

ISSN 1732-9353 (suspended)
eISSN 2543-7496

Scientific Review

Engineering and Environmental Sciences

Przegląd Naukowy
Inżynieria i Kształtowanie Środowiska

Vol. 34 (1)

2025
Quarterly

Issue 107

SCIENTIFIC REVIEW
ENGINEERING AND ENVIRONMENTAL SCIENCES

Quarterly

EDITORIAL BOARD

Libor Ansoerge (T.G. Masaryk Water Research Institute, Czechia), Kazimierz Banasik (Warsaw University of Life Sciences – SGGW, Poland), Jonathan Chan Cheung-Wai (Vrije Universiteit, Brussels, Belgium), Jarosław Chormański (Warsaw University of Life Sciences – SGGW, Poland), Iulii Didovets (Potsdam Institute for Climate Impact Research – PIK, Germany), Tomáš Dostál (Czech Technical University in Prague, Czechia), **Mateusz Grygoruk – Chairman** (Warsaw University of Life Sciences – SGGW, Poland), Jurík Luboš (Slovak Agriculture University, Nitra, Slovak Republic), Bartosz Kaźmierczak (Wrocław University of Science and Technology, Poland), Altaf Hussain Lahori (Sindh Madressatul Islam University, Pakistan), Athanasios Loukas (Aristotle University of Thessaloniki, Greece), Silvia Kohnova (Slovak University of Technology, Slovak Republic), Michael Manton (Vytautas Magnus University, Lithuania), Yasuhiro Matsui (Okayama University, Graduate School of Environmental Science, Japan), Viktor Moshynskiy (National University of Water Management and Nature Resources Use, Ukraine), Mikołaj Piniewski (Warsaw University of Life Sciences – SGGW, Poland), Maja Radziemska (Warsaw University of Life Sciences – SGGW, Poland), Izabela Sówka (Wrocław University of Science and Technology, Poland), Marina Valentukevičienė (Vilniaus Gedimino Technikos Universitetas, Lithuania), Magdalena Daria Vaverková (Mendel University in Brno, Czechia)

EDITORS

Tomasz Gnatowski (Chairman), Barbara Klik, Paweł Marcinkowski (Editorial Assistant Environmental Sciences), Katarzyna Pawluk, Mieczysław Połoński, Sylwia Szporak-Wasilewska, Magdalena Daria Vaverková, Grzegorz Wrzesiński (Editorial Assistant Engineering Sciences)

EDITORIAL STAFF

Weronika Kowalik, Grzegorz Wierzbicki, Justyna Majewska, Robert Michałowski

ENGLISH LANGUAGE EDITING SERVICE

Skrivanek sp. z o.o.

EDITORIAL OFFICE ADDRESS

Wydział Budownictwa i Inżynierii Środowiska SGGW, ul. Nowoursynowska 159, 02-776 Warsaw, Poland
tel. (+48 22) 59 35 363, 59 35 210, 59 35 302
e-mail: srees@sggw.edu.pl
<https://srees.sggw.edu.pl>

Electronic version of the Scientific Review Engineering and Environmental Sciences is primary version

All papers are indexed in the data bases as follows: AGRO(Poznań), BazTech, Biblioteka Nauki, **CrossRef**, **DOAJ**, **Google Scholar**, **Index Copernicus**, INFONA, POL-Index, **SCOPUS**, SIGŻ(CBR)

Scientific Review

Engineering and Environmental Sciences

Przegląd Naukowy

Inżynieria i Kształtowanie Środowiska

Vol. 34 (1)

2025

Issue 107

Spis treści

WIEKE S. Life cycle cost analysis in investment projects – examination of case studies and risk mitigation with Monte Carlo simulation	3
ZIADI E.H., MEKSAOUINE M., MEKKI F. Evaluation of numerical modeling for the seismic response of an arch dam: the case of the Tichy-Haf Dam	19
TKACHENKO T., LIS A., TSIURIUPA Y., MILEIKOVSKYI V., UJMA A., TKACHENKO O., SAKHNOVSKA V. Planning of green roofs for the best thermotechnical effect	42
REZBÁRIK Š., VAVRINCOVÁ L., VALICA M., ADAMCOVÁ V., SEKELY S., REZBÁRIK J., HORNÍK M. Solidification/stabilization of fly ash contaminated with radiocaesium into geopolymers	55
VAVRINCOVÁ L., ADAMCOVÁ V., MACHALOVÁ L., VALICA M., REZBÁRIK Š., HORNÍK M. Effect of soil nutrients on the stability of superabsorbent polymers as a tool for climate change mitigation	73
WIJAYANTI Y., SETYANDITO O. Enhancing urban water utilities: a case study of Utility of the Future framework implementation in Indonesia	89

Wydawnictwo SGGW, Warsaw 2025



Wydawnictwo SGGW



wydawnictwosggw

Editorial work – Anna Dołomisiewicz, Violetta Kaska

ISSN 1732-9353 (suspended) eISSN 2543-7496

Stefan WIEKE  

Mendel University, Faculty of Business and Economics, Czech Republic

Life cycle cost analysis in investment projects – examination of case studies and risk mitigation with Monte Carlo simulation

Keywords: decision-making, life cycle cost analysis, case studies, risk mitigation, Monte Carlo simulation, energy cost

Introduction

Decision-makers need a reliable basis for making appropriate decisions for business development. A company's investment decisions, specifically in technical facilities and equipment that have a primary impact on its success and market assertion, are critical. Such investments are strategic decisions because technical equipment, such as production facilities and machinery, represent a significant long-term financial investment.

Discounted cash flow (DCF) methods are used to estimate the value of investments made in projects. The NPV (net present value) method is the most commonly applied. Life cycle cost (LCC) analysis together with NPV is the preferred method of analysis in the energy sector. The LCC analysis helps decision-makers select the best option. To create a reliable basis, transmission system operator (TSO) owners and operators of natural gas infrastructure in Germany rely on case studies. These studies aim to select the best option for a defined operation task,

such as the decision-making done in compressor stations. Most case studies follow the LCC method of analysis. Although the procedure is straightforward, authors of such case studies encounter challenges that have a considerable impact on the study results and the selection of the best option.

Operational expenditure (OPEX) uncertainties, input data for the NPV calculation, and prediction of future development of input data create the risk of the best investment option not being selected, resulting in the misallocation of limited funds. To address these uncertainties and risks in the evaluation, probabilistic and deterministic methods are proposed. Seven TSO case studies and a single publication (Cierniak, 2001) are examined in this study.

In this study, the impact of input data and the prediction of the future development of input data in case studies on the calculation results of LCC analyses are examined. In retrospect, the case study analysis shows that the prediction of energy costs (among other cost drivers) involves high uncertainty that could result in incorrect decisions. Furthermore, the effectiveness of the Monte Carlo simulation (MCS) probabilistic method for improving the prediction of input data is analyzed. However, the value of the MCS is in quantifying the reliability and validity of results using descriptive statistics. This study focuses on investments in compressor stations in Germany's natural gas infrastructure. The results can be applied to other business areas, such as construction, with machinery involving energy costs as a cost driver.

Material and method

Decision-making in Germany's natural gas infrastructure

Transmission system operators (TSOs) and companies involved in transporting natural gas across Germany operate the high-pressure natural gas pipeline network. These compressor stations maintain pressure in the pipeline system. Before investing in compressor stations, TSOs contract consulting firms to conduct case studies on the intended investment. The most technically and economically advantageous option is developed using the NPV method (Homann et al., 2017). The case studies are prepared by experts. Consequently, the German natural gas industry makes decisions on structured models comprising economic and technical criteria and following LCC and NPV as the commonly used DCF methods. The case studies include capital expenditure (CAPEX) and operational costs for energy and maintenance in the OPEX. Two publications by Heyer and Wieke

(1998) and Cierniak (2001) describe this approach in case studies. Essentially, both follow LCC analysis.

This study examines seven case studies on investments in compressor stations. Six case studies include NPV calculations (following LCC analysis) to determine the best option. Cierniak' paper (2001) in a scientific journal is included in this study. Decision-making in the German natural gas infrastructure is a defined and structured approach based on LCC analysis.

Life cycle cost

Shafiee et al. (2019) explain that LCC calculates all direct costs associated with a project or policy without considering indirect costs (or benefits). The valuation process involves summing the DCF incurred during the project life cycle, assets, and policies using an appropriate discount rate. The main operational cost drivers are the energy and maintenance costs. Project costs comprise CAPEX and OPEX, where CAPEX represents the initial investment, and OPEX includes both the energy and maintenance costs over the lifetime. Other cost factors, such as consumables (e.g. grease or compressed air), can also be considered; however, they are of minor significance.

The LCC method of analysis is widely used in the hydrocarbon industry. Kawauchi and Rausand (1999) conducted a detailed literature survey, online review, and interviews with experts, focusing on examining the basic process of LCC analysis, which contributed to the literature. Furthermore, Kawauchi and Rausand (1999) provide an overview of the codes and standards that establish the details and procedures of LCC analysis. The rules established in the codes and standards are applied in the German gas sector.

A systematic review of the current state-of-the-art and future perspectives on the application of various DMS (decision-making support) methods in the upstream oil and gas industry includes studies published by scholars and practitioners worldwide in relevant English-language journals and conference proceedings between 1977 and 2016 (Shafiee et al., 2019). The literature is identified using databases, such as Scopus, Web of Science, OnePetro, Knovel, IEEE Xplore, the American Society of Mechanical Engineers (ASME) digital collection, and Google Scholar. Related articles are selected based on a set of inclusion criteria, and 110 publications are identified. The LCC has been the most relevant method for decision-making over the past four decades.

Korpi and Ala-Risku (2008) reviewed LCC cases reported in academic and practitioner literature, which is not limited to the energy sector. They found that most of the reported LCC cases were far from ideal. The review highlights the difficulty of conducting a reliable LCC analysis. Further research is encouraged.

The LCC analysis is established in codes and standards such as ISO 15663 Parts 1–3 as an international standard (International Organization for Standardization [ISO], 2000, 2001a, 2001b). The LCC is relevant for decision-making in strategic management and is used to answer a broad range of questions in production processes. It is used to find the best option for an investment project and is established in the German natural gas infrastructure. In fact, not the NPV is calculated, but the discounted cumulated expenditure (DCE). The DCE follows the same rules as the NPV, but does not include revenues. The DCE presents the NPV, but revenues are not included because it is identical for all candidate options for the defined operating cases. In other words, DCE can be considered as the total cost of ownership (TCO) comprising the CAPEX and OPEX.

If all other things are equal, the alternative that is the least expensive over time should be selected (Lee Jr, 2002). For this reason, the option with the lowest DCE is considered the most advantageous.

Managing uncertainties and risks

The LCC analysis is a state-of-the-art method for evaluating infrastructure projects, as they have a long-term horizon in terms of preparation (engineering), execution (construction), and operational lifetime. A lifetime of beyond 20 years is common. Input data and predicting future development involve large uncertainties. Therefore, uncertainties in the input data must be addressed to avoid making incorrect decisions about an investment project. These uncertainties can be addressed in different ways. Ilg et al. (2017) and Scope et al. (2016) conducted systematic literature reviews and identified 115 relevant publications, mostly case studies, in which these uncertainties are addressed. Ilg et al. (2017) and Scope et al. (2016) discuss the different techniques for coping with uncertainty and categorize them as probabilistic, deterministic, possibilistic, and other approaches. Ilg et al. (2017) report that 91 articles mentioned or applied deterministic methods, 90 articles used probabilistic methods, a small number (42 articles) addressed uncertainties using possibilistic methods, and 61 articles applied other methods.

Ilg et al. (2017, p. 280), describe probabilistic methods as “encompassing stochastic techniques that include randomly selected parameters in a variety of sampling methods, e.g. Monte Carlo simulation.” Ally and Pryor (2016) describe

MCS as suitable to quantify the uncertainty of input data in LCC because the key inputs of the model can be randomly and independently varied by their nominal value, which is consistent with a probability distribution function (PDF) to generate a new set of LCC results. The MCS evaluates the impact of simultaneous changes of several input variables on the result – in this case, the NPV. The output of an MCS is an aggregate distribution of these target variables (Ilg et al., 2017). The MCS iterates this process many times, generating new random inputs each time and producing a distribution of LCC outputs that provide a quantified understanding of the uncertainty associated with the LCC model (Ally & Pryor, 2016).

Deterministic methods are used if the input data can be determined, for example, if historical data are available. However, there are several uncertainties associated with the extrapolation of historical data to the future and these uncertainties must be quantified and evaluated. Using deterministic methods, the future development of input data can be evaluated. Scope et al. (2016), besides others, identify sensitivity analysis as a recognized method. Sensitivity analysis is a suitable method for estimating uncertainties. It is straightforward, easily applicable, and provides a comprehensive assessment of the validity of the input data. Also, EN ISO 15663 refers to sensitivity analysis for evaluating uncertainties. Nábrádi and Szöllösi (2007) state that given the uncertainty that may exist about the future, it is often useful to perform sensitivity analyses, which ask a number of “what if” questions.

There are several procedures to reduce uncertainties in the application of LCC. The primary methods for evaluating uncertainties in the long-term development of input data in LCC are probabilistic and deterministic. However, there are no established guidelines regarding the use of these procedures. Experts performing LCCs are responsible for determining the method that must be used to minimize uncertainty. In this respect, a key point is to provide decision-makers with a comprehensive indication of the reliability of the results. Thus, decision-makers’ requirements have a significant influence on the selected procedures. The model’s creator best understands the influencing factors and their reliability and can suggest a method to minimize uncertainties. Recognized recommendations should serve as a guideline for selecting an appropriate method.

With a view to the relevant codes and standards (these are recognized recommendations and represent the state-of-the-art), especially to EN ISO 15663-2 (ISO 2001a), a sensitivity analysis is recommended. The VDI 6025 (Deutsches Institut für Normung [DIN], 2012) guideline also recommends sensitivity analysis.

Besides sensitivity analysis as a deterministic method, a risk assessment, representing probabilistic methods, is also conducted. The probability of the calculated DCE should be ranked and risk mitigated using MCS. To evaluate

the executed studies, MCS and sensitivity analysis are used to improve the decision-making model, which makes it possible to assess the reliability of the results of the model calculation and to provide a strong basis for decision-makers. This work focuses on MCS.

It is shown that the results of the case studies, which are based on assumptions, deviate significantly from the verification with real historical data for energy costs. The prediction of future energy costs is subject to a huge number of publications where related economic theories are discussed. These involve modeling approaches in order to improve prediction. Besides other modeling approaches, MCS is utilized by authors. The broad range of MCS's application is demonstrated by Heck et al. (2016), Tat (2018), Elfarra and Kaya (2021), and Wealer et al. (2021). MCS has been adopted to evaluate the executed case studies for risk assessment. The modeling for the LCC and NPV calculation is Excel-based. For MCS, the open source add-in "XLRisk" has been implemented. The developers point out that "XLRisk" works in a similar fashion to commercial add-ins such as @RISK by Palisade.

Analysis of case studies for investments in Germany's natural gas infrastructure

Compressors and compressor stations are the central components of a natural gas network. Compressors maintain pressure in the system and facilitate natural gas transportation. Investments for compressor stations are above 100 million EUR for a single compressor station. Investment in compressors is long term and associated with considerable monetary resources. During the decision-making process, TSOs rely on case studies.

Seven case studies form the basis for decision-making on investments in the natural gas infrastructure. The analyzed case studies follow LCC, as outlined in EN ISO 15663-1 (ISO 2000), EN ISO 15663-2 (ISO 2001a) and EN ISO 15663-3 (ISO 2001a). These case studies identify the best investment option for compressors in Germany's natural gas infrastructure. The assessed case studies are performed by experts from consulting firms and are reviewed by TSO experts representing the opinions of experts from consulting firms and TSOs. However, these case studies are not accessible publicly, as they are private sector case studies. Therefore, such case studies are typically not available for scientific research. The seven evaluated studies were performed during the period from 2005 to 2015. Additionally, one publication issued in 2001 is examined, meaning a total of eight studies are assessed.

Input data for life cycle cost analysis in case studies

The input data in the analyzed case studies used for calculating the NPV (or DCE) are CAPEX, OPEX (energy costs, maintenance costs, costs for carbon dioxide certificates), operating hours, and macroeconomic data such as discount factor and inflation rate. In this context, CAPEX is the given input data, as expected investments are determined individually for an option based on budget price inquiries or characteristic values.

The set-up of the input data, especially the prediction of future trends in the development of the input data, must be carefully considered. Investment projects have a long-term horizon in terms of preparation (engineering), execution (construction), and operational lifetimes. A lifetime beyond 30 years is not uncommon. The set-up of the input data and future development is associated with high uncertainties. Uncertainties in the input data must be addressed to avoid incorrect investment decisions in projects. Energy costs include costs for electricity and natural gas. Both types of energy are used to drive the compressor motors, which are either gas turbines/gas engines or electric motors. The authors of the case studies applied escalation factors (i.e., 3% per annum) to predict the trends in future energy and maintenance costs.

Modeling with predicted and real historical data

In the executed expert studies, the NPV (DCE) is calculated to investigate the various options available for an investment project. These study models are replicated using the author's input data, and DCEs are recalculated using real historical data. The results of the NPV (DCE) calculations, based on historical data, are compared to those with data applied in the expert studies. The predicted input data (generated with an escalation factor per annum by the authors of the case studies) deviate from the real historical data. Real historical data for energy and maintenance for each year are established during this research. Real costs are historical data from the current perspective and can be generated using data from official sources, such as Statistisches Bundesamt – Destatis (German Federal Statistical Office).

The first step in analyzing the case studies involves replicating the calculation models of the authors' LCC analysis; that is, the algorithm is replicated. Only when the replication results match with those of the authors' calculation models can it be assumed that the repeated algorithm is fully understood, and the second step is prepared. The input values of the case studies are not used in the second step. Instead, real historical (from the current perspective) costs of electrical energy and

natural gas are used. The same applies to the cost of carbon dioxide certificates. Maintenance costs provided by manufacturers are used instead of the authors' data. The result of the second step is a DCE based on real input data. This examination of models shows whether the ranking of options calculated in the expert studies remains unchanged or not when real historical data are used. A comparison of the results demonstrates the robustness of the LCC analysis in the case studies.

Risk assessment with Monte Carlo simulation

The MCS is suitable for quantifying the uncertainty of the LCC because the model's key inputs can be varied randomly and independently with respect to their normal value, which is consistent with the PDF to generate a new set of LCC results (Ally & Pryor, 2016). The MCS is a method to evaluate the impact of simultaneous changes of several input variables on the result; in this case, the NPV. The output of an MCS is an aggregate distribution of these target variables (Choudhry, 2006; Gleißner & Wolfrum, 2019). Jorion (2002) explains that MCS is the most powerful, comprehensive, and potentially accurate method of quantifying risk. However, they state that the price of accurate risk quantification is high. For example, the preliminary work, computational capacity, long computational time, and the know-how of experts are required, making it very expensive to implement (Jorion, 2002; Choudhry, 2006). The LCC is now more accessible due to the significant increases in computer processing capabilities and their availability (Rahman & Vanier, 2004).

Using the MCS macro, 10,000 iterations can be run within a reasonable time, and the number of iterations is inconsequential in terms of generating stable results. The PDF for the following input values must be defined: cost of electricity to run the compressors, cost of natural gas (fuel gas) to run the compressors, and carbon dioxide certificate costs, if included in the respective case study. There are different approaches to determining the PDF. The authors' level of knowledge regarding the historical data of costs should also be considered.

In this study, the following setup is chosen to predict future energy costs. The author's possible knowledge of the historical data of energy costs forms its basis. Here, a graph was created of the annual costs from 2000 to the year the study was prepared. A trend line and extrapolation are generated for this graph. Figure 1 illustrates the trend line and the forecast for natural gas costs in Study 2: The study year is 2011, and historical data are available from 2000 to 2011. The forecast is assessed from 2012 to 2020.

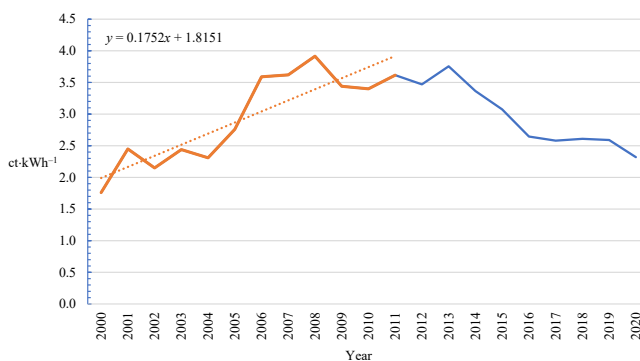


FIGURE 1. Study 2: trend line and forecast of natural gas costs (orange: author’s knowledge of historical data, blue: knowledge of historical data from the current perspective; dotted line: author’s knowledge of trend line for forecast)

Source: own work.

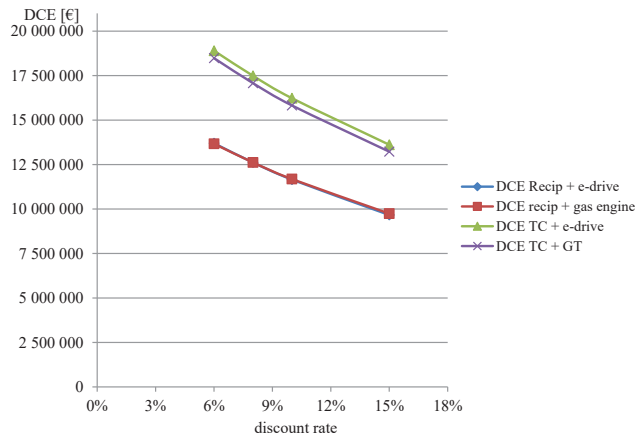
The beta-PERT function is selected as the PDF in the MCS software solution. For the beta-PERT function, the minimum and maximum values, and a most likely value, must be specified as the input data for the above costs. The MCS is applied to each option in each case study for assessment. This implies that all the models for calculating the DCE are re-run with probability distributions for the costs of natural gas, electricity, and carbon dioxide certificates (if included in the case study). Consequently, the following results are available for further evaluation of the DCE calculations for the options examined in the case study: DCE calculation with input data from studies, DCE calculations with real historical input data, and DCE calculations with input data generated from the probability distributions of the MCS. The DCE or the statistical distribution of the DCE is calculated. The results allow the application of descriptive statistics to quantify the associated risks.

Results and discussion

Modeling with predicted and real historical data

The results of the cost models for the input data applied by the authors of the case studies (with predicted input data for energy and maintenance costs) are compared with the results calculated using real historical data. Due to space constraints, the results of the model calculations from one out of eight studies are presented in this study as an example. These results are representative of the results from

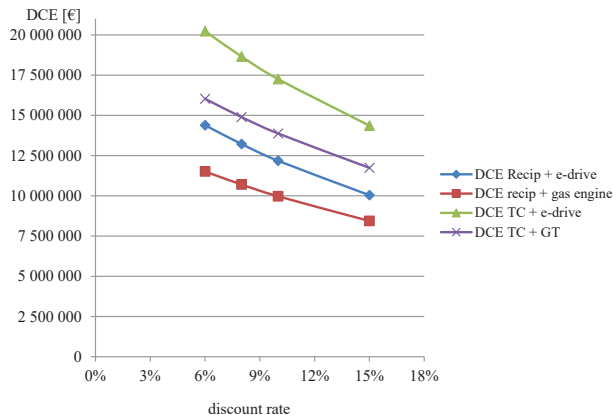
the analysis of all studies. The graphs show not only a comparison between the calculations with predicted input data and real historical data, but also a sensitivity analysis for the interest rate. The results are based on the analysis of Study 2.



Recip: reciprocating compressor; TC: turbo compressor; GT: gas turbine (driven by natural gas); e-drive: electric motor (driven by electricity); period: nine years (2012–2020); operating hours: 2,880 per year

FIGURE 2. Study 2: discounted cumulated expenditure versus discount rate, calculation with authors' input data

Source: own work.



Recip: reciprocating compressor; TC: turbo compressor; GT: gas turbine (driven by natural gas); e-drive: electric motor (driven by electricity); period: nine years (2012–2020); operating hours: 2,880 per year

FIGURE 3. Study 2: discounted cumulated expenditure versus discount rate, calculation with real (historical) input data

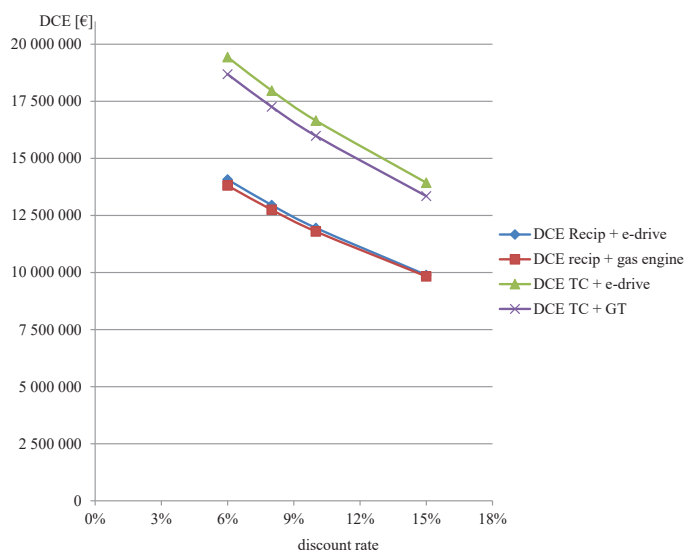
Source: own work.

Study 2 (Figs 2 and 3) shows that the use of real historical data leads to a clear ranking of the options. Using the input data for the study, the two variants are indistinguishable in terms of DCE; with real historical data, there is a clear preference for one option. In the other studies, the ranking of the options remained unchanged, but the distances between the options change. The DCEs are higher with real historical data in some studies, which can influence the decision of whether to invest at all. Some studies show that the ranking changes with the calculation of real historical data. The DCE of an option decreases and receives a higher preference. This recalculation can influence decisions in favor of one or the other option.

Monte Carlo simulation

The following figures show the results of using MCS for Study 2. The DCEs are recalculated using MCS. The relevant figures for Study 2 are:

- calculation of DCE with input data and real historical data (Figs 2 and 3),
- calculations of DCE with input data generated from probability distributions of the MCS based on real historical data (Fig. 4).

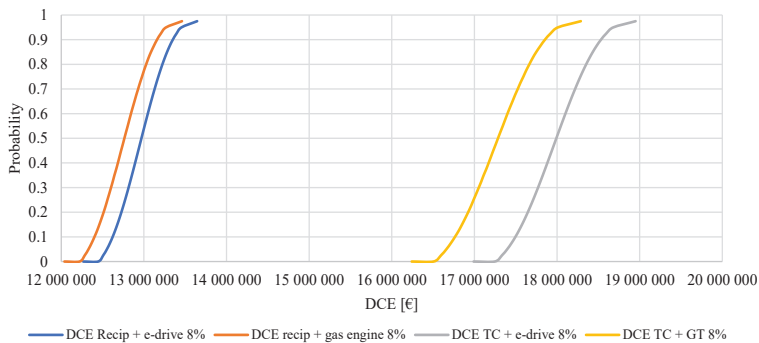


Recip: reciprocating compressor; TC: turbo compressor; GT: gas turbine (driven by natural gas); e-drive: electric motor (driven by electricity); period: nine years (2012–2020); operating hours: 2,880 per year

FIGURE 4. Study 2: Results of Monte Carlo simulation calculation with real historical data

Source: own work.

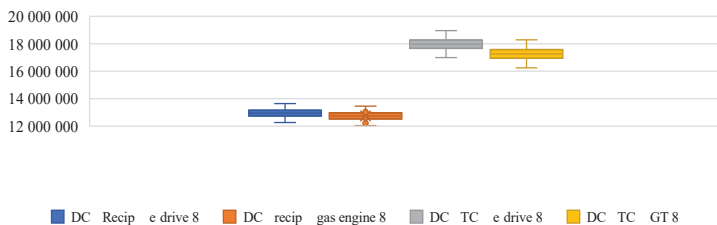
A comparison of the figures for Study 2 shows that using the MCS does not necessarily improve the results of the DCE calculation. Calculations with real historical input data would be expected to match the calculations using data generated from the MCS. However, this is not the case, as the future development of input data cannot be predicted with certainty using MCS. In any case, MCS has an advantage in that the calculated results can be evaluated using descriptive statistics. Descriptive statistics are applied to the probability distributions of the results to generate statistical statements regarding the reliability of the results. The MCS makes it possible to calculate the mean and median values, standard deviations, and confidence levels. Figures 5 and 6 are a sample for Study 2.



Recip: reciprocating compressor; TC: turbo compressor; GT: gas turbine (driven by natural gas); e-drive: electric motor (driven by electricity); period: nine years (2012–2020); operating hours: 2,880 per year

FIGURE 5. Study 2: cumulative probability for discount rate of 8%

Source: own work.



Recip: reciprocating compressor; TC: turbo compressor; GT: gas turbine (driven by natural gas); e-drive: electric motor (driven by electricity); period: nine years (2012–2020); operating hours: 2,880 per year

FIGURE 6. Study 2: box plot for discount rate of 8%

Source: own work.

Conclusions

Decisions regarding investments in compressor stations in Germany's natural gas infrastructure are based on LCC analysis, as described in EN ISO 15663, and this involves a comparison of different options, which must all meet investment requirements. Experts from consulting firms perform seven case studies, and TSO experts review them. These seven studies formed the basis for decision-making on investments in natural gas infrastructure. Moreover, these case studies represent expert opinions, from both the consulting firms and TSOs. The analysis of these seven executed case studies shows that the results of an LCC analysis depend on the input data and the estimate of future development.

As part of the assessment, the models were replicated, and the calculations were repeated using real historical values. A comparison of the results calculated using the authors' data and real historical data shows that changes in the NPV (or DCE) lead, in part, to a change in the ranking of the options. These results clarify that decision-makers require additional measures to validate the results of the case studies and mitigate risks.

The comparison of the results of the DCE-calculations with data from the authors and real historical data shows the discrepancies clearly. The calculation with real, from today's perspective, historical values for energy costs leads to divergent results in the determination of the preferred option. The prediction of energy costs is associated with uncertainties and risks. The MCS is a probabilistic method to address uncertainties and risks. To secure the results of the case studies, MCS is used to recalculate the input data and its future development in the executed case studies. A comparison of the results from calculations with real historical data and calculations with MCS data also shows deviations in the results. This makes it clear that using MCS to establish more reliable input data is limited.

The MCS improves risk mitigation not through more reliable input data but by providing statistical data of the output. The MCS results are the PDF of the DCE, thus making it accessible to descriptive statistics. The probabilities can be analyzed graphically and in box plots. Standard deviations, confidence levels (95%), mean/median values, and other relevant numbers are provided with the MCS. This makes the results of the LCC analysis quantifiable and reduces the risk in the decision-making process.

The MCS is not used in the seven studies examined. Although MCS is a recognized method and limitations in computing are no longer a problem, it is rarely used in the German natural gas infrastructure. Furthermore, the results

can be transferred from natural gas infrastructure to other areas where LCC analysis with OPEX comprising energy, maintenance, or other costs can be applied.

To improve the validation of the case study results, other measures, such as deterministic methods using sensitivity analysis, are suggested. Sensitivity analysis makes it possible to identify the impact of major cost drivers on the results. In addition, a company's success increasingly depends on social acceptance. Therefore, aside from economic requirements, decision-makers at sustainable companies can also consider social and ecological requirements to determine an investment. With the help of a weighted scoring method, these aspects can be incorporated into the decision-making process of a sustainability assessment. Thus, the LCC should be supplemented by a sustainability assessment.

References

- Ally, J., & Pryor, T. (2016). Life cycle costing of diesel, natural gas, hybrid and hydrogen fuel cell bus systems: an Australian case study. *Energy Policy*, 94, 285–294. <https://doi.org/10.1016/j.enpol.2016.03.039>
- Choudhry, M. (2013). *An introduction to value-at-risk*. John Wiley & Sons.
- Cierniak, S. (2001). Life cycle-costs von Kolben- und Turbokompressoren. *Erdöl, Erdgas, Kohle*, 117 (11), 511–517.
- Deutsches Institut für Normung [DIN]. (2012). *Betriebswirtschaftliche Berechnungen für Investitionsgüter und Anlagen [Economy calculation systems for capital goods and plants]* (VDI 6025:2012-11).
- Elfarra, M. A., & Kaya, M. (2021). Estimation of electricity cost of wind energy using Monte Carlo simulations based on nonparametric and parametric probability density functions. *Alexandria Engineering Journal*, 60 (4), 3631–3640. <https://doi.org/10.1016/j.aej.2021.02.027>
- Gleißner, W., & Wolfrum, M. (2019). Grundlagen des Risikomanagements. In *Risikoaggregation und Monte-Carlo-Simulation* (pp. 3–13). Springer. https://doi.org/10.1007/978-3-658-24274-9_2
- Heck, N., Smith, C., & Hittinger, E. (2016). A Monte Carlo approach to integrating uncertainty into the levelized cost of electricity. *Electricity Journal*, 29 (3), 21–30. <https://doi.org/10.1016/j.tej.2016.04.001>
- Heyer, F., & Wieke, S. (1998). Verdichter und Antriebsmaschinen für die Erdgasspeicherung und den Erdgastransport – Auswahl unter technischen und wirtschaftlichen Aspekten [Selection of compressors and drives for storage and transport of natural gas – technical and economical aspects]. *Erdoel Erdgas Kohle*, 114, 548–551.
- Homann, K., Klocke, B., Hühener, T., & Wernekinck, U. (2017). *Handbuch der Gasversorgungstechnik*. DIV Deutscher Industrieverlag.

- Ilg, P., Scope, C., Muench, S., & Guenther, E. (2017). Uncertainty in LCC for long-range infrastructure. Part I: leveling the playing field to address uncertainties. *International Journal Life Cycle Assess*, 22, 277–292. <https://doi.org/10.1007/s11367-016-1154-1>
- International Organization for Standardization [ISO]. (2000). *Petroleum and natural gas industries – Life cycle costing. Part 1: Methodology* (EN ISO 15663-1).
- International Organization for Standardization [ISO]. (2001a). *Petroleum and natural gas industries – Life cycle costing. Part 2: Guidance on application of methodology and calculation methods* (EN ISO 15663-2).
- International Organization for Standardization [ISO]. (2001b). *Petroleum and natural gas industries – Life cycle costing. Part 3: Implementation guidelines* (EN ISO 15663-3).
- Jorion, P. (2002). How informative are value-at-risk disclosures? *The Accounting Review*, 77 (4), 911–931. <https://doi.org/10.2308/ACCR.2002.77.4.911>
- Kawauchi, Y., & Rausand, M. (1999). *Life Cycle Cost (LCC) analysis in oil and chemical process industries*. Toyo Engineering Corp. https://www.researchgate.net/publication/228594034_Life_Cycle_Cost_LCC_Analysis_in_Oil_and_Chemical_Process_Industries
- Korpi, E., & Ala-Risku, T. (2008). Life cycle costing: A review of published case studies. *Managerial Auditing Journal*, 23 (3), 240–261. <https://doi.org/10.1108/02686900810857703>
- Lee, D. B., Jr (2002). Fundamentals of life-cycle cost analysis. *Transportation Research Record*, 1812 (1), 203–210. <https://doi.org/10.3141/1812-25>
- Nábrádi, A., & Szöllösi, L. (2007). Key aspects of investment analysis. *APSTRACT: Applied Studies in Agribusiness and Commerce*, 1 (1), 53–56. <https://doi.org/10.22004/ag.econ.43577>
- Rahman, S., & Vanier, D. J. (2004). Life cycle cost analysis as a decision support tool for managing municipal infrastructure. *CIB 2004 triennial congress*, 2 (1), 11–8. <https://www.irb.fraunhofer.de/CIBlibrary/search-quick-result-list.jsp?A&idSuce=CIB+DC9737>
- Scope, C., Ilg, P., Muench, S., & Guenther, E. (2016). Uncertainty in life cycle costing for long-range infrastructure. Part II: guidance and suitability of applied methods to address uncertainty. *The International Journal of Life Cycle Assessment*, 21, 1170–1184. <https://doi.org/10.1007/s11367-016-1086-9>
- Shafiee, M., Animah, I., Alkali, B., & Baglee, D. (2019). Decision support methods and applications in the upstream oil and gas sector. *Journal of Petroleum Science and Engineering*, 173, 1173–1186. <https://doi.org/10.1016/j.petrol.2018.10.050>
- Tat, A. N. (2018). Electricity price forecasting using Monte Carlo simulation: the case of Lithuania. *Ekonomika*, 97 (1), 76–86. <https://doi.org/10.15388/Ekon.2018.1.11780>
- Wealer, B., Bauer, S., Hirschhausen, C. V., Kemfert, C., & Göke, L. (2021). Investing into third generation nuclear power plants – Review of recent trends and analysis of future investments using Monte Carlo Simulation. *Renewable and Sustainable Energy Reviews*, 143, 110836. <https://doi.org/10.1016/j.rser.2021.110836>
- XLRisk. <https://github.com/pyscripter/XLRisk> [accessed: 14.09.2024].

Summary

Life cycle cost analysis in investment projects – examination of case studies and risk mitigation with Monte Carlo simulation. This work focuses on life cycle cost (LCC) analysis in the German natural gas infrastructure and recommends strategies to mitigate the uncertainties and risks involved using Monte Carlo simulation (MCS). It deals with the impact of input data and predicting the future development of input data on the results of the LCC analysis and discusses MCS for risk mitigation. Seven case studies for investments in Germany's natural gas infrastructure are analyzed. In addition to the executed case studies, a case study from a scientific journal is included. The case studies were conducted between 2005 and 2015. Evaluation with real historical input data shows that the results of an LCC analysis depend on the reliability of input data and predictions on their development. The retrospective view shows that the best options are not always identified. Therefore, the results need to be validated using risk-mitigation methods, such as MCS. The executed case studies reflect the opinions of experts. This work shows how risk is mitigated through MCS while focusing on LCC analysis in the German natural gas infrastructure; however, the proposed risk mitigation with MCS can be adopted for other investment projects comprising capital expenditure (CAPEX) and operational expenditure (OPEX), for example, in construction, machines and other fields.

El Houcine ZIADI¹  

Mohamed MEKSAOUINE¹ 

Feriel MEKKI² 

¹ Badji Mokhtar University, Faculty of Technology, Department of Hydraulic, Laboratory of Soils and Hydraulic, Annaba, Algeria

² Badji Mokhtar University, Faculty of Earth Science, Department of Architecture, Laboratory of Soils and Hydraulic, Annaba, Algeria

Evaluation of numerical modeling for the seismic response of an arch dam: the case of the Tichy-Haf Dam

Keywords: arch dam, finite element method, Midas GTS NX, Mohr–Coulomb, seismic

Introduction

Dams are constructed as blockades to restrain water runoff. They serve a significant role in flood control, electricity generation, water supply, and irrigation (He et al., 2022). Arch dams are favorable to engineers for their high load-bearing capacity (Li et al., 2024). This type of dam is one of the most important engineering structures to provide energy. In both geometry and elevation, they exhibit an arched shape. They are built using a small volume of concrete compared to gravity dams, which means that arch dams require sophisticated engineering knowledge for their design and construction (Bayraktar et al., 2011). Due to their strategic interest, dams are subject to rigorous design criteria, particularly with regard to the risk of exposure associated with earthquakes (Adjadj et al., 2021), especially since failure

of the structure could result in significant loss of life. However, the vibrations from earthquakes may jeopardize the safety of dam construction (Saxena & Patel, 2023). Consequently, it is imperative to develop reliable numerical tools to assess the seismic responses of dams (He et al., 2022). The soil–structure interaction problem has become the primary focus area for major massive structures like arch dams, bridges, and retaining walls (Sharma & Nallasivam, 2023). The factor of dam–foundation rock interaction plays an important role in the 3D analysis of arch dams (Li et al., 2022). The seismic analysis of arch dams, accounting for the interaction between the foundation and the reservoir, is a difficult subject in computational mechanics (Haghani et al., 2022). Various factors influence the behavior of a dam during an earthquake, including the dam’s geometry, the mechanical properties of the construction materials, such as cohesion and internal friction, and the modulus of elasticity (Ebrahimian, 2011). Most existing dams in seismic regions were designed using methods that are now considered simplistic and inaccurate. Before the widespread use of commercial finite element software, physical model tests were the most common method for analyzing structures with complex geometries (Chopra, 2012). Traditional methods used to analyze arch dams, including cylinder theory, the independent arch method, experimental load analysis, and model analysis, have been found to be limited to dams with small heights (Varghese et al., 2014). In recent years, with the development of accessible numerical methods, this type of analysis has taken over as the primary tool for dam safety assessments (Enzell et al., 2021). The most widely used method for evaluating the stability of a dam and foundation is the finite element method – FEM (Lyu et al., 2021). The ease of implementation due to the matrix methodology adopted in FEM formulations makes it highly compatible with modern digital computation facilities (Sarkar et al., 2024). The FEM has a distinct advantage in tackling irregular geometries (Das et al., 2023). A major advantage of FEM lies in its flexibility in modeling complex geometries and geologic conditions. Current FEM codes can simulate a variety of material behaviors and incorporate the influence of construction procedures. FEM analyses provide detailed information on the stress and deformation properties of both the dam and the abutments (Yu et al., 2005).

Among the seismic analysis methods, time history analysis is the most accurate for simulating a structure’s response to an earthquake record (Majidi et al., 2023). For years, researchers have refrained from widely adopting nonlinear time history analysis due to its demanding computational requirements. However, with the advancement of computer technology, it has become relatively easier to conduct a nonlinear time history analysis (Ningthoukhongjam & Singh, 2021). This method is one of the seismic analysis approaches that use a set of seismic

recordings to determine the response of an irregular structure. Among the various existing nonlinear dynamic analyses, time-history dynamic analysis is the most comprehensive. It replicates and records the genuine behavior of a structure responding to varying ground acceleration over time (Suryadi et al., 2023). Assessing the nonlinear response of concrete arch dams to strong or extreme earthquakes is particularly important for evaluating their safety performance, which is highly dependent on input ground motions (Liang et al., 2023).

The year 2021 has witnessed, and continues to witness, a relatively high level of seismic activity in eastern and central Algeria, attributed to the convergence of the Eurasian and African plates near Cape Carbon. Algeria's water resources predominantly reside in dams, which are especially sensitive to seismic events, particularly arch dams. To assess the impact of this seismic activity, it was necessary to analyze the seismic response of the Tichy-Haf Dam, an arch dam located in an earthquake-prone area in northeast Algeria. This study investigates the Tichy-Haf Dam's seismic response using a time history analysis conducted with the Midas software, which can provide displacement, acceleration, and velocity values resulting from earthquake-induced loads. The dynamic load was generated using four accelerograms with peak ground accelerations of 0.12 g, 0.32 g, 0.36 g, and 0.44 g. During the operational period of an arch dam, the influence of attached outlets on stress and deformation is slight under both static and dynamic loads. Therefore, in this study, the finite element analysis for the dam primarily focuses on a model without considering any appurtenant structures to simplify the numerical simulations (Zhang et al., 2024). Validation of the numerical model involves comparing the results obtained from numerical modeling with the actual data collected from dam monitoring.

Material and methods

Geographical and geological location

Tichy-Haf Dam is located on the Oued Bouselam River, about 20 km from the Soummam Valley, 10 km southeast of the city of Akbou, near the village of Mahfouda, in the commune of Bouhamza, Béjaïa Province. The catchment area at the dam site is 3,980 km². The dam, with a height of 80 m, aims to create a reservoir of 150 hm³. The annual allocation of the available water volume is as follows:

- Meeting the drinking water supply needs of the towns along the Akbou-Béjaïa corridor.

- Irrigation of the Sahel and lower Soummam perimeters: the total annual volume allocated for irrigation in these areas is 43 hm³.
- Flood control on the Oued Bousselam: managing flood events along the Oued Bousselam River is crucial to mitigating the impact of flooding in the Soummam Valley.



FIGURE 1. An arch of the Tichy-Haf Dam

Source: Algerian National Agency of Dams and Transfers (ANBT).

The arch dam is founded on Jurassic limestone, which is covered by marl. Tectonic forces have caused detachments within the limestone massif, and a tectonic fold has elevated the limestone above the marl. The reservoir rests on watertight marl. The two banks exhibit quite contrasting features. The left bank is only slightly affected by tectonic activity, with sound limestone that is often karstified. In contrast, the right bank is dolomitic and contains pockets of mylonite or sandy material, with intense fracturing due to tectonic thrusting. The Soummam Valley is a seismic zone, which necessitated the installation of a double anti-seismic belt above and below the auxiliary spillway. This belt serves to prevent any washouts.

Geometric and numerical model

The Tichy-Haf Dam is a double-curvature arch dam with varying radii and angles and is asymmetrical. The dam stands 80 m tall and has a crest length of 275 m. The width at the crest is 5 m, widening to 27.75 m at the base. In the finite element model of an arch of the Tichy-Haf Dam, the flood spillway was excluded due to the small size of the openings between the concrete blocks. The dam structure

was created using the AutoCAD software and then exported to Midas GTS NX. The natural terrain was modeled in 3D in Midas GTS NX, which accounted for the actual geomorphology of the area. Midas GTS NX is a piece of finite element analysis software used for advanced geotechnical analysis, including soil and rock deformation and stability, dynamic vibrations, and soil-structure interaction in both 2D and 3D. It is utilized by geotechnical, civil, and mining engineers for analysis, testing, and design (System, 1989), supporting various geotechnical projects such as subways, tunnels, pile foundations, dams, and mines (Shen, 2022). Figures 2, 3 and 4 illustrate the geometric model of the Tichy-Haf Dam.

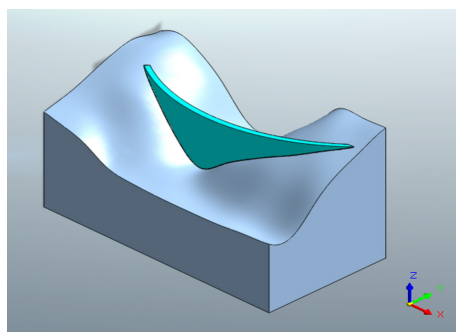


FIGURE 2. Geometric model of the Tichy-Haf Dam

Source: own work.

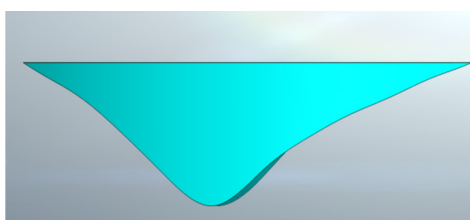


FIGURE 3. Upstream section of the Tichy-Haf Dam

Source: own work.

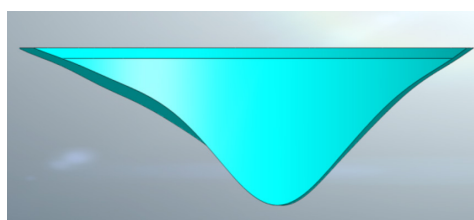


FIGURE 4. Downstream section of the Tichy-Haf Dam

Source: own work.

The finite element model included 59,191 triangular elements and 13,035 nodes. Each node has three degrees of freedom, corresponding to translations in the x, y, and z directions. Figure 5 depicts the finite element model of an arch of the Tichy-Haf Dam and its foundation. The Tichy-Haf Dam's finite element model considers the interaction between the dam and foundation. The static loads

considered are the self-weight of the dam and the water pressure on the upstream side. The boundary conditions applied to the model include fixed support at the base of the foundation and a free displacement boundary at the other edges, allowing the model to interact with dynamic loading.

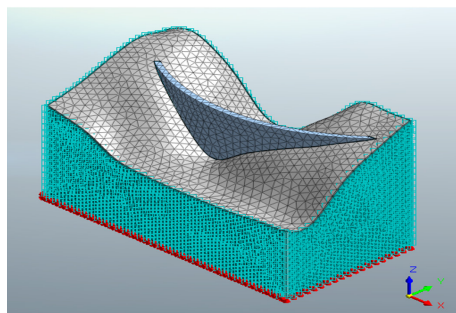


FIGURE 5. Mesh and boundary conditions of an arch of the Tichy-Haf Dam
Source: own work.

The Mohr–Coulomb model was employed to approximate the soil behavior, requiring parameters such as the Young’s modulus, Poisson’s ratio, cohesion, friction angle, and dilatancy angle (Zewdu, 2020). Table 1 provides the values of these parameters for the different materials composing the dam and the foundation.

TABLE 1. Physical-mechanical properties of materials

Specification	Elastic modulus (E) [kN·m ⁻²]	Poisson’s ratio (ν) [-]	Unit weight (γ) [kN·m ⁻³]	Saturated unit weight (γ_{sat}) [kN·m ⁻³]	Cohesion (c) [KN·m ⁻²]	Frictional angle (ϕ) [°]
Dam	10 ⁷	0.39	21.4	21.4	150	25
Foundation	4.10 ⁷	0.32	24.7	24.7	500	45

Source: Algerian National Agency of Dams and Transfers (ANBT).

Eigenvalue module

The eigenvalue problem, also known as modal analysis, is used to determine the natural frequencies of a structure in order to calculate the damping ratio coefficients, accounting for both structural and soil damping (Roësset, 2007). The dynamic behavior of an arch dam is influenced by its dynamic characteristics,

such as the shear modulus and damping ratio. Eigenvalue analysis was utilized to assess the dynamic properties inherent in both the soil and the dam structure (Adjadj et al., 2021). A damping ratio of 5% was assumed for the dam body, which is a typical value for such structures. In this study, the model was subjected to a series of ground motion records. The dynamic loading was derived from four accelerograms with amplitudes of 0.12 g, 0.32 g, 0.36 g, and 0.44 g, respectively.

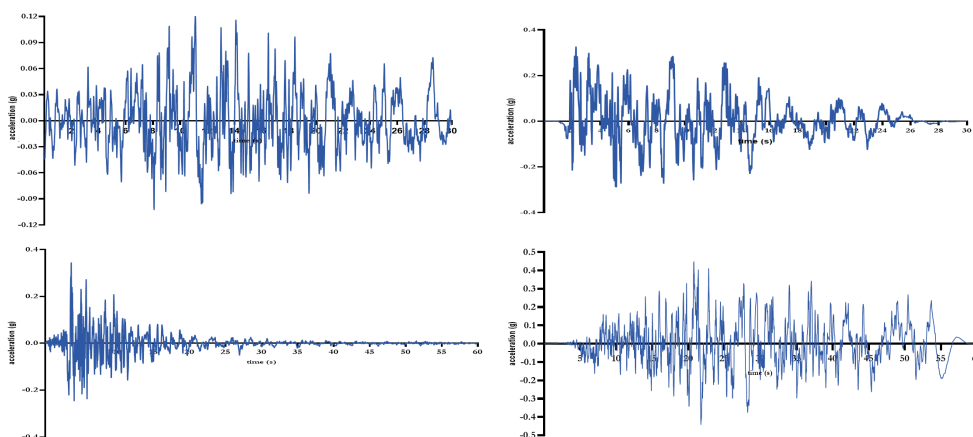


FIGURE 6. Seismic loads used in the modeling

Source: Algerian National Earthquake Engineering Center (CGS).

Figure 6 presents the characteristics of the horizontal accelerograms obtained from seismic loads, with the earthquake's peak horizontal acceleration reaching 0.44 g. This value is consistent with probabilistic studies previously conducted in Algeria.

Dam monitoring

Ensuring the safety of dams through regular monitoring using specialized equipment is crucial for effective dam operation management. Monitoring variables, such as horizontal and vertical displacement data, plays a significant role in evaluating the safety of concrete arch dams. By comparing the actual structural response, including displacement, with model predictions, any abnormal dam behavior can be promptly detected, enabling the timely implementation of corrective measures (He et al., 2022).

Description of the planimetric device

The planimetric system at the Tichy-Haf Dam comprises 7 pillars (Fig. 7) and 18 deformation markers situated on both the crest and downstream face. The distribution of the seven pillars is as follows:

- Pillar 01: downstream of the arch dam,
- Pillar 02: downstream on the left bank of the arch dam,
- Pillar 03: extending from the crest on the right bank of the arch dam,
- Pillar 04: on the crest of the arch dam,
- Pillar 05: extending from the crest on the left bank of the arch dam,
- Pillar 06: downstream on the left bank of the arch dam,
- Pillar 07: at the foot of the arch dam.

There are also 32 planimetric markers, which are smooth bushes capable of accommodating conical targets. These markers are distributed as follows: 14 markers are located on the downstream crest of the arch dam at an elevation of 305 m.



FIGURE 7. Planimetric pillar

Source: Algerian National Agency of Dams and Transfers (ANBT).

The measurements were processed using the Land Surveyor (v2.1) software, which is used to process topographic measurements taken during dam monitoring.

Description of the leveling device

The leveling system at the Tichy-Haf Dam includes 15 benchmarks and 8 reference benchmarks. The vertical displacements of the structure were measured at specific points, as follows (Fig. 8):

- 15 benchmarks are located on the downstream crest of the arch dam at an elevation of 305 m,
- RF 01, RF 02, and RF 03 are situated on the right bank,
- RF 04, RF 05, and RF 06, as well as 100 and 101, are positioned on the crest.



FIGURE 8. Reference benchmark

Source: Algerian National Agency of Dams and Transfers (ANBT).

The measurements were processed using Land Surveyor v2.1. This software is used to determine the most probable height (Z) of all the leveled markers on the dam and to assess the accuracy of the measurements made.

Measurement of radial, tangential and vertical displacement

Tables 2 and 3 present the radial, tangential, and vertical displacements recorded under static loading conditions.

TABLE 2. Radial and tangential displacements

Point	Tangential coordinate [m]	Radial coordinate [m]	First measurement		Second measurement		Third measurement		Fourth measurement	
			X.10 ⁻³ [m]	Y.10 ⁻³ [m]						
Pillar										
1	2 139.7771	5 213.2880	0.1	-0.6	-0.1	-1.5	1.2	-1.7	1.8	1.3
2	2 234.3549	5 145.5580	0	0	0	0	0	0	0	0
3	2 280.7998	5 073.4329	5.2	0.8	0.7	0.6	-0.1	-0.8	2.4	1.0
4	2 128.0069	5 001.9064	0.7	-5	1.7	-3.8	1.6	-2.9	2.3	2.7
5	2 053.6496	5 045.6026	0	0	0	0	0	0	0	0
6	2 061.3379	5 098.1197	0	0	0.1	-1.0	-0.5	0	-0.3	0.8
7	2 180.8727	5 056.8459	-1.6	-0.2	-1.9	-1.1	-1.3	-1.8	0.8	0.3
Arch crest										
1	2 263.2976	5 073.7152	-0.2	2.3	-0.1	3.4	-1.3	-0.3	3.3	2.9
2	2 252.3023	5 059.3807	3.6	-1.4	0.7	-0.3	1.7	-0.3	0.3	-0.5
3	2 241.3327	5 047.0754	4.1	-2.9	-0.1	-0.7	-0.2	-2.3	-0.5	1.8
4	2 228.5392	5 034.7925	3.1	-5.0	0.2	-3.9	0.9	-5.4	-0.7	0.3
5	2 213.3124	5 022.8209	5.4	-5.8	3.8	-4.5	4.3	-3.5	2.2	1.0
6	2 196.6591	5 012.5910	4.2	-5.9	0.7	-5.1	2.7	-6	0	-0.1
7	2 178.2207	5 007.4771	2.8	-7.6	1.6	-5.9	2.8	-5.5	1.1	0.8
8	2 161.0720	5 000.0211	3.3	-6.4	1.0	-4.7	2.3	-3.2	0.1	2.5
9	2 142.8410	4 998.5590	1.6	-3.3	1.7	-5.8	0.1	-6.0	0.5	2.0
10	2 127.0101	5 000.0122	1.3	-5.3	2.3	-3.7	2.3	-2.4	2.0	2.5
11	2 112.8964	5 003.1407	-0.5	-3.3	0.4	-0.7	1.1	-1.2	2.6	3.0
12	2 099.3296	5 007.7667	-0.7	-3.2	-0.9	0.3	0.1	-2.0	2.1	4.0
13	2 086.1626	5 013.6576	-0.2	-1.5	-0.8	1.4	-1.7	1.6	0	4.4
14	2 070.9992	5 022.1910	-0.4	-2.5	-1.4	-1.1	-1.5	0	0.1	-0.4
Downstream section										
17	2 220.8518	5 043.9473	4.3	-1.0	-1.4	-2.3	0	-1.7	0.9	-1.0
18	2 209.4664	5 046.9359	0.4	-1.8	0	0	0.5	-0.9	2.4	1.3
19	2 181.8562	5 024.1640	-2.0	-2.4	-1.1	-4.1	-1.1	-1	-1.2	-7.4
20	2 109.7468	5 018.7815	-0.6	-0.6	-0.2	-0.8	-1.8	-3.3	-0.6	-0.1

X – radial displacements, Y – tangential displacements.

Source: Algerian National Agency of Dams and Transfers (ANBT).

TABLE 3. Vertical displacements

Point	Elevation [m]	Vertical displacement $\cdot 10^{-3}$ [m]			
		first measurement	second measurement	third measurement	fourth measurement
Reference					
01	307.9039	3.7	0.4	-0.2	-1.4
02	310.0502	3.1	-0.2	-0.7	-0.7
03	305.6079	3.7	0.3	-0.1	-1.0
04	286.9498	0	0	0	0
05	285.7634	0	0	0	0
06	286.4792	0	0	0	0
100	286.3762	0	0	0	0
101	288.0259	1.5	1.3	0.4	-0.8
Arch crest					
01	285.2747	1.3	1	-0.2	0
02	285.2878	2.5	1.7	0.8	-0.3
03	285.2854	1.7	1	0.1	-1.6
04	285.3151	2.2	1.6	0.5	-1.2
05	285.2989	0.9	0.5	-0.8	-2.0
06	285.2873	1.7	1.4	-0.1	-1.4
08	285.3012	1.9	0.8	-0.1	-1.6
09	285.3041	1.3	0.3	-0.8	-2.4
10	285.3026	2.2	1.7	0.5	-0.8
11	285.2921	1.4	0.9	0.1	-1.4
12	285.3040	2.4	2	1.4	0
13	285.2950	1.7	1.1	0.7	-0.7
14	285.3078	2.4	1.7	1.4	0.4
15	285.3413	0.1	0.3	0.1	0.9
16	287.6154	1.5	1.7	0.8	0.7

Source: Algerian National Agency of Dams and Transfers (ANBT).

The horizontal and vertical displacement values of the dam were monitored, considering static loads. Static loads are considered permanent loads, and their variation is negligible. An assessment of these parameters is required to evaluate the dam's response to permanent loads and to ensure its long-term

stability. Table 2 shows the radial and tangential displacements of the dam, with maximum values reaching 0.0045 m and -0.007 m, respectively, at the crest of the arch. In contrast, vertical displacements are minimal throughout the dam, particularly at the crest, where a maximum vertical deformation of 0.0037 m is observed (Table 3).

Results and discussion

Calculation stages

In the first phase of this study, we analyzed the dam's behavior by evaluating its displacement under empty conditions. The second phase focused on the dam's response when fully filled, considering the combined effects of its self-weight and the water pressure. In the final phase, a dynamic analysis was conducted to assess the dam's behavior during seismic events, examining key parameters, such as the relative displacement, relative velocity, and relative acceleration, to evaluate its structural performance.

Displacement refers to the overall movement of a point or element within the dam from its original position due to applied loads. In contrast, relative displacement measures the difference in displacement between two points or elements within the structure, providing insights into differential movement between various sections of the dam. This is critical for identifying uneven deformations, which can lead to stress concentrations. Excessive relative displacement may indicate localized strain, potentially leading to cracking or other forms of structural damage.

Relative velocity pertains to the rate at which different sections of the dam move relative to each other when subjected to external forces, such as seismic activity or changes in water pressure. Monitoring relative velocity is essential for assessing deformation rates and the risk of material fatigue over time.

Similarly, relative acceleration describes the rate of change in velocity between different points within the dam under dynamic loading conditions. This parameter plays a crucial role in detecting areas of abrupt movement or stress concentration, which can pinpoint locations prone to cracking or structural failure.

Stability of the dam in the first phase (empty dam)

In the initial state of analysis, the displacement remains consistently at zero (Fig. 9). With the dam empty, only its own weight exerts force on the foundation, resulting in negligible displacements and deformations.

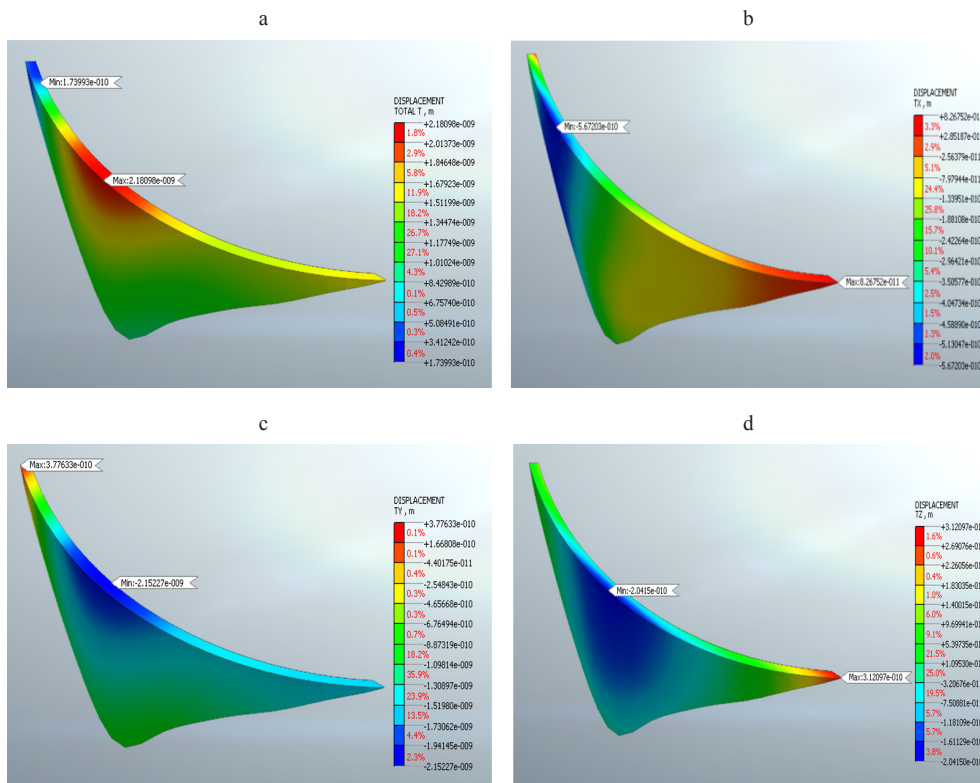


FIGURE 9. Displacements under self-weight effect: a – total displacements, b – radial displacement, c – tangential displacement, d – vertical displacement

Source: own work.

Stability of the dam in the second phase (filled dam)

Figure 10a illustrates the total displacement of the arch dam. Under static loading, the overall displacement of the dam arch is small. The maximum displacement of the dam is 0.015 m, located at the arch crest. In contrast,

the minimum displacement value is 0.0045 m, found at the base of the dam body. The maximum and minimum radial and tangential displacements of Tichy-Haf Dam are presented in Figures 10b and 10c, respectively. The radial and tangential displacements of the investigated arch of the Tichy-Haf Dam on the upstream section are smaller compared to those on the downstream face. The peak values of radial and tangential displacements at the crest were 0.0012 m and -0.0119 m, respectively. Figure 10d illustrates the vertical displacement values in the arch dam under static load. As depicted in Figure 10d, the maximum and minimum vertical displacement values are -0.0095 m and -0.0039 m, respectively. Additionally, this section assesses the capability of Midas GTS NX to simulate the static and dynamic behavior of an arch dam using the FEM. Table 4 compares the results of the static analysis with those from data monitoring (Tables 2 and 3). The findings from Midas GTS NX align with the monitoring data, confirming that the software delivers reliable and consistent results.

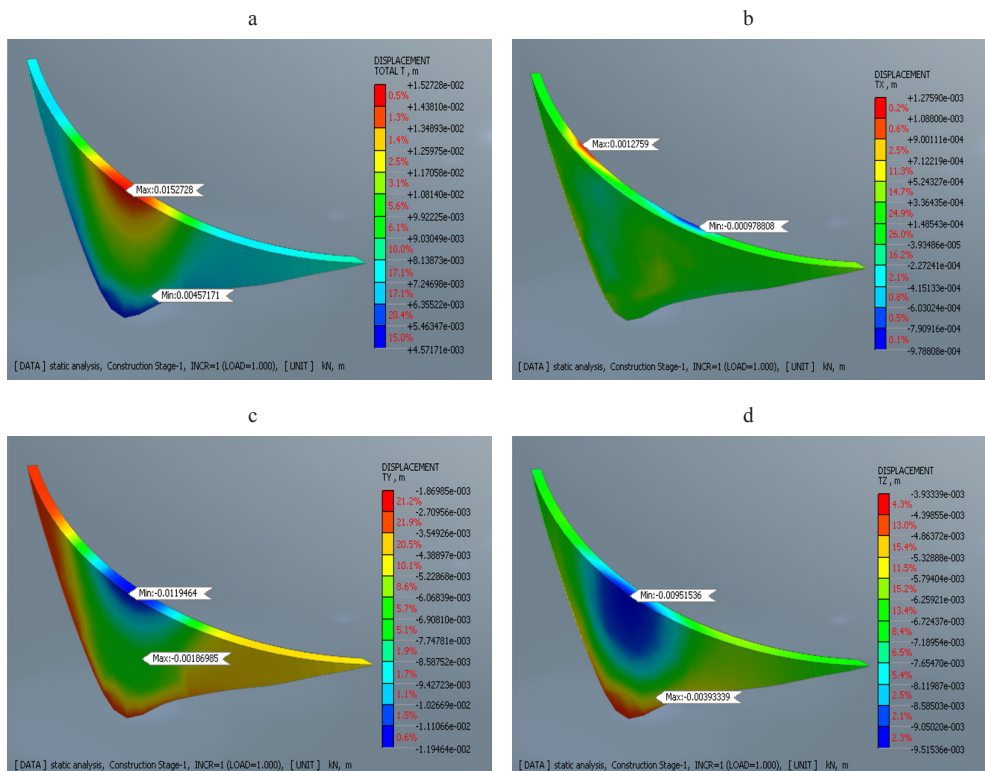


FIGURE 10. Displacements under static loads: a – total displacements, b – radial displacement, c – tangential displacement, d – vertical displacement

Source: own work.

TABLE 4. Summary of displacements calculated by the dam monitoring system and the calculation code

Value [m]	Dam monitoring			Midas GTS NX		
	radial displacement	tangential displacement	vertical displacement	radial displacement	tangential displacement	vertical displacement
Max	0.0045	-0.0070	0.0037	0.0012	-0.0119	-0.0059
Min	0	0	0	0.0009	-0.0018	-0.0039

Source: own work.

Stability of the dam in the final stage of analysis (under dynamic loading)

During this phase of the analysis, the model was subjected to four earthquakes with varying accelerations. Following the first earthquake, a maximum relative displacement of 0.0499 m was observed at the crest of the arch dam, whereas

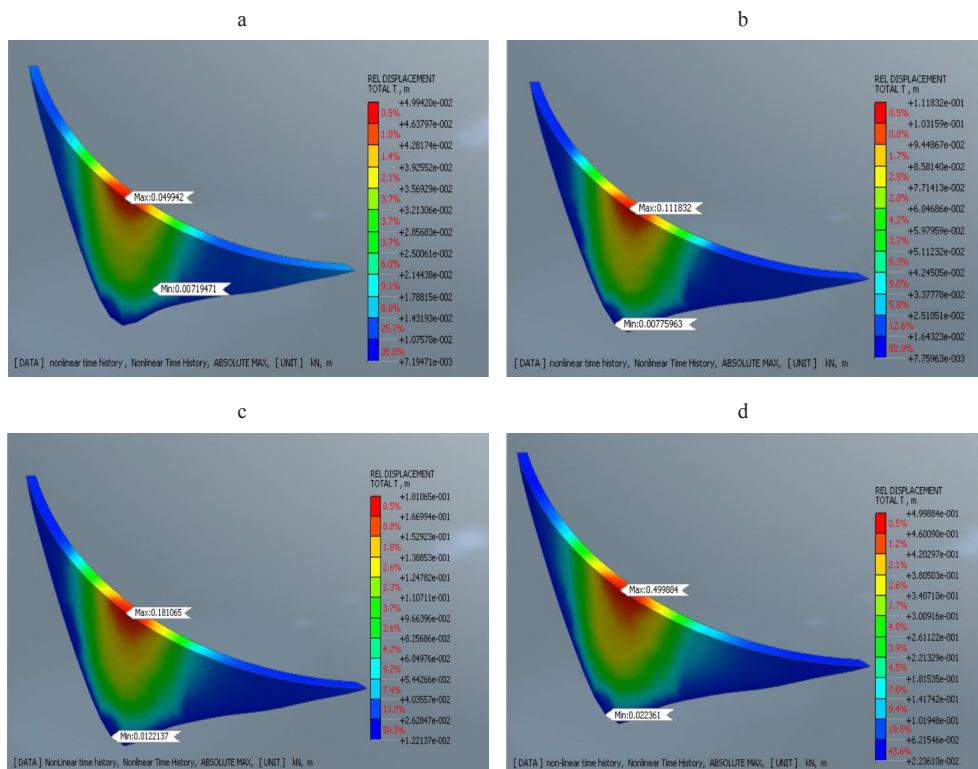


FIGURE 11. Relative displacements under dynamic loads: a – at the end of the first earthquake, b – at the end of the second earthquake, c – at the end of the third earthquake, d – at the end of the fourth earthquake

Source: own work.

the minimum relative displacement, measuring 0.0071 m, was observed at the foundation (Fig. 11a). The minimal relative displacement at the base of the dam can be attributed to the foundation being restrained in all three directions. Additionally, the interaction between the foundation and the dam serves as a significant energy dissipator. The dam modeling demonstrated that the maximum relative displacements are symmetrical with respect to the right and left banks. This behavior was consistently observed in the other models as well (Fig. 11b, 11c, 11d). Furthermore, it was noted that as the intensity of the earthquake increases, the relative displacement of the dam also increases.

Analysis of relative velocity under seismic loading

Figure 12 illustrates the relative velocity distribution across an arch of the investigated dam, the Tichy Haf dam, during a nonlinear time history analysis. The maximum relative velocity is $0.247 \text{ m}\cdot\text{s}^{-1}$, located at the crest of the arch dam (Fig. 12a). This high velocity indicates a significant dynamic response at the dam's uppermost section, which is expected due to the crest's higher exposure to seismic forces and its greater freedom of movement compared to the base. The minimum relative velocity is $0.143 \text{ m}\cdot\text{s}^{-1}$, situated near the base of the dam (Fig. 12a). This lower velocity can be attributed to the constraints imposed by the foundation. The foundation's restraints in all directions effectively reduce movement, resulting in lower relative velocities. The interaction between the dam and the foundation also dissipates energy, contributing to the minimal velocity observed. The gradient of the relative velocity from the base to the crest suggests that the dynamic response of the dam varies significantly along its height. This variation underscores the importance of considering the entire structure during a seismic analysis to understand how the different sections respond to dynamic loading. The velocity distribution appears to be symmetrical along the arch dam.

The same pattern is observed for the second earthquake, with maximum and minimum relative velocities of $0.259 \text{ m}\cdot\text{s}^{-1}$ and $0.142 \text{ m}\cdot\text{s}^{-1}$, respectively (Fig. 12b). The highest and lowest relative velocities during the third earthquake were $0.337 \text{ m}\cdot\text{s}^{-1}$ and $0.176 \text{ m}\cdot\text{s}^{-1}$, respectively (Fig. 12c). For the fourth earthquake, with an intensity of 0.44 g, the highest relative velocity observed was $0.762 \text{ m}\cdot\text{s}^{-1}$ at the crest of the arch dam, while the minimum relative velocity was $0.277 \text{ m}\cdot\text{s}^{-1}$ at the base of the arch dam (Fig. 12d).

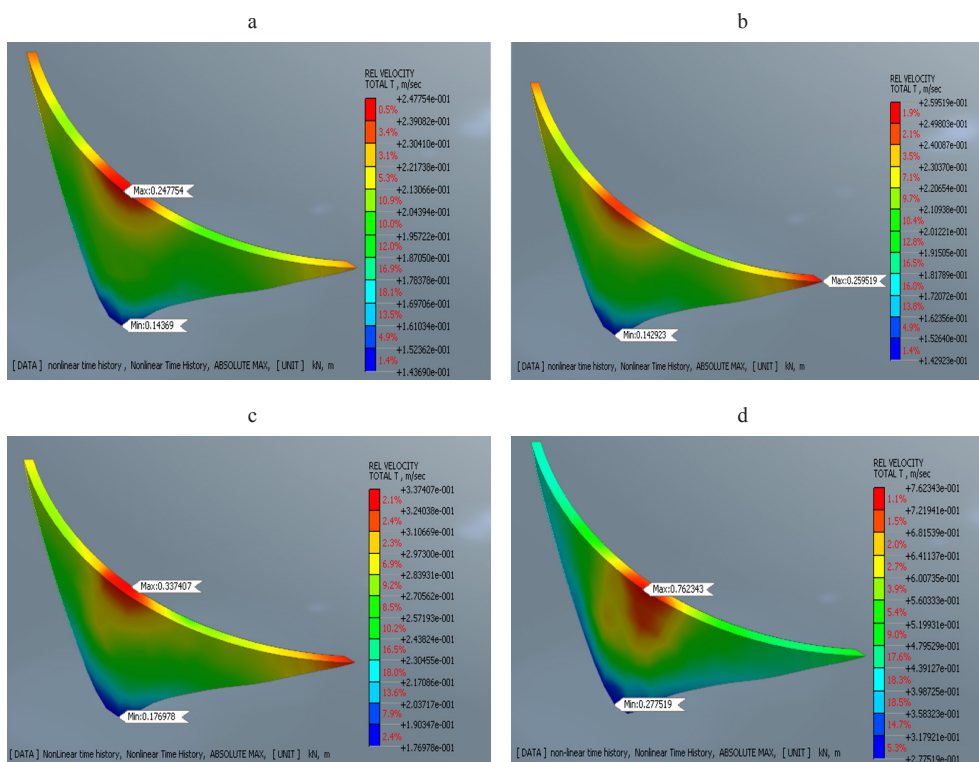


FIGURE 12. Relative velocity under dynamic loads: a – at the end of the first earthquake, b – at the end of the second earthquake, c – at the end of the third earthquake, d – at the end of the fourth earthquake Source: own work.

Analysis of relative acceleration under seismic loading

Figure 13 shows the relative acceleration distribution of the investigated arch of the Tichy-Haf Dam during an earthquake. The maximum relative acceleration is $9.77 \text{ m}\cdot\text{s}^{-2}$, located at the crest of the arch dam (Fig. 13a). This high acceleration indicates that the crest experiences the most significant dynamic response to seismic activity. Being the furthest point from the foundation, the crest is subjected to greater forces and movements during seismic events, leading to higher acceleration values. The minimum relative acceleration is $7.44 \text{ m}\cdot\text{s}^{-2}$, found near the base of the dam (Fig. 13a). This lower acceleration can be attributed to the constraints imposed by the foundation, which limit movement and therefore result in lower acceleration. The gradient of relative acceleration from the base

to the crest indicates a significant variation in the dynamic response along the height of the dam. The observed acceleration peaks (Figs 13b, 13c, 13d) for the second, third, and fourth earthquakes are $9.13 \text{ m}\cdot\text{s}^{-2}$, $10.53 \text{ m}\cdot\text{s}^{-2}$, and $12.84 \text{ m}\cdot\text{s}^{-2}$, respectively. In contrast, the minimum acceleration for this earthquake is $6.05 \text{ m}\cdot\text{s}^{-2}$, $8.25 \text{ m}\cdot\text{s}^{-2}$, and $9.72 \text{ m}\cdot\text{s}^{-2}$, respectively.

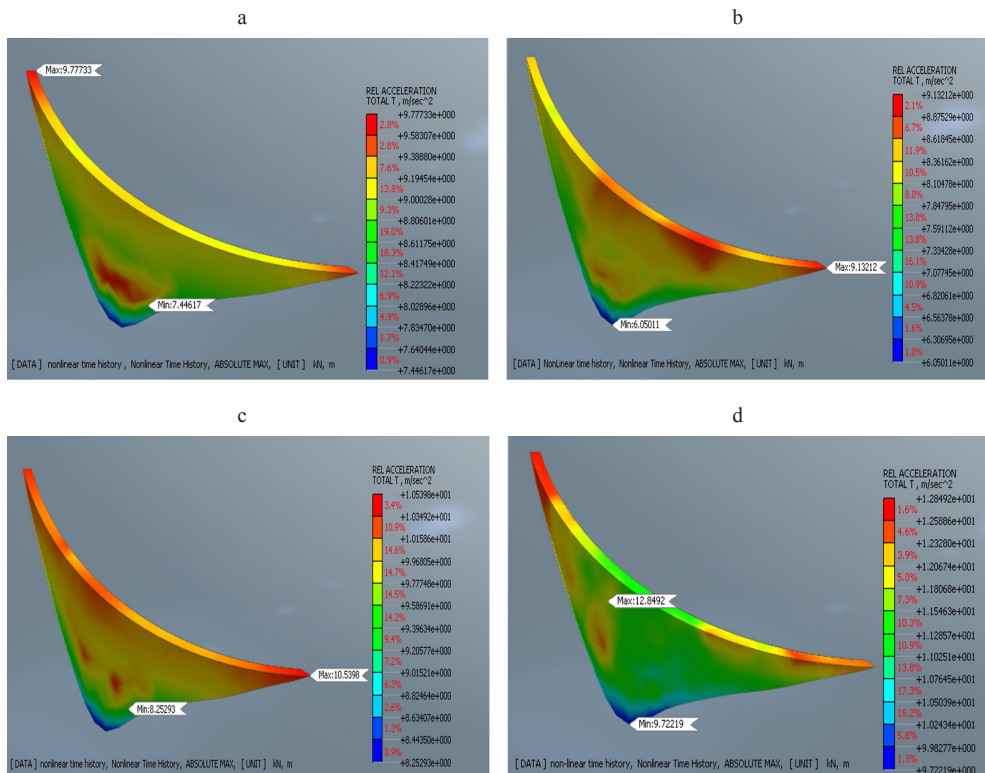


FIGURE 13. Relative acceleration under dynamic loads: a – at the end of the first earthquake, b – at the end of the second earthquake, c – at the end of the third earthquake, d – at the end of the fourth earthquake

Source: own work.

In this section of the study, we evaluated the stability of the dam by selecting four reference points for analysis (Fig. 14). These points are located on the crest, at the base of the arch dam, and on both the right and left banks.

Figure 15 depicts the displacement curves observed during the four earthquakes. The loads applied to the arch dam in its initial state consist of dead weight and water thrust. These loads, at this juncture, have caused minimal

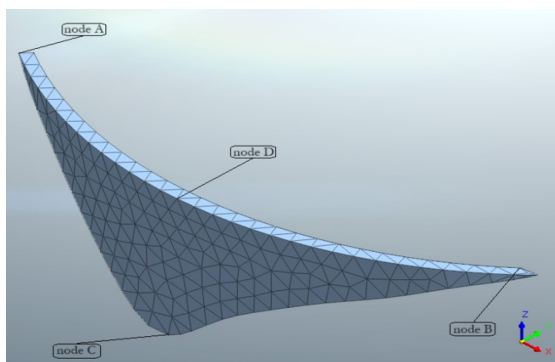


FIGURE 14. Reference points for the behavior dam analysis
Source: own work.

impact on the dam, resulting in only a slight displacement. The discrepancy in displacement among various nodes underscores the non-uniform distribution of dynamic loads within the structure. Nodes A and B experience moderate displacements, while Node D undergoes the most significant deformation, and Node C remains relatively unaffected. The maximum displacements recorded during

Earthquakes 1, 2, 3, and 4 were 0.048 m at 5 s, 0.106 m at 16 s, 0.18 m at 10 s, and 0.499 m at 15 s, respectively, with no further evolution until the conclusion of each earthquake.

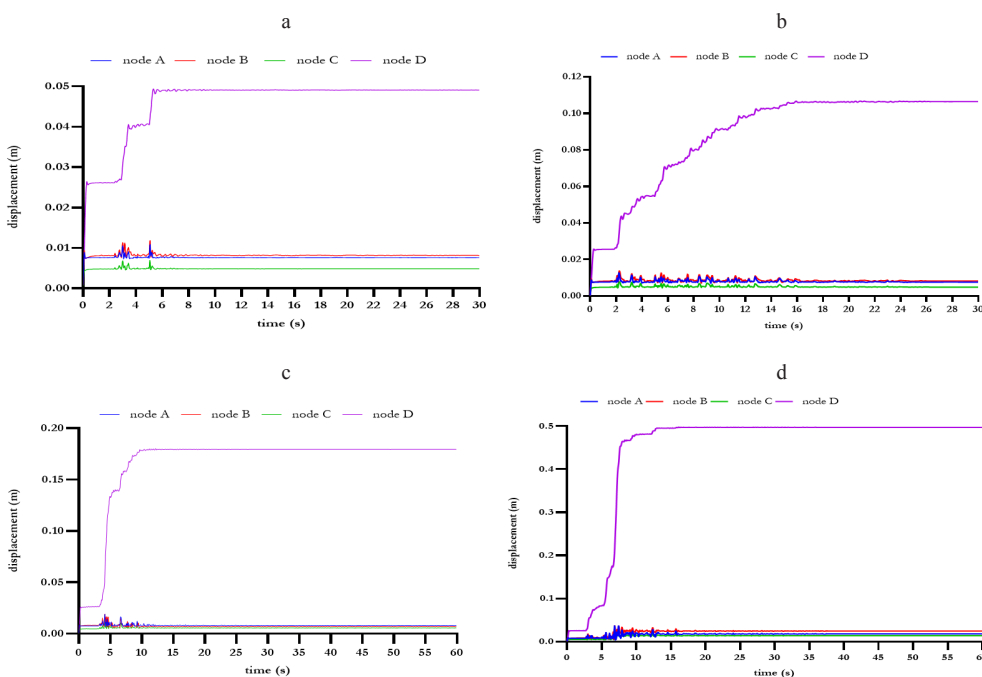


FIGURE 15. Displacement–time curve during the four earthquakes: a – first earthquake, b – second earthquake, c – third earthquake, d – fourth earthquake

Source: own work.

Conclusions

The current study numerically evaluates the seismic response of the investigated arch of the Tichy-Haf Dam, focusing on relative displacement, relative velocity, and relative acceleration. We developed the numerical model using Midas GTS NX, based on the FEM. In any seismic analysis, a single seismic load is insufficient to determine the general behavior of a structure. Therefore, to understand the behavior of the evaluated arch of the Tichy-Haf Dam, we used four earthquakes with varying intensities. The key conclusions are summarized further in the text.

The maximum relative displacement observed at the crest of the dam at the end of the fourth earthquake was 0.49 m. On the right and left banks, the relative displacement did not exceed 0.5% of the dam's height, indicating minimal impact in these areas due to the lesser influence of hydrostatic forces. In the foundation, the relative displacement did not exceed 0.5%, which is attributed to the significant role of the dam–foundation interaction in dissipating energy. The displacement–time response for the four nodes provides valuable insights into the structural behavior under seismic loading. Nodes with higher displacements (e.g., Node D) indicate regions that may require additional reinforcement to prevent structural failure. In contrast, nodes with minimal displacement (e.g., Node C) highlight stable areas with minimal dynamic impact. This analysis is essential for designing earthquake-resistant structures and ensuring safety and integrity during seismic events. The observed relative velocities and accelerations highlight critical areas where seismic forces have the most impact. The crest, with its maximum relative velocity, is a crucial area for structural reinforcement. The minimal movement at the base implies that the foundation design is effective in mitigating seismic energy transfer. Understanding these dynamics is essential for designing retrofitting measures or improving future dam designs to enhance seismic resilience. By addressing the areas with the highest dynamic response, engineers can ensure the overall stability and safety of the dam during earthquake events. To validate the model, we compared the results obtained under a static load with the monitoring data. The values are close, confirming the effectiveness of the program in numerical modeling the Tichy-Haf Dam. Finally, numerical simulations provide a reliable and practical way to evaluate the behavior of arch dams under seismic loads. The findings of this study can assist engineers in making informed decisions about the design and construction of such dams.

References

- Adjadj, M., Aliouche, Y., & Meksaouine, M. (2021). Three-dimensional non-linear analysis based on the temporal evolution of an RCC dam including the alluvium effect. *GeoScience Engineering*, 67(1), 11–20. <https://doi.org/10.35180/gse-2021-0047>
- Autodesk (2008). Land Surveyor 2.1.
- Autodesk (2024). AutoCAD.
- Bayraktar, A., Sevim, B., & Can Altunişik, A. (2011). Finite element model updating effects on nonlinear seismic response of arch dam reservoir foundation systems. *Finite Elements in Analysis and Design*, 47(2), 85–97. <https://doi.org/10.1016/j.finel.2010.09.005>
- Chopra, A. K. (2012). Earthquake analysis of arch dams: Factors to be considered. *Journal of Structural Engineering*, 138(2), 205–214. [https://doi.org/10.1061/\(ASCE\)ST.1943-541X.0000431](https://doi.org/10.1061/(ASCE)ST.1943-541X.0000431)
- Das, S. K., Mandal, K. K., & Niyogi, A. G. (2023). Finite element-based direct coupling approach for dynamic analysis of dam–reservoir system. *Innovative Infrastructure Solutions*, 8(44), 1–15. <https://doi.org/10.1007/s41062-022-01013-5>
- Ebrahimian, B. (2011). Numerical analysis of nonlinear dynamic behavior of earth dams. *Frontiers of Architecture and Civil Engineering in China*, 5(1), 24–40. <https://doi.org/10.1007/s11709-010-0082-6>
- Enzell, J., Ulfberg, A., Sas, G., & Malm, R. (2021). Post-peak behavior of concrete dams based on nonlinear finite element analyses. *Engineering Failure Analysis*, 130, 105778. <https://doi.org/10.1016/j.engfailanal.2021.105778>
- Haghani, M., Neyra, B. N., Ahmadi, M. T., & Amiri, J. V. (2022). A new numerical approach in the seismic failure analysis of concrete gravity dams using extended finite element method. *Engineering Failure Analysis*, 132, 105835. <https://doi.org/10.1016/j.engfailanal.2021.105835>
- He, Q., Gu, C., Valente, S., Zhao, E., Liu, X., & Yuan, D. (2022). Multi-arch dam safety evaluation based on statistical analysis and numerical simulation. *Scientific Reports*, 12(1), 1–19. <https://doi.org/10.1038/s41598-022-13073-9>
- Liang, C., Chen, J., Xu, Q., & Li, J. (2023). Evaluation of nonlinear response biases of arch dams due to amplitude scaling via three-component record selection based on conditional spectra. *Engineering Structures*, 287, 116169. <https://doi.org/10.1016/j.engstruct.2023.116169>
- Li, Z. Y., Hu, Z. Q., Lin, G., & Li, J. B. (2022). A scaled boundary finite element method procedure for arch dam-water-foundation rock interaction in complex layered half-space. *Computers and Geotechnics*, 141, 104524. <https://doi.org/10.1016/j.compgeo.2021.104524>
- Li, Y., Zhao, E., Zhang, J., Shao, C., & Li, Z. (2024). Hybrid reliability evaluation of arch dam during long-term service with multi-dimensional parallelepiped convex model. *Engineering Failure Analysis*, 157, 107937. <https://doi.org/10.1016/j.engfailanal.2023.107937>
- Lyu, W., Zhang, L., Yang, B., & Chen, Y. (2021). Analysis of stability of the Baihetan arch dam based on the comprehensive method. *Bulletin of Engineering Geology and the Environment*, 80, 1219–1232. <https://doi.org/10.1007/s10064-020-02009-0>

- Majidi, N., Riahi, H. T., Zandi, S. M., & Hajirasouliha, I. (2023). Development of practical down-sampling methods for nonlinear time history analysis of complex structures. *Soil Dynamics and Earthquake Engineering*, 175, 108247. <https://doi.org/10.1016/j.soildyn.2023.108247>
- Midas (2025). Midas GTS-NX. Midas.
- Ningthoukhongjam, S. S., & Singh, K. D. (2021). Analysis of mid-rise moment resisting steel frames by Nonlinear Time History Analysis using Force Analogy Method. *Journal of The Institution of Engineers (India): Series A*, 102, 901–918. <https://doi.org/10.1007/s40030-021-00577-2>
- Roësset, J. M. (2007). Review of dynamics of structures: theory and applications to earthquake engineering, Third Edition, by Anil K. Chopra. *Journal of Structural Engineering*, 133(5), 752–752. [https://doi.org/10.1061/\(asce\)0733-9445\(2007\)133:5\(752\)](https://doi.org/10.1061/(asce)0733-9445(2007)133:5(752))
- Sarkar, A., Ghodke, S., & Bagchi, A. (2024). Performance of 2D-spectral finite element method in dynamic analysis of concrete gravity dams. *Structures*, 59, 105770. <https://doi.org/10.1016/j.istruc.2023.105770>
- Saxena, S., & Patel, M. (2023). Evaluating dynamic behaviour of a concrete dam using modal analysis. *Materials Today: Proceedings*, 93(P3), 296–301. <https://doi.org/10.1016/j.matpr.2023.07.259>
- Sharma, A., & Nallasivam, K. (2023). Static analysis of a concrete gravity dam using the finite element technique. *Asian Journal of Civil Engineering*, 24, 2939–2957. <https://doi.org/10.1007/s42107-023-00686-2>
- Shen, Y. (2022). Stability analysis of high slope based on MIDAS GTS digital simulation. In *2022 World Automation Congress Proceedings* (pp. 575–580). IEEE. <https://doi.org/10.23919/WAC55640.2022.9934489>
- Suryadi, A., Wijaya, H., & Yuwono, A. (2023). Nonlinear Time History Pada Fondasi Tiang Pancang Dengan Program Midas Gts Nx. *JMTS: Jurnal Mitra Teknik Sipil*, 6(2), 383–392. <https://doi.org/10.24912/jmts.v6i2.21674>
- System (1989). *New eXperience of analysis*. System.
- Varghese, B., Saju, A., & John, S. (2014). Finite element analysis of arch dam. *International Journal of Research in Engineering and Technology*, 03(07), 180–193. <https://doi.org/10.15623/ijret.2014.0307032>
- Yu, X., Zhou, Y. F., & Peng, S. Z. (2005). Stability analyses of dam abutments by 3D elasto-plastic finite-element method: A case study of Houhe gravity-arch dam in China. *International Journal of Rock Mechanics and Mining Sciences*, 42(3), 415–430. <https://doi.org/10.1016/j.ijrmms.2005.01.001>
- Zewdu, A. (2020). Modeling the slope of embankment dam during static and dynamic stability analysis: a case study of Koga dam, Ethiopia. *Modeling Earth Systems and Environment*, 6, 1963–1979. <https://doi.org/10.1007/s40808-020-00832-8>
- Zhang, M. Z., Wang, X. C., Liu, Y. L., Wang, J. T., Yi, K., Yan, J. H., & Chen, H. J. (2024). Effect of attached outlets on the dynamic response of arch dams. *Engineering Structures*, 302, 117392. <https://doi.org/10.1016/j.engstruct.2023.117392>

Summary

Evaluation of numerical modeling for the seismic response of an arch dam: the case of the Tichy-Haf Dam. The seismic stability of concrete arch dams has always been a key parameter in seismic safety evaluation. For this purpose, this paper presents a numerical analysis of the seismic response of an arch of the Tichy-Haf Dam using the Midas GTS NX software. The study employs the finite element method and a nonlinear time history analysis to evaluate the stability of the structure. Several reference nodes on the dam body were selected to assess displacement, velocity, and acceleration during seismic events. To determine the values of these parameters, nonlinear time-history analyses were conducted using four accelerograms with amplitudes of 0.25 g, 0.32 g, 0.36 g, and 0.44 g, respectively. The dynamic numerical analysis revealed that the dam performed well during the seismic events, maintaining its structural integrity. The numerical model was validated by comparing the results from the static analysis with the actual monitoring data from the dam. This comparison demonstrated the effectiveness of the numerical simulation method in analyzing the stability of the arch dam.

Tetiana TKACHENKO¹✉ 

Anna LIS² 

Yurii TSIURIUPA¹ 

Viktor MILEIKOVSKYI¹ 

Adam UJMA³ 

Oleksii TKACHENKO⁴ 

Viktoriiia SAKHNOVSKA¹ 

¹ Kyiv National University of Construction and Architecture, Faculty of Engineering Systems and Ecology, Ukraine

² Czestochowa University of Technology, Building Faculty, Poland

³ University of Applied Sciences in Nysa, Faculty of Technical Sciences, Poland

⁴ Kyiv National University of Construction and Architecture, Faculty of Architecture, Ukraine

Planning of green roofs for the best thermotechnical effect

Keywords: green roof, heat gains, solar radiation

Introduction

The energy-efficient provision of indoor comfort for buildings is one of the most important requirements for modern construction. It can be achieved in two main ways: energy-efficient engineering systems and using natural measures such as the greening of buildings.

The last group of measures provides more opportunities. The experience in using these measures is significant, starting from sod roofs, invented in prehistory

(Berg, 1989). Despite this, the most limiting factor is the lack of systematic research on the positive effects.

Most of the energy-efficient engineering solutions consist of the optimally orientating buildings (Zhelykh et al., 2020), increasing the air-tightness (Corcoran & Duffy, 2019; Kuhnhenne et al., 2020) and the thermal resistance (Brunoro, 2024; Štastný et al., 2024) of the building envelopment; effective heating systems (Cholewa et al., 2018; Voznyak et al., 2021), etc.; optimizing ventilation strategies (Gładyszewska-Fiedoruk et al., 2019; Brunoro, 2024); effective inlet air treatment (Alsayah et al., 2024; Bari et al., 2024); optimizing air exchange organization (Voznyak et al., 2019; Voznyak et al., 2022); optimizing air volume control (Kim & Cho, 2022; Nassif, 2022); solar radiation protection (Muñoz-Viveros, 2022); and using renewable energy (Zhelykh et al., 2016; Shapoval et al., 2019a; Shapoval et al., 2019b; Shapoval et al., 2021; Venhryn et al., 2021; Voznyak et al., 2023). These measures are single-task solutions, which can only decrease the energy demands.

In contrast, increasing amounts of research is being devoted to all-in-one measures, such as green structures as a combination of living plants and building structures. They are solving different tasks simultaneously, including decreasing energy demands (Gioannini et al., 2018; Rey et al., 2020) and mitigating the urban heat island effect (Fallmann et al., 2014; Luthfiyyah & Widjajanti, 2019), heat insulation, and cooling effect through evaporative cooling caused by evapotranspiration; increasing the roof durability (Gioannini et al., 2018); cleaning pollution from the air (Chen et al., 2020); oxygenating the air by photosynthesis (Zhang et al., 2021); suppressing noise (Gioannini et al., 2018); effectively managing and treating rainwater (Chen et al., 2018; Zeng et al., 2019); supporting biodiversity, including pollinators (Gill et al., 2020); creating a close-to-natural aesthetic (Gioannini et al., 2018) environment, which provides mental health, calming (Nwankwo et al., 2022), eco-regulation and passive rehabilitation; inducing passive environmental education (Gioannini et al., 2018); and increasing the areas for recreation and business, including urban agriculture (Qiu et al., 2013).

Most of the works above are more qualitative than quantitative. Some of them are case studies, and the results cannot be applied broadly in most cases. Thus, optimizing such green structures is a problem requiring additional research.

In contrast to the above-mentioned works, there is a complex of multidisciplinary, quantitative and qualitative, laboratory and field research on the thermotechnical properties of grass layers revealing a significant cooling effect up

to 4 K (Tkachenko & Mileikovskiy, 2018a; Tkachenko & Mileikovskiy, 2020a); solar protection (Tkachenko & Mileikovskiy, 2018b; Tkachenko & Mileikovskiy, 2020b); rainwater management (Hlushchenko et al., 2022; Tkachenko et al., 2023b; Kravchenko et al., 2024; Tkachenko et al., 2024a); rainwater cleaning (Kravchenko et al., 2024); carbon dioxide sequestration (Tkachenko et al., 2019; Tkachenko & Mileikovskiy, 2022); air cleaning (Tkachenko et al., 2019); reparation of historical places with out-of-context building (Tkachenko et al., 2024); and biodiversity (Tkachenko et al., 2023a).

Extensive green roofs that do not provide access for people usually cover the roof surface with grass and small shrubs, providing thermotechnical effects to the whole roof surface. Semi-intensive green roofs have paths for the people, which are usually covered by some pavement, which absorbs solar radiation and converts it to heat. If the roof is combined with the ceiling, the heat will pass to it and load the air-conditioning systems. The proposed solution for such roofs is to build these paths over the auxiliary premises, such as corridors, storage rooms, wardrobes, etc., which have low microclimate requirements.

This recommendation has been proposed without calculations based only on the presence of the effect. Thus, this should also be checked.

The work aims to estimate the heat distribution in green roofs with paths to ground the recommendations for planning green roofs for the maximum thermotechnical effect. The research object is green roofs combined with ceilings as the effective biotechnology of joining the building structures and living plants. The research subject is the heat transfer process inside green roofs combined with the ceiling.

Material and methods

To show the specifics of the heat transfer, we built a 3D model of a semi-intensive green roof fragment combined with a ceiling of a room, coated at the top by the ZinCo Perennial Garden system (ZinCo USA, Inc., n.d. a) and a ZinCo Hard Landscape system (ZinCo USA, Inc., n.d. b) path (Fig. 1, Table 1). We ignore very thin layers, such as the root barrier and the system filter, which cannot influence the heat transfer. The thermotechnical properties of most of the layers have not yet been researched. Thus, we will apply analogical materials according to Table 1.

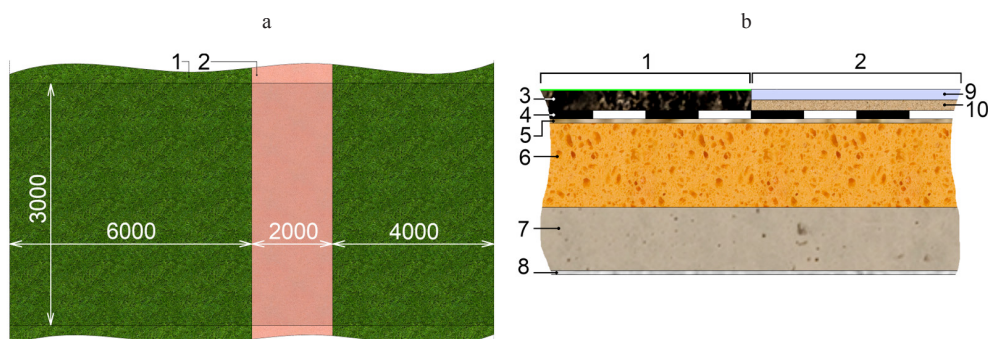


FIGURE 1. A semi-intensive green roof: a – top view, b – section; 1 – green part, 2 – path, 3 – substratum, 4 – drainage, 5 – protection layer, 6 – insulation, 7 – slab, 8 – plaster, 9 – pavement, 10 – bedding (see Table 1); the computational domain in Figure 1a is darkened

Source: own work.

Paths on green roofs are the heat-conductive inclusions. Such nodes cannot be analytically calculated. They should be simulated using the Fourier–Kirchhoff equation (Hojny et al., 2023). The simulation is performed using the finite element method:

$$\frac{c\rho\partial\theta}{\partial t} = \nabla^T (\lambda\nabla\theta) \Phi_V \text{ [W]}, \quad (1)$$

where: c – specific heat [$\text{J}\cdot\text{kg}^{-1}\cdot\text{K}^{-1}$], ρ – density [$\text{kg}\cdot\text{m}^{-3}$], θ – temperature [K], t – time [s], a – thermal diffusivity [$\text{m}^2\cdot\text{s}^{-1}$], ∇^T – thermal gradient, Φ_V – power of internal heat sources per volume [$\text{W}\cdot\text{m}^{-3}$].

TABLE 1. Layers

Position in Fig. 1	Layer	Material or analogue	Density (ρ) [$\text{kg}\cdot\text{m}^{-3}$]	Specific heat (c) [$\text{J}\cdot\text{kg}^{-1}\cdot\text{K}^{-1}$]	Thermal conductance (λ) [$\text{W}\cdot\text{m}^{-1}\cdot\text{K}^{-1}$]	Thickness (δ) [mm]
3	substratum	claydite ^a	300	972	0.13	100
4	drainage	polycarbonate 40 ^a	102.5	1 010	0.072	40
5	protection	synthetic carpet ^a	160	2 500	0.06	20
6	insulation	polystyrene	1 050	1 800	0.14	400
7	slab	cast concrete	2 000	1 000	1.13	300
8	plaster	lightweight plaster	600	1 000	0.16	20
9	pavement	cast concrete ^a	2 000	1 000	1.13	50
10	bedding	gravel ^a	1 840	840	0.36	50

^aAnalogue.

Source: own work based on Farenjuk et al. (2014); ZinCo USA, Inc. (n.d. a); ZinCo USA, Inc. (n.d. b).

The precision of Equation (1) corresponds to the precision of the thermophysical properties of the materials and boundary conditions. The main assumptions and boundary conditions are the following. There is no contact thermal resistance between materials. Air conditioning in the room below the roof maintains constant temperature θ_{IDA} equal to 298.15 K. The ceiling surface transfers heat with constant heat transfer coefficient α equal to $8.7 \text{ W}\cdot\text{m}^{-1}\cdot\text{K}^{-1}$ (Hojny et al., 2023):

$$\Phi_A = \alpha(\theta_{\text{ceil}} - \theta_{IDA}) [\text{W}\cdot\text{m}^{-2}], \quad (2)$$

where: Φ_A – thermal flow density from the ceiling to the indoor air [$\text{W}\cdot\text{m}^{-2}$], α – heat transfer coefficient [$\text{W}\cdot\text{m}^{-1}\cdot\text{K}^{-1}$], θ_{ceil} – ceiling surface temperature [K], and θ_{IDA} – indoor air temperature [K].

The path surface absorbs the convective heat (or transfers if negative) with constant heat transfer coefficient α equal to $23 \text{ W}\cdot\text{m}^{-1}\cdot\text{K}^{-1}$ (Hojny et al., 2023):

$$\Phi_A = \alpha(\theta_{ODA} - \theta_{\text{path}}) [\text{W}\cdot\text{m}^{-2}], \quad (3)$$

where: θ_{ODA} – outdoor temperature [K], and θ_{path} – path surface temperature [K].

The path surface also absorbs solar radiation with a constant absorbance of 0.5. The solar radiation is calculated for the corresponding date and time moment. The surface under the grass has a temperature (Tkachenko & Mileikovskiy, 2020a):

$$\theta_{\text{grass}} = \theta_{ODA} - \Delta\theta [\text{K}], \quad (4)$$

where: θ_{grass} – surface temperature under the grass [K], and $\Delta\theta$ – cooling effect of the grass;

$$\Delta\theta = (0.508 \operatorname{atan}(v) + 0.543) \operatorname{atan}^2(v) + 0.752 [\text{K}], \quad (5)$$

where: v – wind speed [$\text{m}\cdot\text{s}^{-1}$];

The regime of the heat conduction is quasi-periodical: the outdoor temperature change during each day is to be assumed as the same by repeating the weather data of a representative day until the temperature field change on the ceiling on the final day repeats the previous one with a maximum deviation less than 0.2 K.

The sun's movement will produce a temperature change on the outer surface of the paths, causing a thermal wave. It will attenuate in the structure's layers due to thermal inertia and cause some heat trace on the ceiling below.

Results and discussion

The simulation results were performed for two days: a warm day on July 11, 2024, and August 11, 2024, with moderate temperatures (Fig. 2). On both days, the path gives a trace of higher heat transfer on the ceiling (Fig. 3). Due to the thermal capacity of the concrete slab, the trace does not change from night to day.

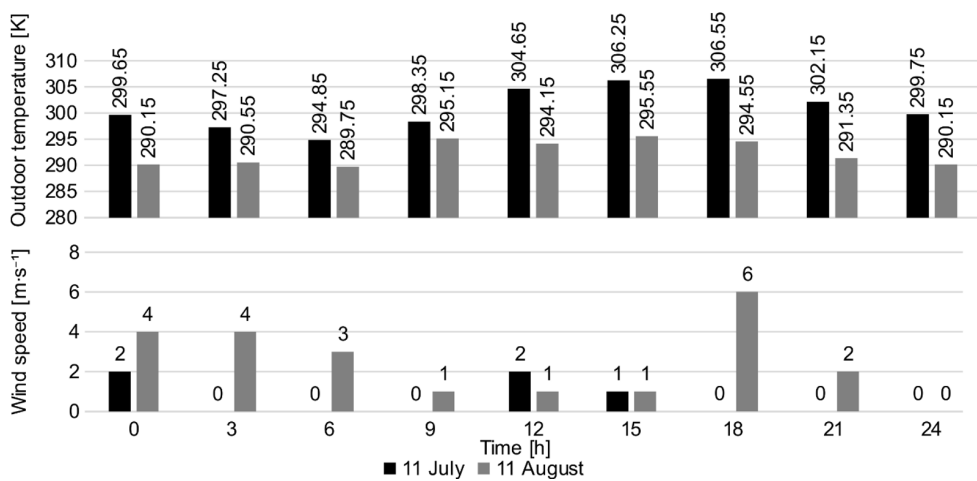


FIGURE 2. Weather conditions

Source: own work.

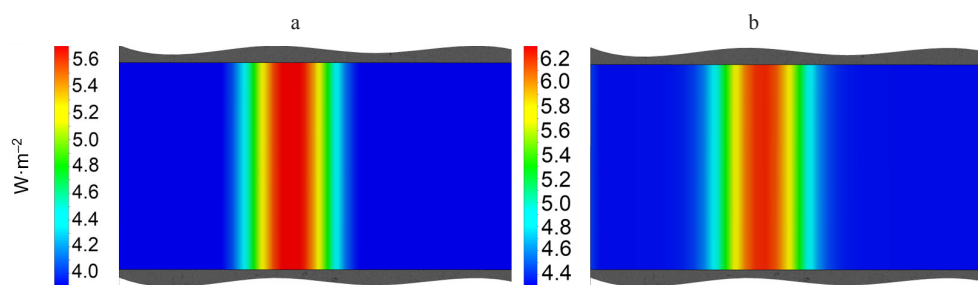


FIGURE 3. Results of simulation of heat flow density across the whole day: a – with a moderate temperature (August 11, 2024); b – warm (July 11, 2024)

Source: own work.

The heat transfer difference is $2 W \cdot m^{-2}$ for the warm day and $1.8 W \cdot m^{-2}$ for the moderate temperatures. This value is not very big, but is significant. For a living room of $6 \times 3 m$, the heat gain is 32–36 W, which is comparable

to LED illumination (up to 32 W). Thus, avoiding these unnecessary heat gains should improve the energy efficiency of air-conditioning.

Let us consider the recommendation to align, if possible, the traditional paths with the auxiliary premises such as corridors or pantries. If these rooms have no external walls, the heat gained will be distributed to other air-conditioned rooms with some lag due to thermal inertia. If this lag continues after the end of the hot period, some energy demand decrease will appear. But in a steady state, it will be minimal.

For auxiliary rooms with external walls, some heat will be dissipated. If the additional heat gains $\Delta\Phi$ [W] appears, the temperature of the auxiliary room will slightly rise by $\Delta\theta$ [K]. If the hot period is long enough to achieve near-to-steady heat transfer, this heat will be distributed to other rooms and the environment through indoor and outdoor enclosures with a U -factor of U_i [$\text{W}\cdot\text{m}^{-1}\cdot\text{K}^{-1}$] and area A_i [m^2]. The portion and total will be, respectively:

$$\Delta\Phi_i = U_i A_i \Delta\theta \text{ [W]}; \quad (6)$$

$$\Sigma\Delta\Phi_i = \Delta\Phi \text{ [W]}. \quad (7)$$

From Equations (6) and (7):

$$\Delta\Phi_i = \frac{\Delta\Phi U_i A_i}{\sum(U_i A_i)} \text{ [W]}. \quad (8)$$

Thus, in steady-state mode, the dissipated part of the heat gain through external wall number i equals 0:

$$\frac{\Delta\Phi_0}{\Delta\Phi} = \frac{U_0 A_0}{\sum(U_i A_i)} \text{ [W]}. \quad (9)$$

In energy-efficient buildings, $U_0 \ll U_j, j \neq 0$, and in most buildings, $A_0 < \Sigma A_i$. Thus, most heat will be kept in the building and will load the air conditioning. For example, a corridor of size $1.2 \times 3 \times 3$ m with one external wall 1.2×3 m with a U -factor of $0.2 \text{ W}\cdot\text{m}^{-1}\cdot\text{K}^{-1}$ and internal walls with a U -factor of $2.7 \text{ W}\cdot\text{m}^{-1}\cdot\text{K}^{-1}$ in a steady state will dissipate to the environment only 0.92% of the additional gains.

It is possible to conclude that aligning the roof paths half-measure, which can mitigate the additional consumption by thermal inertia. We should therefore find stronger measures.

There are alternative options, which can produce the maximum effect based on planting the paths: using plant-permit pavement analogous to eco-parking, makes it possible to plant on pathways, or barefoot-in-dew systems such as ZinCo Soft Landscape with a denser substrate. Walking on lawns is a common European trend, which promotes more natural conditions close to the wild nature. In addition to the thermotechnical effect of covering all surfaces with cooling plants, it soothes and supports rest, and the rainwater drainage and retention abilities will increase through activation of the whole area. For green roofs with a lightweight substratum, the “virtual” paths with a denser substratum should be definitively highlighted by a noticeable difference in the appearance of the grass.

In both cases, a special grass should be planted for walking: perennial ryegrass (*Lolium perenne*), red fescue (*Festuca rubra*), meadow fescue (*Lolium pratense*), bluegrass (*Poa pratensis*), or clovers (*Trifolium* sp.). We did not see such innovative “green path” solutions on available green roofs.

Another possibility is using pavements with maximum reflectivity (cool roof). This solution has a disadvantage: it requires regular cleaning because dust and dirt, which are common on paths, absorb solar radiation.

Conclusions

The literature review shows that there is not enough research on the positive effects of green roofs to make recommendations for aligning green roof design and space-planning solutions. The simulation of a semi-intensive green roof with the ceiling of the room below combined with a roof path shows that the path induces a trace of higher heat transfer on the ceiling. The difference in the density of the heat flow below the path and the grass is not huge but is still significant, as it varies in the range of 1.8–2.0 W·m⁻². Calculations show that such alignment of the paths above the auxiliary premises is a half-measure that operates almost due to inertia and lags in heat flows. Better solutions, which are innovative for green roofs, allow planting on the paths – from plant-permit pavement analogous to eco-parking and barefoot-in-dew systems such as ZinCo Soft Landscape with a denser substrate. It is necessary to use grass that can be walked on – perennial ryegrass (*Lolium perenne*), red fescue (*Festuca rubra*), meadow fescue

(*Festuca pratensis*, *Lolium pratense*), bluegrass (*Poa pratensis*), or clovers (*Trifolium* sp.). In the future, the authors plan to simulate the influence of joints and other linear and point inclusions on the thermal performance.

Acknowledgements

This work was performed within the framework of the grant program of Erasmus Plus “Multilevel Local, Nation- and Regionwide Education and Training in Climate Services, Climate Change Adaptation and Mitigation – ClimEd,” 619285-EPP-1-2020-1-FI-EPPKA2-CBHE-JP, 15.11.2020 – 14.05.2025.

References

- Alsayah, A. M., Faraj, J. J., & Eidan, A. A. (2024). A review of recent studies of both heat pipe and evaporative cooling in passive heat recovery. *Open Engineering*, 14(1), 1–18. <https://doi.org/10.1515/eng-2024-0012>
- Bari, M. A., Münsch, M., Schöneberger, B., Schlagbauer, B., Tiu, A. A., & Wierschem, A. (2024). Heat recovery optimization of a shell and tube bundle heat exchanger with continuous helical baffles for air ventilation systems. *International Journal of Air-Conditioning and Refrigeration*, 32(2), 1–16. <https://doi.org/10.1007/s44189-023-00046-4>
- Berg, A. (1989). *Norske tømmerhus frå mellomalderen*. Vol. 1. Landbruksforlaget.
- Brunoro, S. (2024). Passive envelope measures for improving energy efficiency in the energy retrofit of buildings in Italy. *Buildings*, 14(7), 2128. <https://doi.org/10.3390/buildings1407212>
- Chen, H., Ma, J., Wang, X., Xu, P., Zheng, S., & Zhao, Y. (2018). Effects of biochar and sludge on carbon storage of urban green roofs. *Forests*, 9(7), 413. <https://doi.org/10.3390/f9070413>
- Chen, Y., Zheng, B., & Hu, Y. (2020). Numerical simulation of local climate zone cooling achieved through modification of trees, albedo and green roofs – a case study of Changsha, China. *Sustainability*, 12(7), 2752. <https://doi.org/10.3390/su12072752>
- Cholewa, T., Balen, I., & Siuta-Olcha, A. (2018). On the influence of local and zonal hydraulic balancing of heating system on energy savings in existing buildings – Long term experimental research. *Energy and Buildings*, 179, 156–164. <https://doi.org/10.1016/j.enbuild.2018.09.009>
- Corcoran, L., & Duffy, A. (2019). Experimental field-trial design to investigate the effects of a defective internal vapour layer on timber frame wall constructions including initial findings. *MATEC Web of Conferences*, 282, 02047. <https://doi.org/10.1051/mateconf/201928202047>
- Fallmann, J., Emeis, S., & Suppan, P. (2014). Mitigation of urban heat stress – a modelling case study for the area of Stuttgart. *Journal of the Geographical Society of Berlin*, 144(3–4), 202–216. <https://doi.org/10.12854/erde-144-15>

- Fareniuk, H., Kolesnyk, E., Fareniuk, Ye., Pavliuk, P., Bilous, O., Prishchenko, A., & Tymofeiev, M. (2014). *Methods for choosing of insulation material for insulation of buildings* (DSTUB V.2.6-189:2013). Minrehion Ukrainy. <https://eurobud.ua/wp-content/uploads/2022/08/dstu-b-v.2.6-189-2013-metody-vyboru-teploizolyacziynogo-materialu-dlya-uteplennya-budivel.pdf>
- Gill, A. S., Purnell, K., Palmer, M. I., Stein, J., & McGuire, K. L. (2020). Microbial composition and functional diversity differ across urban green infrastructure types. *Frontiers in Microbiology*, 11, 912. <https://doi.org/10.3389/fmicb.2020.00912>
- Gioannini, R., Al-Ajlouni, M., Kile, R., VanLeeuwen, D., & St. Hilaire, R. (2018). Plant communities suitable for green roofs in arid regions. *Sustainability*, 10(6), 1755. <https://doi.org/10.3390/su10061755>
- Gładyszewska-Fiedoruk, K., Zhelykh, V., & Pushchinskyi, A. (2019). Simulation and analysis of various ventilation systems given in an example in the same school of indoor air quality. *Energies*, 12(15), 2845. <https://doi.org/10.3390/en12152845>
- Hlushchenko, R., Tkachenko, T., Mileikovskiy, V., Kravets, V., & Tkachenko, O. (2022). “Green structures” for effective rainwater management on roads. *Production Engineering Archives*, 28(4), 295–299. <https://doi.org/10.30657/pea.2022.28.37>
- Hojny, M., Głowacki, M., Bała, P., Bednarczyk, W., & Zalecki, W. (2023). Multiscale model of heating-remelting-cooling in the Gleeble 3800 thermo-mechanical simulator system. *Archives of Metallurgy and Materials*, 64(1), 401–412. <https://doi.org/10.24425/amm.2019.126266>
- Kim, H., & Cho, Y. (2022). Optimization of supply air flow and temperature for VAV terminal unit by artificial neural network. *Case Studies in Thermal Engineering*, 40, 102511. <https://doi.org/10.1016/j.csite.2022.102511>
- Kravchenko, M., Trach, Y., Trach, R., Tkachenko, T., & Mileikovskiy, V. (2024). Improving the efficiency and environmental friendliness of urban stormwater management by enhancing the water filtration model in rain gardens. *Water*, 16(10), 1316. <https://doi.org/10.3390/w16101316>
- Kuhnhenne, M., Reger, V., Pyschny, D., & Döring, B. (2020). Influence of airtightness of steel sandwich panel joints on heat losses. *E3S Web of Conferences*, 172, 05008. <https://doi.org/10.1051/e3sconf/202017205008>
- Luthfiyyah, D. N., & Widjajanti, R. (2019). Green Roof to Overcome Urban Heat Island Effects in the Center of Semarang. *E3S Web of Conferences*, 125, 07018. <https://doi.org/10.1051/e3sconf/201912507018>
- Muñoz-Viveros, C., Pérez-Fargallo, A., & Rubio-Bellido, C. (2022). Influence of the type of solar protection on thermal and light performance in classrooms. *Energy Reports*, 8, 5329–5340. <https://doi.org/10.1016/j.egy.2022.04.007>
- Nassif, N., Tahmasebi, M., Ridwana, I., & Ebrahimi, P. (2022). New optimal supply air temperature and minimum zone air flow resetting strategies for VAV systems. *Buildings*, 12(3), 348. <https://doi.org/10.3390/buildings12030348>
- Nwankwo, M., Meng, Q., Yang, D., & Liu, F. (2022). Effects of forest on birdsong and human acoustic perception in urban parks: a case study in Nigeria. *Forests*, 13(7), 994. <https://doi.org/10.3390/f13070994>

- Qiu, G., Li, H., Zhang, Q., Chen, W., Liang, X., & Li, X. (2013). Effects of evapotranspiration on mitigation of urban temperature by vegetation and urban agriculture. *Journal of Integrative Agriculture*, 12(8), 1307–1315. [https://doi.org/10.1016/s2095-3119\(13\)60543-2](https://doi.org/10.1016/s2095-3119(13)60543-2)
- Rey, C. V., Franco, N., Peyre, G., & Rodríguez, J. P. (2020). Green roof design with engineered extensive substrates and native species to evaluate stormwater runoff and plant establishment in a neotropical mountain climate. *Sustainability*, 12(16), 6534. <https://doi.org/10.3390/su12166534>
- Shapoval, S., Spodyniuk, N., Zhelykh, V., Shepichak, V., & Shapoval, P. (2021). Application of rooftop solar panels with coolant natural circulation. *Pollack Periodica*, 16(1), 132–137. <https://doi.org/10.1556/606.2020.00218>
- Shapoval, S., Zhelykh, V., Venhryn, I., & Kozak, K. (2019a). Simulation of thermal processes in the solar collector which is combined with external fence of an energy efficient house. *Lecture Notes in Civil Engineering*, 47, 510–517. https://doi.org/10.1007/978-3-030-27011-7_65
- Shapoval, S., Zhelykh, V., Venhryn, I., Kozak, K., & Krygul, R. (2019b). Theoretical and experimental analysis of solar enclosure as part of energy-efficient house. *Eastern-European Journal of Enterprise Technologies*, 2(8), 38–45. <https://doi.org/10.15587/1729-4061.2019.160882>
- Štastný, P., Antošová, N., Kalús, D., & Mučková, V. (2024). The importance of using active thermal protection following restoration work on old buildings. *Acta Polytechnica*, 64(2), 118–127. <https://doi.org/10.14311/ap.2024.64.0118>
- Tkachenko, T., Kravchenko, M., Voloshkina, O., Mileikovskiy, V., Tkachenko, O., & Sipakov, R. (2024a). Evaluating rain-garden bands: filtration properties and implications for urban water management. *World Environmental and Water Resources Congress, 2024*, 960–968. <https://doi.org/10.1061/9780784485477.085>
- Tkachenko, T., & Mileikovskiy, V. (2018a). Energy efficiency of “Green structures” in cooling period. *International Journal of Engineering & Technology*, 7(3.2), 453–457. <https://doi.org/10.14419/ijet.v7i3.2.14570>
- Tkachenko, T., & Mileikovskiy, V. (2018b). Geometric basis of the use of “Green constructions” for sun protection of glazing. *Advances in Intelligent Systems and Computing*, 809, 1096–1107. https://doi.org/10.1007/978-3-319-95588-9_94
- Tkachenko, T., & Mileikovskiy, V. (2020a). Methodology of thermal resistance and cooling effect testing of green roofs. *Songklanakarin Journal of Science and Technology (SJST)*, 42(1), 50–56. <https://doi.org/10.14456/sjst-psu.2020.8>
- Tkachenko, T., & Mileikovskiy, V. (2020b). Assessment of light transmission for comfort and energy efficient insolation by “Green Structures.” *Advances in Intelligent Systems and Computing*, 1296, 139–151. https://doi.org/10.1007/978-3-030-63403-2_13
- Tkachenko, T., & Mileikovskiy, V. (2022). Capturing carbon dioxide from human-driven vehicles by green structures for carbon neutrality. *IOP Conference Series Earth and Environmental Science*, 1111(1), 012056. <https://doi.org/10.1088/1755-1315/1111/1/012056>
- Tkachenko, T., Mileikovskiy, V., Kravchenko, M., & Konovaliuk, V. (2023a). Simulation of illumination and wind conditions for green and fed cities using CFD software. *IOP Conference Series Earth and Environmental Science*, 1275(1), 012014. <https://doi.org/10.1088/1755-1315/1275/1/012014>

- Tkachenko, T., Mileikovskiy, V., & Ujma, A. (2019). Field study of air quality improvement by a “Green Roof” in Kyiv. *System Safety Human – Technical Facility – Environment*, 1(1), 419–424. <https://doi.org/10.2478/czoto-2019-0054>
- Tkachenko, T., Mileikovskiy, V., Ujma, A., & Hajiyev, M. (2024b). Treatment of out-of-context buildings during the restoration of historical territories using green structures. *International Journal of Conservation Science*, 15(SI), 129–140. <https://doi.org/10.36868/ijcs.2024.si.11>
- Tkachenko, T., Voloshkina, O., Mileikovskiy, V., Sipakov, R., Hlushchenko, R., & Tkachenko, O. (2023b). Using rain-garden bands for rainwater drainage from roads. *IOP Conference Series: Earth and Environmental Science*, 1254, 1207–1214. <https://doi.org/10.1061/9780784484852.110>
- Venhryn, I., Shapoval, S., Voznyak, O., Datsko, O., & Gulai, B. (2021). *Modelling of optical characteristics of the Thermal Photovoltaic Hybrid Solar Collector*. 2021 IEEE 16th International Conference on Computer Sciences and Information Technologies (CSIT), Lviv, Ukraine. <https://doi.org/10.1109/csit52700.2021.9648738>
- Voznyak, O., Savchenko, O., Spodyniuk, N., Sukholova, I., Kasynets, M., & Dovbush, O. (2022). Improving of ventilation efficiency at air distribution by the swirled air jets. *Pollack Periodica*, 17(1), 123–127. <https://doi.org/10.1556/606.2021.00419>
- Voznyak, O., Spodyniuk, N., Antypov, I., Dudkiewicz, E., Kasynets, M., Savchenko, O., & Tarasenko, S. (2023). Efficiency improvement of Eco-Friendly solar heat supply system as a building coating. *Sustainability*, 15(3), 2831. <https://doi.org/10.3390/su15032831>
- Voznyak, O., Spodyniuk, N., Savchenko, O., Sukholova, I., & Kasynets, M. (2021). Enhancing energetic and economic efficiency of heating coal mines by infrared heaters. *Naukovyi Visnyk Natsionalnoho Hirnychoho Universytetu*, 2, 104–109. <https://doi.org/10.33271/nvn-gu/2021-2/104>
- Voznyak, O., Yurkevych, Y., Dovbush, O., & Serediuk, Y. (2019). The influence of chairs and passengers on air velocity in bus passenger compartment. *Lecture Notes in Civil Engineering*, 47, 518–525. https://doi.org/10.1007/978-3-030-27011-7_66
- Zeng, J., Huang, G., Luo, H., Mai, Y., & Wu, H. (2019). First flush of non-point source pollution and hydrological effects of LID in a Guangzhou community. *Scientific Reports*, 9(1), 13865. <https://doi.org/10.1038/s41598-019-50467-8>
- Zhang, J., Zhang, Q., Shuang, S., Cun, Z., Wu, H., & Chen, J. (2021). The Responses of Light Reaction of Photosynthesis to Dynamic Sunflecks in a Typically Shade-Tolerant Species *Panax notoginseng*. *Frontiers in Plant Science*, 12, 718981. <https://doi.org/10.3389/fpls.2021.718981>
- Zhelykh, V., Kozak, C., & Savchenko, O. (2016). Using of thermosiphon solar collector in an air heating system of passive house. *Pollack Periodica*, 11(2), 125–133. <https://doi.org/10.1556/606.2016.11.2.11>
- Zhelykh, V., Shapoval, P., Shapoval, S., & Kasynets, M. (2020). Influence of orientation of buildings facades on the level of solar energy supply to them. *Lecture Notes in Civil Engineering*, 100, 499–504. https://doi.org/10.1007/978-3-030-57340-9_61
- ZinCo USA, Inc. (n.d. a). *Perennial Garden* | ZinCo Green Roof Systems USA. <https://zinco-usa.com/systems/perennial-garden>
- ZinCo USA, Inc. (n.d. b). *Walkways on roofs and plaza decks* | ZinCo Green Roof Systems USA. <https://zinco-usa.com/systems/walkways>

Summary

Planning of green roofs for the best thermotechnical effect. The energy-efficient provision of indoor comfort for buildings is one of the most important requirements for modern construction. The greening of buildings is a natural measure to achieve this, for which the most limiting factor is the lack of systematic research on its positive effects. At the Kyiv National University of Construction and Architecture, a series of research on thermotechnical benefits and gas exchange in plant layers has been performed. The cooling effect of plants is up to 4 K. Semi-intensive green roofs on rooms have paths, which absorb solar radiation and load the air-conditioning systems. The proposed solution is to build the paths on the auxiliary premises with low microclimate requirements. The work aims to estimate the heat distribution in green roofs with paths to test the recommendation. Simulation using the Fourier–Kirchhoff equation shows that the path has a trace of higher heat transfer on the ceiling up to an additional $1.8\text{--}2.0\text{ W}\cdot\text{m}^{-2}$. Thus, aligning the paths above the auxiliary premises is recommended, if possible. A better solution is to allow planting of the paths. Using plant-permit pavements and barefoot-in-dew systems such as ZinCo Soft Landscape are examples of such solutions. It is necessary to use grass that can be walked on.

Šimon REZBÁRIK^{1,2}

Lenka VAVRINCOVÁ¹

Martin VALICA¹ 

Vanda ADAMCOVÁ¹ 

Stanislav SEKELY²

Ján REZBÁRIK²

Miroslav HORNÍK¹  

¹ University of Ss. Cyril and Methodius in Trnava, Faculty of Natural Sciences, Institute of Chemistry and Environmental Sciences, the Slovak Republic

² GEOFIX, s.r.o., the Slovak Republic

Solidification/stabilization of fly ash contaminated with radiocaesium into geopolymers

Keywords: fly ash, geopolymers, solidification/stabilization, ¹³⁷Cs, leachability, compressive strength

Introduction

Nuclear power is developing rapidly due to its high energy potential and environmental benefits (Danish, 2021; Zhan et al., 2021). Although nuclear power offers significant economic and social benefits, it produces radioactive wastes (RAWs) with varying levels of hazard and radioactivity. In terms of protection of the environment, the safe disposal of these RAWs has become an increasingly serious problem in a way that hinders the further development of the nuclear industry (Liu et al., 2024). Three radionuclides – ¹³⁷Cs ($T_{1/2} = 30.2$ y), ⁹⁰Sr ($T_{1/2} = 28.2$ y) and ⁷⁹Se ($T_{1/2} = 3.26 \times 10^5$ y) – occur in the produced

RAWs with significant risk characteristics, such as relatively high radioactivity levels, long half-lives and significant radiation energies (Abass et al., 2022; Durmus & Erenturk, 2023). The potential release of radionuclides from RAWs poses serious risks to the environment and human health. Consequently, it becomes necessary to ensure their proper and safe treatment and storage (Liu et al., 2024).

Currently, more than 60% of electricity in the Slovak Republic is generated by nuclear power and this share is steadily increasing due to the gradual closure of thermal power plants as significant producers of carbon dioxide and other greenhouse gases. However, nuclear power plants (NPPs) are responsible for producing huge amounts of RAWs and spent nuclear fuel. The production of solid RAWs was on an upward trend from 2005 to 2020 at the Mochovce NPP, rising from 14.6 t in 2005 to 16.5 t in 2020. In contrast, at the Jaslovské Bohunice NPP, the production of solid RAWs was down by 49.9% over the same period. In the case of liquid RAWs, a significant decrease in their production was observed in the period 2005–2020, with a decrease from 127.5 m³ in 2005 to 11.7 m³ in 2020 in Mochovce and from 48.0 m³ to 15.1 m³ in Jaslovské Bohunice (these data do not include the amount of RAWs produced in the framework of the decommissioning of the A1 and V1 power plants by JAVYS, a.s.) (Enviroportál, 2023).

In Slovakia, JAVYS, a.s. is practically the only company responsible for the implementation of the treatment and storage of the above mentioned RAWs, as well as institutional RAWs (JAVYS, 2024).

In order to ensure the safe disposal of RAWs, a number of variables need to be considered that lead to the most appropriate disposal method for a particular type of RAW. There are different pre-treatment processes, RAW treatments and final storage systems. As mentioned above, in addition to the conventional methods (e.g. adsorption, chemical precipitation, extraction, membrane separation, etc.), attention is also being given to alternative remediation technologies, such as biosorption and phytoremediation for the separation of radionuclides using biological systems (e.g. microorganisms or plants) as a first step in the treatment of RAWs. In the next step, the aim is to achieve a reduction in the volume of RAWs (e.g. contaminated biomass), e.g. by incineration, which results in contaminated ash. The final step in the treatment of RAWs is to convert the contaminated material into a safe form with respect to its final storage. Solidification is used to convert RAWs into a solid and long-term stable form. Apart from cementation, as the longest used method of final RAW treatment, technology based on the production of geopolymer matrices is proving to be a suitable method of RAW solidification.

The concept and notion of geopolymers was first introduced in 1972 by French scientist Joseph Davidovits (Davidovits, 2011). Geopolymers belong to a group of mineral binders related to natural zeolites. The term geopolymers refers to

aluminosilicate inorganic polymers with an amorphous three-dimensional network structure of a silica-oxygen tetrahedron and an aluminum-oxygen tetrahedron connected via an oxygen bridge (Hu et al., 2020). They are prepared using alkaline activation without the presence of a lime component and thus belong to the group of alkali-activated materials. The material, which is formed by the geopolymerization of an active aluminosilicate precursor and an alkali activator, is distinguished by excellent mechanical properties, high durability, resistance to acid and high temperatures, and low cost and carbon dioxide emissions (Amran et al., 2020). Due to these excellent properties, geopolymers are widely used in various manufacturing fields, such as building blocks (Singh et al., 2020), coatings (Lv et al., 2019), adhesives (Kürklü & Görhan, 2019) and refractories (Gao et al., 2020), and for the immobilization of hazardous wastes and materials (Fu et al., 2020) and emergency repairs (Bhutta et al., 2019).

In 2024, an interesting review paper was published by Liu et al. (2024), which addresses the solidification performance and mechanism of typical radioactive nuclear waste by geopolymers and geopolymer ceramics. It highlights the fact that for the last two years, papers dealing with the solidification and adsorption of cesium by cement, metakaolin- and fly ash-based geopolymers have been published in scientific databases. The use of metakaolin-based geopolymers in the solidification of cesium has been studied in works by Tian et al. (2022), Mukiza et al. (2023), and Tan et al. (2024). In recent years, inexpensive precursors for the preparation of geopolymers for the solidification of hazardous wastes have also been explored, of which fly ash has received significant attention (Wang et al., 2018; Pu et al., 2024). In this context, several works have shown that fly ash-based geopolymers may be suitably applicable in the solidification and immobilization of radiocesium ^{137}Cs (Tian et al., 2019; Jain et al., 2022a; Jain et al., 2022b). Li et al. (2013) described the solidification of Cs^+ by fly ash-based geopolymer as an encapsulation matrix and discovered that geopolymers could better meet the safe disposal requirements of radioactive waste compared to cement.

Based on these facts, it seems to be an interesting idea to use fly ashes obtained after the incineration of radioactive wastes containing ^{137}Cs radiocesium or to apply fly ashes as adsorbents of ^{137}Cs occurring in liquid radioactive wastes and subsequently solidify them using geopolymers. The aim of this work was to evaluate the possibility of solidifying fly ash contaminated with radiocesium ^{137}Cs into geopolymer matrices. Within the individual experimental steps, the work focused on the preparation of fly ash originating from the Vojany thermal power plant (TPP) (Slovak Republic) and artificially contaminated with the radionuclide ^{137}Cs , on the design and verification of the recipe for solidifying fly ash into

a geopolymer matrix (commercially available under the name Geocem, produced by GEOFIX, a.s., Slovak Republic), and on evaluating the qualitative parameters of the final product in terms of its long-term storage in the RAW repository.

Material and methods

Matrices used for the preparation of geopolymers

A three-component geopolymer mixture commercially available under the name Geocem, produced by GEOFIX, s.r.o. (Trnava, Slovak Republic), was used in the preparation of the geopolymer matrices. This mixture consists of three basic components, namely Geosil A consisting of sodium polysilicate, sodium hydroxide and potassium hydroxide; Geosil B containing calcium oxide, silicon oxide, aluminum oxide and magnesium oxide; and Geosil C including calcium oxide, silicon oxide and aluminum oxide.

The fly ash as waste studied came from the Vojany TPP (Slovak Republic). The sample was obtained at the end of 2020, as fly ash K5 (annual sample collection). The physico-chemical analysis of this fly ash was carried out by Eurofins Environment Testing Slovakia, s.r.o. (Slovak Republic), which included the determination of selected metals and semi-metals (Sb, As, Ba, Be, Bi, B, Sn, Al, Mg, Cr, Cd, Cu, Ni, Pb, Hg, Se, Tl, Te, V, Ca, Fe, and Zn) using different analytical methods (HG-AAS, ICP-OES, F-AAS, AAS-AMA, or UV-Vis), oxides (K_2O , P_2O_5 , Al_2O_3 , MgO , SiO_2 , MnO , Na_2O , TiO_2 , CaO , and Fe_2O_3), specific weight, solids content, loss of organic matter by annealing at $550^\circ C$, total sulfur, pyrite sulfur, sulfate sulfur, combustible matter at $830^\circ C$, loss by drying, dry matter at $105^\circ C$, bulk density, and determination of total chlorine. In addition, grain size testing, according to ČSN EN ISO 17892-4 (Česká agentura pro standardizaci [ČSN], 2017), and at the Výskumný ústav pre hnedé uhlie (Research Institute for Brown Coal) in Most (VUHU, a.s., Czech Republic), determination of the percentage of water, and the pH of the fly ash reaction according to STN ISO 10390 (Slovenski inštitut za standardizacijo [STN], 2005) were carried out.

Artificial contamination of fly ash

Before the artificial contamination of the fly ash with the radioisotope ^{137}Cs , the possible level of this radionuclide was analyzed by scintillation gamma-spectrometry in a sample of original fly ash (1 kg) placed in a Marinelli-type

beaker. An accurately weighed quantity of fly ash was transferred into an Erlenmeyer flask containing a CsCl solution in deionized water spiked with $^{137}\text{CsCl}$ of known activity, chemical concentration, and pH value. The pH of the solution was adjusted by the addition of $1 \text{ mol}\cdot\text{dm}^{-3}$ NaOH solution to a final value of pH 5.5. The exposure was carried out under stirring on a rotary shaker (150 min^{-1}) at 25°C and the risk of evaporation of the water from the solution was prevented by covering the neck of the flask with parafilm. After 48 h of exposure, fly ash with bound ^{137}Cs activity was collected on filter paper. Subsequently, an aliquot of the solution was removed and filtered through a syringe filter (13 mm diameter; $0.45 \mu\text{m}$ permeability) to remove any residual fly ash, and the residual ^{137}Cs activity in the solution was determined using a scintillation gamma-spectrometer. The captured fly ash was allowed to dry in a laboratory oven at 40°C for several days to a constant weight.

Solidification of fly ash

Plastic samplers with a circular base with a diameter of 35 mm and a height of 50 mm were designed and fabricated to prepare the cylindrical geopolymer waste forms. Before loading the geopolymer matrix, these plastic samplers were covered with parafilm on the base to prevent the unsolidified geopolymer matrix from leaking out of the samplers.

The preparation of the geopolymer mass containing different percentages by weight of fly ash (5%, 10%, 20%, and 40%) artificially contaminated with ^{137}Cs followed the proposed recipes shown in Table 1. From each variant, four samples were prepared in the form of cylinders of the geopolymer waste forms. The samples were allowed to cure for 45 days under laboratory conditions (25°C).

TABLE 1. Proposed recipes for preparation of geopolymer waste forms containing different percentages by weight of fly ash (5%, 10%, 20%, and 40%) artificially contaminated with ^{137}Cs

Geopolymer waste forms with proportion of fly ash [wt.%]	Fly ash [g; d.w.]	Geosil A [g; d.w.]	Geosil B [g; d.w.]	Geosil C [g; d.w.]	Technical water [g]	Final product [g]	NaOH [g; d.w.]
0.00	0.00	42.00	24.00	123.00	111.00	300.00	15
5.00	15.00	38.67	22.10	113.23	111.00	300.00	15
10.00	30.00	35.33	20.19	103.48	111.00	300.00	15
20.00	60.00	28.67	16.38	83.95	111.00	300.00	15
40.00	120.00	15.33	8.76	44.91	111.00	300.00	15

Source: own work.

Leachability test

In the first step, the initial ^{137}Cs activity bounds in a given formed geopolymer waste form was determined based on the known specific activity of ^{137}Cs ($\text{Bq}\cdot\text{g}^{-1}$; d.w.) in the used, artificially contaminated fly ash sample, the percentage by weight of this fly ash in the final product, and the total dry weight of the formed geopolymer waste forms.

The leachability test was performed according to ANSI/ANS-16.1 (American National Standard [ANSI], 1986). The test itself was carried out in sealed plastic beakers with a total volume of 1 dm^3 , to which was added an exact volume of deionized water ($0.05\text{ }\mu\text{S}\cdot\text{cm}^{-1}$) calculated as ten times the surface area of the sample of the geopolymer waste form. The geopolymer waste form sample was then immersed in the deionized water and exposed under laboratory conditions at 25°C . After 2 h, the sample was removed from the water and immersed in a new plastic beaker of fresh deionized water of identical volume as above. The water sample obtained after exposure was analyzed for pH, conductivity, and ^{137}Cs activity released from the geopolymer waste form using Marinelli-type beakers and scintillation gamma-spectrometry. Similar procedures were subsequently followed for exposure times of 4 h, 7 h, 24 h, 48 h, 72 h, 96 h, and 120 h.

As the fly ash was artificially contaminated with radiocaesium ^{137}Cs , its long half-life of $T_{1/2} = 30.2\text{ y}$ allows us to ignore its radioactive decay during the testing in terms of the activity determined in the leachates. Under such conditions, the effective diffusivity can be calculated using the following mathematical relationship (Eq. 1):

$$D = \left(\frac{A_n}{A_0} \frac{1}{\Delta t_n} \right)^2 \left(\frac{V}{S} \right)^2 T, \quad (1)$$

where: D – effective diffusivity [$\text{cm}^2\cdot\text{s}^{-1}$], V – volume of the geopolymer waste form sample [cm^3], S – geometric surface area of the geopolymer waste form sample [cm^2], A_n – activity released from the geopolymer waste form sample during the leaching interval n [Bq], A_0 – total activity solidified in the geopolymer waste form sample at the beginning of the first leaching interval [Bq], $\Delta t_n = t_n - t_{n-1}$ = duration of the n^{th} interval [s], T – mean time of the leaching interval [s], which is calculated using relation (Eq. 2):

$$T = \left\{ \frac{1}{2} \left(t_n^2 + t_{n-1}^2 \right) \right\}^2. \quad (2)$$

The leachability index L_i is then calculated using the following equation (Eq. 3):

$$L_i = \frac{1}{n} \sum_{1}^n \left(\frac{\beta}{D} \right)_n, \quad (3)$$

where: L_i – leachability index, n – number of leaching intervals, β – constant ($\beta = 1$) [$\text{cm}^2 \cdot \text{s}^{-1}$], D – effective diffusivity [$\text{cm}^2 \cdot \text{s}^{-1}$].

Compressive strength test

The compressive strength test of the formed geopolymer waste form was carried out using a prototype of a piece of compressive strength measurement equipment (GEOFIX, s.r.o.). It was a manual hydraulic press with an integrated manometer and a maximum pressure of 20 t. The compressive strength measurement was preceded by the pressing of the geopolymer waste form samples into perfectly flat surfaces. The prepared sample was inserted between the contact surfaces of the hydraulic press and the pressure on the sample was increased by stepwise pumping. The pressure at which sample destruction occurred was then read on the manometer.

Scintillation gamma-spectrometry

A scintillation gamma-spectrometer with a 3" diameter NaI(Tl) well-type crystal 76BP76/3 (Enviet, 2024) coupled with the evaluation program ScintiVision-32 (Ortec, USA) was used to determine the initial and residual ^{137}Cs activity in the solutions from the experiments aimed at artificial contamination of fly ash with radionuclide ^{137}Cs , and to determine the bound ^{137}Cs activity directly in the fly ash. The detector was placed in a cylindrical lead shield with a height of 250 mm and a wall thickness of 35 mm of Pb to minimize the background effect. For the leachate samples obtained from the leachability test, the ^{137}Cs activity was measured on an identical scintillation detector, but with the difference that the leachate samples with a volume of 600–800 cm^3 were analyzed in Marinelli-type beakers (type 1040G; max. volume 1,000 cm^3) and on a detector placed in a lead shield designed for high-resolution gamma-spectrometry (Enviet, Czech Republic; height 400 mm, wall thickness 100 mm Pb). The scintillation gamma-spectrometers were calibrated in terms of γ -photon energies and measurement efficiencies using the above evaluation program and the built library of analyzed radioisotopes: ^{109}Cd ($E_\gamma = 88.04$ keV), ^{137}Cs ($E_\gamma = 661.66$ keV), and ^{60}Co ($E_\gamma = 1,173.24$ keV), using

standard solutions of the given radioisotopes. The calibration considered the geometry of the measurement, either in the form of vials inserted into the detector well or in the form of Marinelli-type beakers placed on the detector. The duration of the sample analysis was 600 s, which ensured a relative measurement uncertainty of up to 2%.

Graphical and statistical evaluation of data

The obtained data were statistically evaluated and processed into graphical dependencies using Origin Pro 2016 (OriginLab Corporation, 2016) and MS Excel 2016 (Microsoft Corporation, 2016).

Results and discussion

Characterization of fly ash

In the first step, we characterized in detail the fly ash sample studied. Based on the results obtained, we can say that the studied fly ash sample did not contain heavy metals (Cu, Zn, Hg, Cr, Cd, or Pb) in concentrations that would be abnormal or unnatural for the given sample type. We also found that the fly ash sample studied contained naturally high concentrations of the elements Al, Mg, and Ca, which also form an important component within the geopolymers. Al was present in the fly ash sample at a concentration of $107 \text{ g}\cdot\text{kg}^{-1}$ (10.7%), Ca at $101 \text{ g}\cdot\text{kg}^{-1}$ (10.1%), and Mg at $10.5 \text{ g}\cdot\text{kg}^{-1}$ (1.05%).

Other important chemical components of geopolymers in terms of their final structure and polymerization include oxides, in particular aluminum oxide, magnesium oxide, silicon oxide, and calcium oxide. For this reason, analyses were also carried out to determine the abundance of oxides in the studied fly ash sample. We found that the fly ash sample contained silicon oxide at a percentage by weight of 39.5%, aluminum oxide at 20.2%, calcium oxide at 14.1% and magnesium oxide at a percentage of 1.74% (Table 2). It should be noted at this point that the mechanism of the effect of some oxides, such as CaO and SO_3 , on the mechanical properties and dimensional stability of fly ash-based geopolymers is not clear. Chen et al. (2022) observed that the mechanical properties of fly ash-based geopolymers initially increase and then decrease with the increasing CaO and SO_3 content.

TABLE 2. Proportion of oxides in fly ash sample originating from Vojany TPP (Slovak Republic)

Oxide	Weight proportion [%; d.w.]	Measurement uncertainty [%]	Analytical method
K ₂ O	2.01	10	F-AAS
P ₂ O ₅	0.53	15	ICP-OES
Al ₂ O ₃	20.2	15	ICP-OES
MgO	1.74	15	ICP-OES
SiO ₂	39.5	not determined	gravimetry
MnO	0.12	not determined	ICP-OES
Na ₂ O	0.66	10	F-AAS
TiO ₂	0.81	not determined	ICP-OES
CaO	14.1	15	ICP-OES
Fe ₂ O ₃	6.78	20	ICP-OES

ICP-OES – inductively coupled plasma optical emission spectrometry; F-AAS – flame atomic absorption spectrometry. Source: own work.

In the final analyses, we focused on the abundance of basic elements such as sulfur in its various chemical forms, and total chlorine, as well as on the solids content, loss of organic matter by annealing at 550°C, combustible matter at 830°C, loss by drying, dry matter determined at 105°C, bulk density, and specific weight. These analyses were supplemented by the determination of the pH reaction of the fly ash in suspension with water (weight ratio of fly ash to deionized water equals 1 : 5). We found that the fly ash showed a strongly basic character with a pH of 12.2.

Based on these facts, it can be assumed that the studied fly ash represents a suitable material that chemically complements the basic components of the geopolymer mixture, which implies that the evaluated fly ash can be applied to this mixture in significant weight proportions, representing tens of percent. This assumption is also the basis of the extensive review work by Li et al. (2022), which deals with the preparation, properties, and application possibilities of fly ash-based geopolymers.

Preparation and characterization of geopolymer waste forms

For the artificial contamination of a fly ash sample with ¹³⁷Cs, we found that with the increasing CsCl concentration in deionized water, the percentage of ¹³⁷Cs bound activity by the studied fly ash sample decreased significantly.

The conducted experiments also showed that the amount of initial ^{137}Cs activity in the deionized water had a significant effect on the ^{137}Cs specific binding values obtained in $\text{Bq}\cdot\text{g}^{-1}$ d.w. The specific ^{137}Cs activity bound in the individual fly ash samples ranged from $420 \text{ Bq}\cdot\text{g}^{-1}$ (d.w.) to $969 \text{ Bq}\cdot\text{g}^{-1}$ (d.w.). The fly ash samples thus artificially contaminated with radiocaesium ^{137}Cs were subsequently applied for the preparation of geopolymer waste forms containing different percentages by weight of fly ash (5%, 10%, 20%, and 40%), whose physico-chemical and geometric characteristics are presented in Table 3.

TABLE 3. Physico-chemical and geometric characteristics of prepared geopolymer waste forms

Proportion of fly ash [%]	Average weight of samples [g]	Average height of samples [cm]	Average sample volume [cm^3]	Average surface area of samples [cm^2]	Initial ^{137}Cs activity of samples [Bq]
5.00	58.0 ± 0.3	4.25 ± 0.03	40.9 ± 0.3	66.0 ± 0.4	2 137
10.00	52.3 ± 0.5	4.80 ± 0.06	46.2 ± 0.6	72.1 ± 0.6	6 475
20.00	45.1 ± 0.3	4.64 ± 0.02	44.6 ± 0.2	70.2 ± 0.3	6 543
40.00	35.7 ± 3.8	5.31 ± 0.51	51.1 ± 4.9	77.6 ± 5.6	5 830

Source: own work.

Many authors point out that several factors will play an important role in the preparation of fly ash-based geopolymers for the successful and highly efficient solidification or immobilization of Cs, as well as the microstructure of the formed geopolymers. Jain et al. (2022a; 2022b) found that the critical process parameters are the curing time and curing temperature, followed by the interaction between the curing temperature and the Cs dosage. They also explained (Jain et al., 2022a) that the Cs dosage affected the resulting phase compositions and pore structure of fly ash-based geopolymers, eventually influencing the Cs immobilization in these matrices. In our case, we worked with the radioisotope ^{137}Cs and simulated radioactive wastes originating from NPP operations, which are characterized by very low Cs concentrations but not negligible radiochemical characteristics. In addition, Tian et al. (2019) showed that a high Si/Al ratio could contribute to a more compact of geopolymer, as confirmed by the decrease in the pore volume with the increasing Si/Al ratio. In contrast, the geopolymer with a low Si/Al ratio had a higher Cs^+ immobilization efficiency than the geopolymer with a high Si/Al ratio due to the high adsorption density.

Leachability test

The leachability test performed according to the ANSI/ANS-16.1 standard is implemented in the operations of the National Radioactive Waste Repository (NRWR) in Mochovce (Slovak Republic) as an important parameter determining the suitability of the solidified RAWs for their storage.

While performing the leachability test and at the specified times of 2 h, 4 h, 7 h, 24 h, 48 h, 72 h, 96 h, and 120 h, the ^{137}Cs activity in the whole volume of deionized water was determined, and the pH and conductivity of the water were measured. Figure 1 shows graphically the changes in the pH, conductivity, and ^{137}Cs activity values in the deionized water released from the prepared geopolymer waste forms with different fly ash contents. As can be seen, there was a gradual decrease in the above measured values at short time periods, i.e. after 2 h, 4 h, and 7 h of exposure. A similar dependence was observed for measurements that proceeded at daily intervals, i.e., after one day, two days, three days, four days, and five days of exposure. In the case of conductivity, we found that the highest values of conductivity, in $\text{mS}\cdot\text{cm}^{-1}$, probably originating from the release of chemical components of the prepared geopolymer waste forms, were observed for the samples exhibiting the lowest fly ash proportions. The conductivity values ranged from approx. $1 \text{ mS}\cdot\text{cm}^{-1}$ to $5 \text{ mS}\cdot\text{cm}^{-1}$. This was not clearly demonstrated for the pH values of the water; the pH of the deionized water increased from an initial pH 5.5 to pH values of 10.6–11.8 within the individual times of measurement. Regarding the ^{137}Cs activity released into the water, the opposite phenomenon was observed, namely that the highest values of the measured activities were observed for the geopolymer waste form samples containing the highest applied content of fly ash (40 wt.%).

We also evaluated the ^{137}Cs leachability within individual samples and measurements in the context of the initial ^{137}Cs activity determined in a given cylinder of the geopolymer waste forms through the applied fly ash contaminated with ^{137}Cs . We found that the highest percentage releases of ^{137}Cs activity within the individual measurements were observed for the geopolymer waste form samples containing fly ash at 40% by weight. At the same time, these results showed that we confirmed a slightly higher percentage release of ^{137}Cs activity than 1% in only one case of exposure time.

Within this leachability test and in accordance with the ANSI/ANS-16.1 standard, parameters such as the effective diffusivity (D) and, in particular, the dimensionless leachability index (L_i) were evaluated, based on which solidified RAWs are determined to be suitable or unsuitable for storage in RAW repositories.

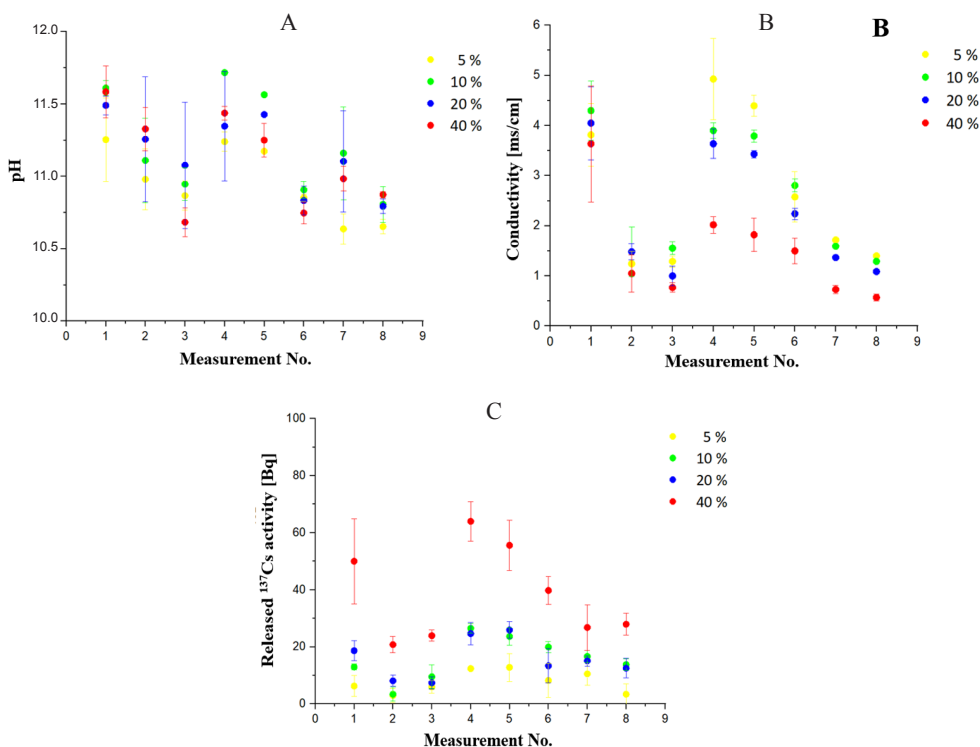


FIGURE 1. Changes in pH (A), conductivity (B), and ¹³⁷Cs activity (C) values in deionized water released from prepared geopolymer waste forms with different fly ash contents (5 wt.%, 10 wt.%, 20 wt.%, and 40 wt.%). After each measurement, the deionized water was replaced with fresh water and the duration of exposure of the geopolymer waste form sample from the beginning of the leachability test was as follows: 1st measurement – after 2 h of exposure; 2nd measurement – after 4 h; 3rd measurement – after 7 h; 4th measurement – after 24 h; 5th measurement – after 48 h; 6th measurement – after 72 h; 7th measurement – after 96 h; 8th measurement – after 120 h of exposure. The values represent the arithmetic means and the error bars describe the standard deviation of three independent experiments
Source: own work.

This standard defines that if the L_i value is greater than 6, the solidified RAWs are suitable for storage in an RAW repository. Conversely, if the L_i value is less than 6, the solidified product does not meet the criteria for storage in a repository, e.g. the NRWR in Mochovce. Based on the calculated L_i values, we found that the prepared geopolymer waste form samples with 5%, 10%, and 20% fly ash content by weight showed L_i values ranging from 6.34 to 6.54, and thus met this criterion. For the sample with 40% fly ash content, we obtained a value of L_i equal to 5.58, from which we can conclude that this solidified RAWs did not pass the leachability test and therefore cannot be stored in a RAW repository.

Jain et al. (2022b) found that for prepared fly ash-based geopolymers and Cs immobilization, the leachability index L_i ranged from 7.4 to 14.6 (determined according to the ANSI/ANS-16.1-1 standard), which significantly exceeded the minimum acceptable value of 6. They explained these very high L_i values via the combination of the chemical (within the amorphous gel and zeolitic phase) and physical (adsorbed on surfaces and trapped within porosity) immobilization of Cs in fly ash-based geopolymers. They also emphasized that the remarkable improvement in the performance is due to the formation of the Cs-bearing zeolitic phase (pollucite) found in properly processed fly ash-based geopolymers.

Compressive strength test

As in the leachability test, the compressive strength test of solidified RAWs is considered a critical parameter determining their suitability or unsuitability for storage in RAW repositories planned for hundreds of years. In each country, the value of the pressure at which the solidified RAW is destroyed may vary according to the standards adopted for this purpose. In the conditions of the Slovak Republic, a minimum pressure on the wall of a solidified RAW of at least 5 MPa has been set for a given solidified RAW to be able to resist pressure. In Figure 2, we present the results of the material compressive strength tests for the individual prepared geopolymer waste form samples. As can be seen, the samples with fly ash contents ranging from 0 wt.% to 35 wt.% met the above limit. At the same time, we found that the value of the pressure at which the destruction of a given sample occurred decreased from a value of approx. 12 MPa determined for the sample without fly ash addition to a value of 8 MPa for the geopolymer waste form sample containing 35 wt.% of fly ash. As with the leachability test, the sample containing 40 wt.% fly ash proved to be unsuitable for storage in the RAW repository, with the destruction occurring at a pressure of only 4 MPa.

From the point of view of comparing our results concerning the effect of fly ash content in geopolymer waste forms on their compressive strength with the results reported in scientific databases, there are papers that show a different pattern of this dependence. For example, Carrillo-Beltran et al. (2021), when studying the effect of the percentage amount of fly ash originating from the combustion of olive tree biomass in prepared geopolymers (from 10 wt.% to 40 wt.%) on their compressive strength, found that this parameter increased with the increasing fly ash percentage

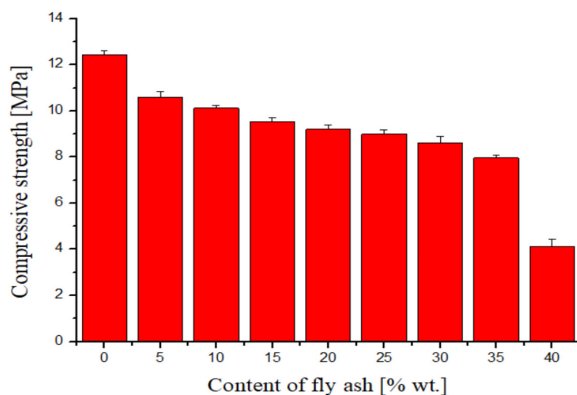


FIGURE 2. Compressive strength measured for prepared geopolymer waste forms with different fly ash contents. The values represent the arithmetic means and the error bars describe the standard deviation of three independent experiments

Source: own work.

up to 30 wt.% and then started to decrease slightly, reaching compressive strength values in the tens of MPa in all the cases analyzed. Also, Teixeira et al. (2022) confirmed in their work the synergistic effect of adding fly ash derived from biomass combustion on improving the characteristics of concrete containing fly ash derived from coal combustion.

Conclusions

This work investigated the possibility of solidifying fly ash contaminated with radiocaesium ^{137}Cs into geopolymer matrices (commercially available under the name Geocem, produced by GEOFIX, s.r.o., Slovak Republic). The fly ash sample originated from the Vojany TPP (Slovak Republic) and was artificially contaminated with the radionuclide ^{137}Cs . The main aim of the study was to design and validate the recipe for solidifying fly ash into a geopolymer matrix such that the final product meets the qualitative leachability and compressive strength test parameters to allow its long-term storage in the NRWR in Mochovce.

In terms of physico-chemical characterization of the fly ash sample, it was found that the fly ash sample studied contained naturally high concentrations of the elements Si, Al, Mg, and Ca, especially in the form of their oxides, which also form an important component within geopolymers.

The fly ash was artificially contaminated with radiocaesium ^{137}Cs through its relatively short-term exposure (48 h) in a $^{137}\text{CsCl}$ solution. These experiments showed that with the increasing CsCl concentration in deionized water, the percentage of ^{137}Cs bound activity by the studied fly ash sample decreased significantly. Also, the initial ^{137}Cs activity in the deionized water had a significant effect on the specific ^{137}Cs activity bound in the individual fly ash samples subsequently used to prepare geopolymer matrices containing different percentages by weight of fly ash (5%, 10%, 20%, and 40%) ranging from 420 to 969 $\text{Bq}\cdot\text{g}^{-1}$ (d.w.).

The leachability test carried out according to the ANSI/ANS-16.1 standard for five days, which is also adopted in the NRWR in Mochovce, showed that the geopolymer waste forms with fly ash contents of 5%, 10%, and 20% met the required limits of the leachability index L_i being more than 6. For the sample with a fly ash content of 40%, this index reached the value of L_i less than 6, which indicates the unsuitability of this material for storage in the NRWR in Mochovce.

The compressive strength test confirmed that the geopolymer waste forms with a fly ash content of 40% did not meet the required 5 MPa limit for its disposal. Samples with fly ash contents ranging from 0 to 35 wt.% met the above limit. At the same time, it was found that the value of the pressure at which the destruction of a given sample occurred decreased from a value of approx. 12 MPa, determined for the sample without a fly ash addition, to a value of 8 MPa, measured for the geopolymer waste form sample containing 35 wt.% of fly ash.

Based on the obtained results, it can be concluded that the geopolymer mixture used is capable of absorbing significant amounts of fly ash as RAW representing up to 30% of the total mass of the geopolymer waste forms prepared, while also meeting the required limits determined by the leachability and compressive strength tests that have been adopted in the operation of the NRWR in Mochovce as a RAW repository.

Acknowledgements

This work was supported by the Slovak Research and Development Agency under the contract No. APVV-15-0098 and Scientific Grant Agency of the Slovak Republic under the contract No. VEGA 1/0018/22.

References

- Abass, M. R., Breky, M. M. E., & Maree, R. M. (2022). Removal of ^{137}Cs and ^{90}Sr from simulated low-level radioactive waste using tin(IV) vanadate sorbent and its potential hazardous parameters. *Applied Radiation and Isotopes*, 189, 110417. <https://doi.org/10.1016/j.apradi-so.2022.110417>
- American National Standards Institute [ANSI]. (1986). *Measurement of the leachability of solidified low-level radioactive wastes by a short-term test procedure* (ANSI/ANS-16.1-1986). American National Standards Institute.
- Amran, Y. M., Alyousef, R., Alabduljabbar, H., & El-Zeadani, M. (2020). Clean production and properties of geopolymer concrete; A review. *Journal of Cleaner Production*, 251, 119679. <https://doi.org/10.1016/j.jclepro.2019.119679>
- Bhutta, A., Farooq, M., & Bantia, N. (2019). Performance characteristics of micro fiber-reinforced geopolymer mortars for repair. *Construction and Building Materials*, 215, 605–612. <https://doi.org/10.1016/j.conbuildmat.2019.04.210>
- Carrillo-Beltran, R., Corpas-Iglesias, F. A., Terrones-Saeta, J. M., & Bertoya-Sol, M. (2021). New geopolymers from industrial by-products: Olive biomass fly ash and chamotte as raw materials. *Construction and Building Materials*, 272, 121924. <https://doi.org/10.1016/j.conbuildmat.2020.121924>
- Česká agentura pro standardizaci [ČSN]. (2017). *Geotechnický průzkum a zkoušení – Laboratorní zkoušky zemín. Část 4: Stanovení zrnitosti [Geotechnical exploration and testing – Laboratory testing of soils. Part 4: Determination of grain size]* (ČSN EN ISO 17892-4).
- Chen, X., Zhang, J., Lu, M., Chen, B., Gao, S., Bai, J., Zhang, H., & Yang, Y. (2022). Study on the effect of calcium and sulfur content on the properties of fly ash based geopolymer. *Construction and Building Materials*, 314, 125650. <https://doi.org/10.1016/j.conbuildmat.2021.125650>
- Danish, Khan, S. U. D., & Ahmad, A. (2021). Testing the pollution haven hypothesis on the pathway of sustainable development: accounting the role of nuclear energy consumption. *Nuclear Engineering and Technology*, 53(8), 2746–2752. <https://doi.org/10.1016/j.net.2021.02.008>
- Davidovits, J. (2011). *Geopolymer chemistry and applications*. Geopolymer Institute.
- Durmuş, R. K. I., & Erenturk, S. A. (2023). Evaluation of adsorption behaviour of selenium onto zeolite-based composite barrier material for intermediate deep radioactive waste repository. *Progress in Nuclear Energy*, 158, 104604. <https://doi.org/10.1016/j.pnucene.2023.104604>
- Envinet (2024). *Produkty*. Envinet. <https://www.nuvia.com/cz/subjekty/ceska-republika/>
- Enviroportál (2023). *Radioactive waste*. Enviroportál. <https://www.enviroportal.sk/indicator/detail?id=805>
- Fu, S., He, P., Wang, M., Cui, J., Wang, M., Duan, X., Yang, Z., Jia, D., & Zhou, Y. (2020). Hydrothermal synthesis of pollucite from metakaolin-based geopolymer for hazardous wastes storage. *Journal of Cleaner Production*, 248, 119240. <https://doi.org/10.1016/j.jclepro.2019.119240>

- Gao, H., Liu, H., Liao, L., Mei, L., Zhang, F., Zhang, L., Li, S., & Lv, G. (2020). A bifunctional hierarchical porous kaolinite geopolymer with good performance in thermal and sound insulation. *Construction and Building Materials*, 251, 118888. <https://doi.org/10.1016/j.conbuildmat.2020.118888>
- GEOFIX (2024). *Hazardous waste processing*. GEOFIX, s.r.o. <https://www.geofixsro.sk/>
- Hu, S., Zhong, L., Yang, X., Bai, H., Ren, B., Zhao, Y., Zhang, W., Ju, X., Wen, H., Mao, S., Tao, R., & Li, C. (2020). Synthesis of rare earth tailing-based geopolymer for efficiently immobilizing heavy metals. *Construction and Building Materials*, 254, 119273. <https://doi.org/10.1016/j.conbuildmat.2020.119273>
- Jain, S., Banthia, N., & Troczynski, T. (2022a). Leaching of immobilized cesium from NaOH-activated fly ash-based geopolymers. *Cement and Concrete Composites*, 133, 104679. <https://doi.org/10.1016/j.cemconcomp.2022.104679>
- Jain, S., Banthia, N., & Troczynski, T. (2022b). Conditioning of simulated cesium radionuclides in NaOH-activated fly ash-based geopolymers. *Journal of Cleaner Production*, 380, 134984. <https://doi.org/10.1016/j.jclepro.2022.134984>
- JAVYS (2024). *Nuclear and decommissioning company*. JAVYS. <https://www.javys.sk/en/index.php>
- Kürklü, G., & Görhan, G. (2019). Investigation of usability of quarry dust waste in fly ash-based geopolymer adhesive mortar production. *Construction and Building Materials*, 217, 498–506. <https://doi.org/10.1016/j.conbuildmat.2019.05.104>
- Li, Q., Sun, Z., Tao, D., Xu, Y., Li, P., Cui, H., & Zhai, J. (2013). Immobilization of simulated radionuclide $^{133}\text{Cs}^+$ by fly ash-based geopolymer. *Journal of Hazardous Materials*, 262, 325–331. <https://doi.org/10.1016/j.jhazmat.2013.08.049>
- Li, X., Bai, C., Qiao, Y., Wang, X., Yang, K., & Colombo, P. (2022). Preparation, properties and applications of fly ash-based porous geopolymers: A review. *Journal of Cleaner Production*, 359, 132043. <https://doi.org/10.1016/j.jclepro.2022.132043>
- Liu, J., Xu, Y., Zhang, W., Ye, J., & Wang, R. (2024). Solidification performance and mechanism of typical radioactive nuclear waste by geopolymers and geopolymer ceramics: a review. *Progress in Nuclear Energy*, 169, 105106. <https://doi.org/10.1016/j.pnucene.2024.105106>
- Lv, X., Wang, K., He, Y., & Cui, X. (2019). A green drying powder inorganic coating based on geopolymer technology. *Construction and Building Materials*, 214, 441–448. <https://doi.org/10.1016/j.conbuildmat.2019.04.163>
- Microsoft Corporation (2016). *Microsoft Excel*. Microsoft Corporation.
- Mukiza, E., Phung, Q. T., Frederickx, L., Jacques, D., Seetharam, S., & De Schutter, G. (2023). Co-immobilization of cesium and strontium containing waste by metakaolin-based geopolymer: Microstructure, mineralogy and mechanical properties. *Journal of Nuclear Materials*, 585, 154639. <https://doi.org/10.1016/j.jnucmat.2023.154639>
- Origin Lab Corporation (2016). *Origin Pro 2016*. Origin Lab Corporation.
- Pu, S., Xu, B., Cai, G., Duan, W., Liu, Y., Lang, L., Shen, Z., & Yao, H. (2024). Strongly acidic lead contaminated soil solidification/stabilization using metakaolin-modified fly ash phosphoric-based geopolymer. *Chemical Engineering Journal*, 496, 154336. <https://doi.org/10.1016/j.cej.2024.154336>

- Singh, S., Aswath, M. U., & Ranganath, R. V. (2020). Performance assessment of red mud based geopolymer bricks and prisms. *Journal of Building Engineering*, 32, 101462. <https://doi.org/10.1016/j.jobe.2020.101462>
- Slovenský ústav technickej normalizácie [SUTN]. (2005). *Kvalita pôdy. Stanovenie pH [Soil quality. Determination of pH]* (STN ISO 10390). Slovenský ústav technickej normalizácie.
- Tan, G., Liu, Z., Ma, X., Zheng, Z., Zhang, G., Wu, B., Zhang, L., & Liu, L. (2024). Phosphoric acid-activated metakaolin-based geopolymer: Optimizing P/A molar ratio to solidify Cs⁺ and Sr²⁺ in nuclear waste. *Nuclear Engineering and Design*, 424, 113300. <https://doi.org/10.1016/j.nucengdes.2024.113300>
- Teixeira, E. R., Camões, A., & Branco, F. G. (2022). Synergetic effect of biomass fly ash on improvement of high-volume coal fly ash concrete properties. *Construction and Building Materials*, 314, 125680. <https://doi.org/10.1016/j.conbuildmat.2021.125680>
- Tian, Q., Nakama, S., & Sasaki, K. (2019). Immobilization of cesium in fly ash-silica fume based geopolymers with different Si/Al molar ratios. *Science of the Total Environment*, 687, 1127–1137. <https://doi.org/10.1016/j.scitotenv.2019.06.095>
- Tian, Q., Wang, H., Pan, Y., Bai, Y., Chen, C., Yao, S., Guo, B., & Zhang, H. (2022). Immobilization mechanism of cesium in geopolymer: Effects of alkaline activators and calcination temperature. *Environmental Research*, 215, 114333. <https://doi.org/10.1016/j.envres.2022.114333>
- Wang, Y., Han, F., & Mu, J. (2018). Solidification/stabilization mechanism of Pb(II), Cd(II), Mn(II) and Cr(III) in fly ash based geopolymers. *Construction and Building Materials*, 160, 818–827. <https://doi.org/10.1016/j.conbuildmat.2017.12.006>
- Zhan, L., Bo, Y., Lin, T., & Fan, Z. (2021). Development and outlook of advanced nuclear energy technology. *Energy Strategy Reviews*, 34, 100630. <https://doi.org/10.1016/j.esr.2021.100630>

Summary

Solidification/stabilization of fly ash contaminated with radiocaesium into geopolymers. The main goal of this work was to evaluate the possibilities of solidifying fly ashes contaminated with ¹³⁷Cs into geopolymer waste forms. In the first step, physico-chemical characterization of fly ash originating from the thermal power plant in Vojany (Slovak Republic) was carried out. Before the preparation of the geopolymer waste forms (ternary mixture Geocem, GEOFIX, s.r.o., Slovak Republic) containing fly ash at percentage weight proportions of 5%, 10%, 20%, and 40%, the fly ash was artificially contaminated with a ¹³⁷CsCl solution. The ¹³⁷Cs activity was measured by scintillation gamma-spectrometry. The leachability test conducted according to the American National Standard ANSI/ANS-16.1-1986 over five days showed that the geopolymer waste forms with fly ash contents of 5%, 10% and 20% met the required leachability index limits with values more than 6. The compressive strength test also confirmed that the samples with 40% ash content did not meet the required 5 MPa limit for their disposal as a radioactive waste.

Lenka VAVRINCOVÁ

Vanda ADAMCOVÁ ✉ 

Linda MACHALOVÁ 

Martin VALICA 

Šimon REZBÁRIK

Miroslav HORNÍK 

University of Ss. Cyril and Methodius in Trnava, Institute of Chemistry and Environmental Sciences,
Faculty of Natural Sciences, Slovak Republic

Effect of soil nutrients on the stability of superabsorbent polymers as a tool for climate change mitigation

Keywords: superabsorbent polymers, agriculture, drought, nutrients, metals, hydrogel formation

Introduction

Climate change and drought are closely interrelated, as climate change significantly influences precipitation patterns, leading to drought in many regions of the Earth. Climate change refers to long-term shifts in average meteorological conditions, including temperature, precipitation, wind, and other atmospheric phenomena (Cook et al., 2018). The growing global demand for water, coupled with the impacts of climate change, is placing immense pressure on water resources (Oladosu et al., 2019). Abiotic factors, such as temperature,

salinity, and drought, are key drivers affecting agricultural production. These factors are projected to increasingly contribute to soil degradation and reduced crop yields. Thus, it is crucial to develop innovative agricultural practices that enhance water use efficiency. Superabsorbent polymers (SAPs) are one potential solution in this regard.

Superabsorbent polymers (SAPs) are three-dimensional cross-linked hydrophilic polymers capable of absorbing and storing large quantities of water, which can be gradually released during periods of drought. Since the American Department of Agriculture made the first SAP available in the 1970s, SAPs offer promising applications in a variety of fields, including modern agriculture, materials for personal hygiene products, biomedicine, drug delivery systems, sewage treatment, construction, healthcare, electronics and so on for their excellent water-absorption and retention capabilities. Currently, SAPs are widely used in products, such as diapers, sanitary napkins, tampons, and nursing pads (Ahmed, 2015; Mignon et al., 2019; Prasad et al., 2023; Chavan et al., 2024; Wang et al. 2024a).

SAPs could be groundbreaking technologies for the adaptation of agriculture to climate change. When applied to cultivated soil, SAPs absorb and retain water from irrigation (both artificial and natural) and prevent rapid loss through drainage and evaporation. As the soil dries, the stored water is released from the hydrogel via diffusion, keeping the soil or substrate moist for extended periods. The application of hydrogels improves soil density, structure, and permeability, enhances water infiltration, and reduces evaporation rates, all while decreasing water runoff and soil erosion, ultimately leading to improved crop productivity (Nnadi & Brave, 2011; Frioni et al., 2024). Another advantage of SAPs is their ability to retain nutrients in the soil and serve as carriers for slow-release fertilizers. In addition to improving soil water-use efficiency, SAPs are also used for the controlled release of fertilizers. It has been reported that approx. 40–70% of the nitrogen (N) and 80–90% of the phosphorus (P) in conventional fertilizers cannot be absorbed by crops due to their high solubility and rapid diffusion into the surrounding environment (Hou et al., 2017).

SAPs can be classified based on various factors, including chemical composition, source, and application. SAPs are generally classified from the point of view of their origin as natural, synthetic, or semisynthetic. Natural SAPs, such as those derived from cellulose, starch, and chitosan, are easily biodegradable, but they have a lower water absorption capacity and must therefore be used in larger quantities. On the other hand, synthetic SAPs, such as polyacrylic acid and polyacrylamide, have a higher water absorption capacity and are more cost-effective, but their lower biodegradability may negatively impact

the environment and plant growth (Chang et al., 2021; Chavan et al., 2024). Semisynthetic polymers, which combine the properties of both natural and synthetic polymers, are frequently used in applications like drug delivery. For instance, chitosan can be crosslinked with polyacrylic acid for use in medicinal delivery systems (Chang et al., 2021; Chavan et al., 2024).

In recent years, driven largely by increasing concerns about environmental sustainability, there has been growing interest in developing biodegradable SAPs for commercial agricultural applications. The development of biodegradable SAPs from renewable resources is gaining significant attention from scientists and researchers worldwide. In contrast to synthetic SAPs, biodegradable alternatives offer ecological benefits and contribute to environmental protection. Many companies that produce hydrogel products are now focusing on the development of environmentally friendly absorbent materials derived from renewable resources, rather than synthetic SAPs made from petroleum byproducts (Mali et al., 2018; Calcagnile et al., 2019; Godwin et al., 2019; Chavan et al., 2024). Cellulose and its derivatives present a sustainable alternative due to their renewable, biodegradable, and abundant characteristics, and show promise as a source for the production of eco-friendly SAPs (Dodangeh et al., 2024).

SAPs consist of three-dimensional crosslinked hydrophilic networks capable of absorbing and retaining vast amounts of water. This water absorption capacity is a key parameter used to describe SAPs, defined as the ratio of the weight of absorbed water [g] to the dry weight of the SAP [g]. While retaining their physical structure, three-dimensional hydrophilic networks of polymer chains can absorb, expand, and hold aqueous solutions up to 1,000-time their weight, while standard SAPs can retain a maximum of 10-times their weight (Chen et al., 2022; Prasad et al., 2024; Wang et al., 2024b). A typical SAP is defined as a highly hydrophilic material whose absorption mechanism is based on osmotic pressure, which is a direct result of its extreme hydrophilicity and cross-linked structure. SAPs draw water into their three-dimensional network through osmotic pressure, thanks to the compatibility between water and polymer chains. To achieve excellent absorption properties, SAPs must contain a sufficient number of strongly hydrophilic groups, which are generally highly polar or ionic (following neutralization by metal ions – M). Examples include –OH, –COOH/–COO-M, –CONH₂, –SO₃H/–SO₃-M, and others (Dodangeh et al., 2024).

There are four primary mechanisms by which absorbent materials absorb water: (i) reversible changes in their crystal structure (e.g. silica gel and anhydrous inorganic salts); (ii) physical capture of water by capillary forces in macroporous structures (e.g. soft polyurethane sponges); (iii) a combination of capillary action

and hydration of functional groups (e.g. tissue paper); (iv) a combination of the above with the natural dissolution of hydrophilic polymer chains, which is the primary mechanism of SAP formation (Matjašič et al., 2021).

Two types of cross-linking are commonly used in SAP production: bulk cross-linking and surface cross-linking. Bulk cross-linking, also known as core cross-linking, usually occurs during the polymerization stage of SAP production. For example, in the polymerization of acrylic acid, a dialkene cross-linking agent is used, and its molecules are incorporated directly into the main polymer chain during radical polymerization. This process results in SAPs with higher cross-linking densities, which provide greater structural stability and gel strength. However, this may reduce their water absorption due to the dense cross-linking, which limits the free space for water molecules. Once the pores allowing water entry into the core become blocked, further water penetration is prevented, leading to “gel blocking” (Kiatkamjornwong, 2007).

To mitigate this issue, surface cross-linking methods are now widely used. In this process, a surface coating helps maintain sufficient gel strength while allowing adequate water absorption into the core. Surface cross-linking typically occurs on a side group (e.g. carboxyl group) of a preformed base polymer (Dabhi et al., 2013).

The aim of this study was to assess the effect of soil nutrients on the stability of superabsorbent polymers (SAPs). SAPs derived from starch and mixtures of acrylic acid and acrylamide were tested. First, a physicochemical characterization of the SAPs was performed, which included optimization of the water absorption volume, determination of the maximum water absorption capacity, and analysis of the water binding kinetics. Then, we also investigated the effects of selected nutrients and metals on the water absorption capacity of SAPs.

Material and methods

Superabsorbent polymer

A sample of superabsorbent polymer (SAP) was obtained from PEWAS, Ltd. (Bratislava, Slovakia) under the trade name AquaVantage AV200. The polymer is a complex mixture consisting of 60% (by weight) starch-based polymers and 40% (by weight) of a blend of acrylic acid and acrylamide (in a weight ratio of 10 : 1).

It appeared as a fine white-cream colored powder with a grain size of 200 mesh. The sample was stored in a dry environment until the experiments were conducted. Before use, the SAP was dried in a hot air oven at 60°C for 24 h.

Evaluation of the effect of nutrients and metals on the formation of hydrogels

The water absorption capacity of the SAP was evaluated through experiments using two types of gravimetric methods: (i) the tea bag method for evaluating hydrogel formation, and (ii) the test tube method using a Microfil filtration system (Millipore, 2017) with membrane cellulose filters.

The objective of the first experiment was to determine the water absorption capacity of the SAP, i.e., the maximum volume of water that the polymer can absorb. A precisely weighed 100 mg sample of the SAP was placed into a pre-weighed empty tea bag. The tea bag containing the SAP was then placed at the bottom of a two-liter plastic container, and specific volumes of ultrapure water (30 mL, 40 mL, 50 mL, 75 mL, 100 mL, 200 mL, and 500 mL) were added. Three parallel samples were tested for each volume. After 2 h, the tea bag with the swollen hydrogel was removed from the water, allowed to drip for 10 s, and then weighed. The water absorption capacity of the polymer was calculated using the following equation (Eq. 1):

$$Q = \frac{m_1 - m_0}{m_0}, \quad (1)$$

where: Q – hydrogel swelling capacity [$\text{g} \cdot \text{g}^{-1}$]; m_0 – weight of SAP in the tea bag before swelling [g]; m_1 – mass of swollen hydrogel [g].

The second experiment focused on evaluating the swelling kinetics of the hydrogel. The procedure was identical to that of the water volume optimization experiment, but using 100 mL of ultrapure water as the optimized volume. Measurements were taken at time intervals of 5 min, 15 min, 30 min, 60 min, 120 min, 180 min, 240 min, and 1,440 min, with three parallel samples for each time of exposure. The hydrogel swelling capacity was calculated using the same equation (Eq. 1).

As an alternative method for evaluating the swelling kinetics, the gravimetric method using a Microfil filter system and pre-weighed cellulose membrane filters (47 mm in diameter) was employed. A five-milligram sample of SAP was weighed into a test tube, followed by the addition of 10 mL of ultrapure water. The contents were mixed in a vortex mixer for 5 s. Samples were taken at the same time intervals as in the case of the tea bag method (5 min, 15 min, 30 min, 60 min, 120 min, 180 min, 240 min, and 1,440 min) with three parallel series. The water-hydrogel mixture was then separated into the filter system, excess water was removed using the filtration system, and the hydrogel was retained on the filter. The hydrogel swelling capacity was calculated using the same equation (Eq. 1).

To evaluate the stability of the hydrogel in the presence of Hoagland's medium (Hoagland, 1920), test tube experiments were conducted using a gravimetric analysis. An exact amount of 5 mg of SAP was weighed into test tubes (two parallel series), and prepared solutions of Hoagland's medium (10% and 100% of ionic strength) were added to the tubes. After the solutions were added, the samples were vortexed for uniform mixing. Following a two-hour swelling period, the samples containing the formed hydrogel were separated onto the filter system, and the solution was removed using a vacuum filtration system. The hydrogel retained on the filter was then weighed, and the hydrogel swelling capacity was calculated using Equation (1).

To assess the stability of the hydrogel in the presence of nutrients and metal ions at concentrations equimolar to the potassium content in the SAP, test tube experiments were conducted with a gravimetric analysis using the Microfil filtration system. Metal solutions of Na, K, Zn, Co, Cu, Cs, and Cd (in the form of chlorides) were prepared in 200 mL volumetric flasks, each with a concentration equimolar to the potassium content in the SAP. A precise amount of 5 mg of the SAP was weighed into test tubes (three parallel series), and 10 mL of each prepared metal solution was added. The samples were then vortexed. After a two-hour swelling period, the samples were filtered through the Microfil filter system, and the hydrogel was retained on the filter and weighed. The hydrogel swelling capacity was calculated according to Equation (1).

Flame photometry

Determination of the potassium (K) in a mineralized SAP sample was performed using an ATS 200MKI flame photometer (Switzerland). A calibration curve and the equation of the calibration line for calculating the concentration of K in the SAP sample were obtained using standard K solutions in the concentration

range of 5–100 mg·L⁻¹. During the analysis of both the standard calibration solutions and the mineralized SAP sample, the solution was atomized using a nebulizer and combusted in a non-luminous propane-butane/air flame at temperatures between 1,600°C and 1,900°C. The concentration of K in the SAP sample was calculated based on the measured signal and by substituting the result into the equation derived from the calibration curve for determining K.

Scintillation gamma-spectrometry

To determine the potassium content in the analyzed SAP, a gamma-spectrometric analysis was performed using a 76BP76/3scintillation gamma-spectrometer equipped with a NaI(Tl) well-type crystal and lead shielding for high-sensitivity and high-resolution gamma-spectrometry (Envinet, 2024). The analysis was carried out using the ScintiVision-32 evaluation program (Ortec, USA). Initially, a background measurement was conducted with a measurement time of 5,000 s. Following this, a standard containing a known quantity of potassium, specifically the radioisotope potassium-40 (⁴⁰K) in the form of potassium chloride (KCl), was measured using Marinelli containers (1040G). The weight of the measured standard was 1,200 g. During the measurement, a peak with an energy of 1,460 keV was detected, which is characteristic of gamma-photons emitted during the decay of ⁴⁰K. The measurement time for the standard was 5,000 s. Subsequently, a sample of the analyzed SAP, weighing 983 g, was measured under the same conditions. Based on the measured activity of ⁴⁰K in the sample, the potassium content in the analyzed SAP was determined.

Graphical and statistical evaluation of data

The data processing and evaluation were performed using the Microsoft Excel (Microsoft Corporation, 2016) and Origin Pro 2016 (Origin Lab Corporation, 2016) software.

Results and discussion

The initial phase of the experiments focused on optimizing the conditions for hydrogel formation, specifically the volume of the absorbate and the kinetics of the hydrogel swelling process. Once the optimal conditions were determined, further experiments were conducted to evaluate hydrogel formation in different solutions, including Hoagland's medium and in the presence of metal ions.

Optimization of water volume (tea bag method)

The first experiment was aimed at optimizing the volume of water to determine the water absorption capacity of the SAP, i.e., the maximum volume of water that the SAP can absorb. Various water volumes were tested to establish the optimal hydrogel swelling capacity of the polymer.

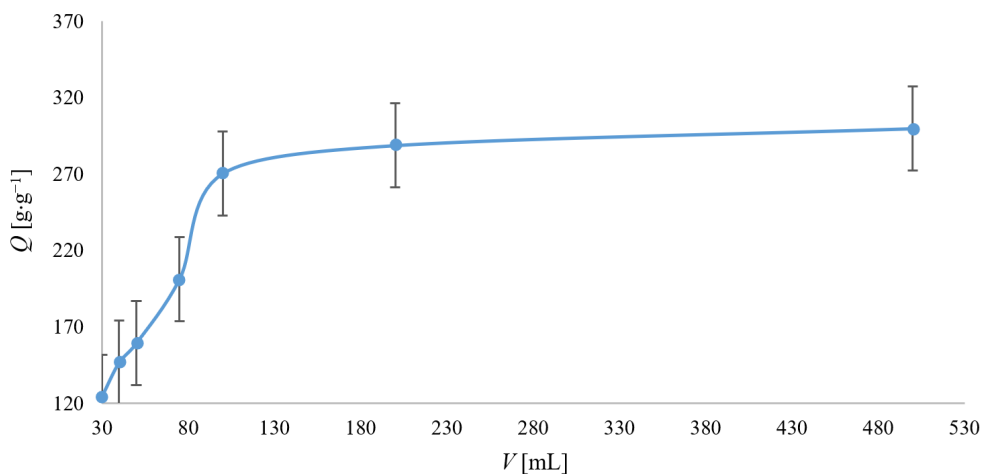


FIGURE 1. Dependence of SAP's water absorption capacity (Q) on water volume (V). The values represent the arithmetic means, and the error bars describe the standard deviation of three independent experiments

Source: own work.

Based on Figure 1, the trend of the water absorption capacity of SAP increases linearly with the volume of added water up to 100 mL. Beyond this point, the water absorption capacity shows minimal change, even as the water volume increases. Consequently, 100 mL was chosen as the optimal volume for determining the water absorption capacity in subsequent experiments, as further increases did not significantly improve this water absorption. It can therefore be concluded that after 2 h of exposure of SAP to various volumes of water, the SAP was saturated with water molecules from a volume of 100 ml and thus the maximum water absorption capacity was achieved.

The results from the volume optimization experiment were further analyzed using the Origin 2016 program to determine the maximum water absorption capacity of the SAP with ultrapure water as the sorbate. The obtained data were fitted by Langmuir's adsorption isotherm to provide a deeper understanding of the water absorption behavior.

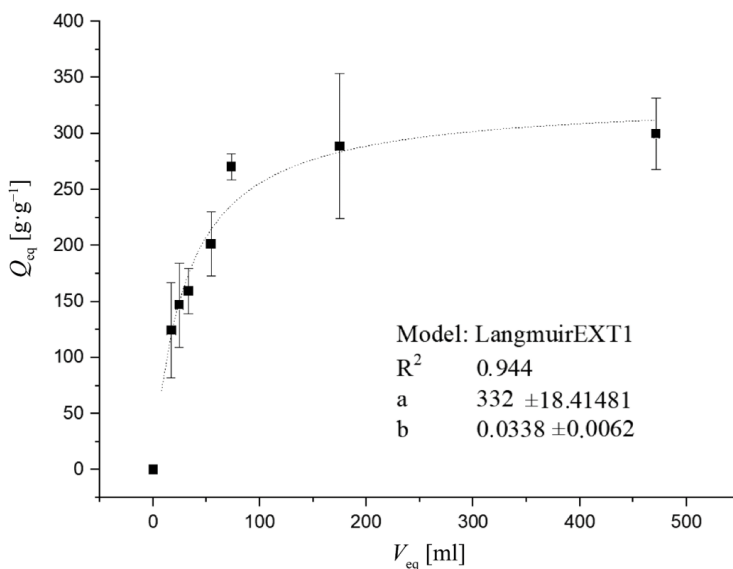


FIGURE 2. Dependence of equilibrium water absorption capacity (Q_{eq}) on equilibrium volumes of unabsorbed water (V_{eq}) described by Langmuir's adsorption isotherm using a nonlinear regression method. The values represent the arithmetic means, and the error bars describe the standard deviation of three independent experiments

Source: own work.

In Figure 2, the maximum water absorption capacity (Q_{max}) of the SAP for ultrapure water, based on Langmuir's adsorption isotherm, is shown to be $322 \pm 18 \text{ g}\cdot\text{g}^{-1}$ (parameter a in the graph). However, it is important to note that during the experiments using tea bags, a partial release of the hydrogel through the tea bag material was visually observed.

Kinetics of the hydrogel swelling process (tea bag method)

The second experiment aimed to evaluate the kinetics of the hydrogel swelling process, specifically how the water absorption capacity of the SAP changes with the exposure time. The goal was to determine the optimal hydrogel swelling time of the polymer.

Based on Figure 3, it can be concluded that the hydrogel swelling process was most intense during the first 2 h of exposure, after which the hydrogel swelling capacity values changed only minimally. This suggests that the optimal hydrogel swelling time is 2 h. This conclusion was also supported by the results from the kinetics experiments using test tubes with a Microfil filter system. Consequently, a hydrogel swelling time of 2 h was applied in all subsequent experiments.

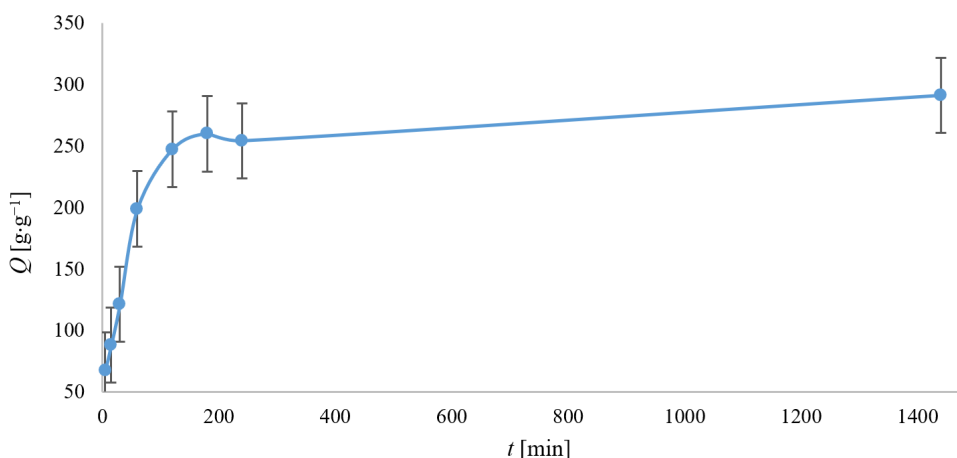


FIGURE 3. Dependence of SAP's water absorption capacity (Q) on exposure time (t). The values represent the arithmetic means, and the error bars describe the standard deviation of three independent experiments

Source: own work.

Kinetics of the hydrogel swelling process (test tube and filtration experiments)

As the second method for evaluating the kinetics of the hydrogel swelling process, the gravimetric method with the Microfil filter system was used.

From the curve described in Figure 4, it can be observed that the kinetics of hydrogel formation, whether in tea bags or test-tube experiments, followed a similar pattern, with intense hydrogel swelling during the first 2 h of exposure. After this period, the hydrogel swelling capacity increased only minimally. In this experiment, the maximum hydrogel swelling capacity (Q) after 2 h was recorded at $522 \pm 14 \text{ g}\cdot\text{g}^{-1}$, which was higher than in the tea bag experiment, where Q was only $247 \pm 14 \text{ g}\cdot\text{g}^{-1}$ after 2 h of exposure. The lower hydrogel swelling capacity observed in the tea bag method was attributed to the partial release of the hydrogel through the tea bag material, as previously mentioned.

A similar trend in the water absorption curve was also observed by Wang et al. (2024), who studied the kinetics of hydrogel formation for superabsorbent polymers. It is also noteworthy that the studied SAP exhibits relatively high-water absorption capacity compared to the starch-based SAPs used in similar experimental conditions, as demonstrated in the works of Lee et al. (2018), Lejcuš et al. (2018) and Chang et al. (2021).

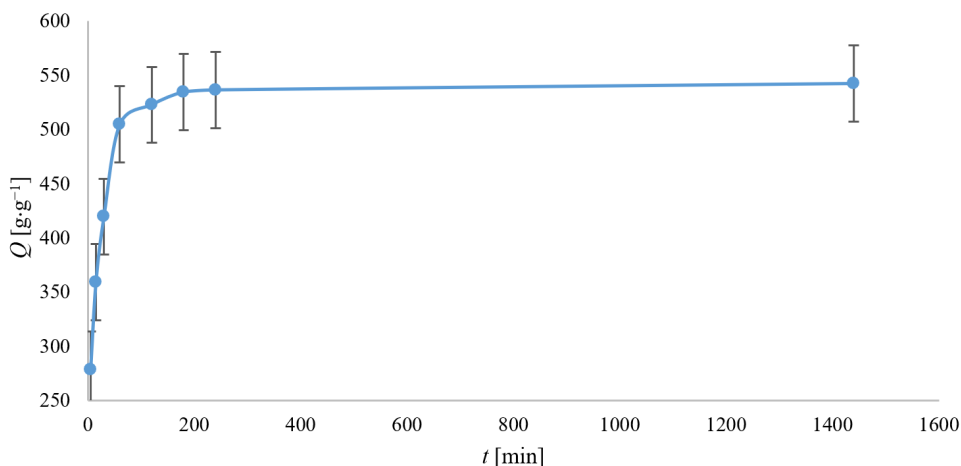


FIGURE 4. Dependence of SAP's water absorption capacity (Q) on exposure time (t). The values represent the arithmetic means, and the error bars describe the standard deviation of three independent experiments

Source: own work.

Evaluation of hydrogel stability in the presence of nutrients or metals

To assess the stability of the hydrogel, expressed as the value of the water absorption capacity of SAP, determined in the presence of nutrients (individually or as complex Hoagland's medium) or selected metals, test tube experiments were performed, where the hydrogel formation was evaluated gravimetrically.

Hoagland's solution is a hydroponic nutrient medium that contains essential nutrients for plant growth and development, including N, P, K, Ca, Mg, S, and trace elements, such as Fe, Zn, Cu, and Mn. As shown in Figure 5, the formation of hydrogel significantly decreased even with a 10% diluted Hoagland's medium. In the case of 100% Hoagland's medium, hydrogel formation was minimal compared to water. This indicates that the components of Hoagland's medium have a considerable impact on the ability of the SAP to bind water and form a hydrogel.

The potassium content in the SAP sample was determined using two analytical methods: flame photometry and scintillation gamma-spectroscopy. The measurements revealed that the potassium content in the analyzed SAP was 16.8%. To assess the hydrogel's stability in the presence of metal ions with an equimolar concentration to the potassium content in the SAP, test tube experiments were conducted. The gravimetric assessment of hydrogel formation was performed using the Microfil filtration system.

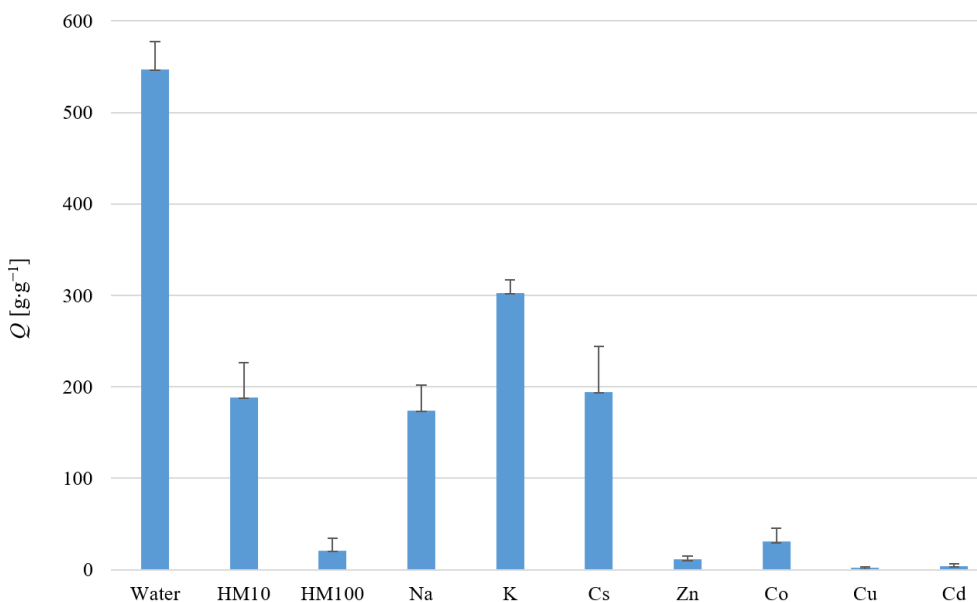


FIGURE 5. Water absorption capacity (Q) of SAP determined in the presence of Hoagland's medium (10% and 100% strength) and metal ions with an equimolar concentration to the potassium content in the SAP. The values represent the arithmetic means, and the error bars describe the standard deviation of three independent experiments

Source: own work.

As shown in Figure 5, the hydrogel formation decreased significantly in the presence of all the investigated ions. The hydrogel swelling capacity decreased by approx. half in the presence of K^+ ions and by around two-thirds in the presence of Na^+ and Cs^+ ions. Minimal or no hydrogel formation was observed for the heavy metal ions studied. Mignon et al. (2019) explained that the osmotic pressure forces water into a polymer due to a higher ionic concentration inside the polymer compared to the surrounding solution because of the presence of charged and hydrophilic moieties onto the ionic monomers. The combination of these charged groups and additional polar moieties in a SAP (hydroxyl, carbonyl or amine functionalities) attracts water and induces hydrogen bonding. The amount of polar and/or ionic groups is directly proportional to the hydrogel's swelling capacity. Introducing the SAP into a solution with a lower ionic concentration will lead to a higher hydrogel swelling capacity and, in the case of higher ion concentrations being present in the solution, the water absorption capacity of the SAP will be lower.

Conclusions

The experiments were focused on evaluating the effect of soil nutrients on the stability of superabsorbent polymers (SAPs) and their potential application in agriculture to improve water management, enhance crop resistance, and support agricultural production under the conditions of drought.

The first part of the study involved the physicochemical characterization of SAP as a mixture consisting of starch-based polymers and acrylic acid/acrylamide, including the assessment of its water absorption capacity, water binding kinetics, and optimization of experimental conditions.

In the second part, the effect of soil nutrients in the form of Hoagland's hydroponic nutrient solution and various macro- and microelement solutions on the water absorption capacity of SAP was examined. Based on the experiments and analyses, the SAP exhibited relatively high-water absorption capacity $Q = 522 \pm 14 \text{ g}\cdot\text{g}^{-1}$. However, a significantly reduced hydrogel swelling capacity was observed when Hoagland's medium or metal ion solutions with an equimolar concentration to potassium were used. The hydrogel's swelling capacity decreased by half in potassium (K) solutions and by two-thirds in sodium (Na) and cesium (Cs) solutions. Minimal hydrogel formation was observed in the presence of heavy metal ions with an equimolar concentration to potassium, and complete inactivation of the SAP occurred in the case of copper (Cu) solution.

The results of these experiments indicate that SAPs have potential applications in agriculture to enhance the efficiency of water use, increase drought tolerance in crops, and boost agricultural productivity. However, the composition of the soil solution or nutrient medium significantly affects the SAPs' properties, particularly their water absorption capacity and stability. This must be considered when considering the use of SAPs in agricultural practices. It would be desirable for follow-up research in the field of evaluating the application of SAP to focus on finding new substances forming SAPs that meet the criteria of biodegradability and higher stability in soil in terms of maintaining their water absorption capacities.

Acknowledgments

This work was supported by the Slovak Research and Development Agency under contract No. APVV-17-0150 and Scientific Grant Agency of the Slovak Republic under contract No. VEGA 1/0018/22.

References

- Ahmed, E. M. (2015). Hydrogel: Preparation, characterization and applications: A review. *Journal of Advanced Research*, 6(2), 105–121. <https://doi.org/10.1016/j.jare.2013.07.006>
- Calcagnile, P., Sibillano, T., Giannini, C., Sannino, A., & Demitri, C. (2019). Biodegradable poly (lactic acid)/cellulose-based superabsorbent hydrogel composite material as water and fertilizer reservoir in agricultural applications. *Journal of Applied Polymer Science*, 136(21), 47546. <https://doi.org/10.1002/app.47546>
- Chang, L., Xu, L., Liu, Y., & Qiu, D. (2021). Superabsorbent polymers used for agricultural water retention. *Polymer Testing*, 94, 123–130. <https://doi.org/10.1016/j.polymertesting.2020.107021>
- Chavan, V. D., Pinjari, D. V., Waghmare, N. G., Juikar, V. C., & Sayyed, A. J. (2024). A critical review on technological development of cellulosic material as a sustainable alternative for superabsorbent polymers and its recent applications. *Chemical Engineering Journal*, 499, 156487. <https://doi.org/10.1016/j.cej.2024.156487>
- Chen, J., Wu, J., Raffa, P., Picchioni, F., & Koning, C. E. (2022). Superabsorbent polymers: from long-established, microplastics generating systems, to sustainable, biodegradable and future proof alternatives. *Progress in Polymer Science*, 125, 101475. <https://doi.org/10.1016/j.progpolymsci.2021.101475>
- Cook, B. I., Mankin, J. S., & Anchukaitis, K. J. (2018). Climate change and drought: From past to future. *Current Climate Change Reports*, 4, 164–179. <https://doi.org/10.1007/s40641-018-0093-2>
- Dabhi, R., Bhatt, N., & Pandit, B. (2013). Superabsorbent polymers – an innovative water saving technique for optimizing crop yield. *International Journal of Innovative Research in Science, Engineering and Technology*, 2(10), 5333–5340.
- Dodangeh, F., Nabipour, H., Rohani, S., & Xu, C. (2024). Applications, challenges and prospects of superabsorbent polymers based on cellulose derived from lignocellulosic biomass. *Biore-source Technology*, 408, 131204. <https://doi.org/10.1016/j.biortech.2024.131204>
- Envinet (2024). *Products*. Envinet. <https://www.nuvia.com/cz/subjekty/ceska-republika/>
- Frioni, T., Bonicelli, P. G., Ripa, C., Tombesi, S., & Poni, S. (2024). Superabsorbent hydrogels: A new tool for vineyard water management? *Agricultural Water Management*, 306, 109145. <https://doi.org/10.1016/j.agwat.2024.109145>
- Godwin, P. M., Pan, Y., Xiao, H., & Afzal, M. T. (2019). Progress in preparation and application of modified biochar for improving heavy metal ion removal from wastewater. *Journal of Bioresources and Bioproducts*, 4(1), 31–42. <https://doi.org/10.21967/jbb.v4i1.180>
- Hoagland, D.R. (1920). Optimum nutrient solutions for plants. *Science*, 52(1354), 562–564.
- Hou, X. Q., Li, R., He, W., Dai, X., Ma, K., & Liang, Y. (2017). Superabsorbent polymers influence soil physical properties and increase potato tuber yield in a dry-farming region. *Journal of Soils and Sediments*, 18, 816–826. <https://doi.org/10.1007/s11368-017-1818-x>
- Kiatkamjornwong, S. (2007). Superabsorbent polymers and superabsorbent polymer composites. *ScienceAsia*, 33(1), 39–43. [https://doi.org/10.2306/scienceasia1513-1874.2007.33\(s1\).039](https://doi.org/10.2306/scienceasia1513-1874.2007.33(s1).039)

- Lee, J., Park, S., Roh, H. G., Oh, S., Kim, S., Kim, M., Kim, D., & Park, J. (2018). Preparation and characterization of superabsorbent polymers based on starch aldehydes and carboxymethyl cellulose. *Polymers*, 10(6), 605. <https://doi.org/10.3390/polym10060605>
- Lejcuš K., Špitalniak M., & Dąbrowska, J. (2018). Swelling behaviour of superabsorbent polymers for soil amendment under different loads. *Polymers*, 10(3), 271. <https://doi.org/10.3390/polym10030271>
- Mali, K. K., Dhawale, S. C., Dias, R. J., Dhane, N. S., & Ghorpade, V. S. (2018). Citric acid cross-linked carboxymethyl cellulose-based composite hydrogel films for drug delivery. *Indian Journal of Pharmaceutical Sciences*, 80(4), 657–667. <https://doi.org/10.4172/pharmaceutical-sciences.1000405>
- Matjašič, T., Simčič, T., Medvešček, N., Bajt, O., Dreo, T., & Mori, N. (2021). Critical evaluation of biodegradation studies on synthetic plastics through a systematic literature review. *Science of the Total Environment*, 752, 141–145. <https://doi.org/10.1016/j.scitotenv.2020.141959>
- Microsoft Corporation (2016). *Microsoft Excel*. Microsoft Corporation.
- Millipore (2017). *Microfil Filtration System*. Millipore.
- Mignon, A., De Belie, N., Dubruel, P., & Van Vlierberghe, S. (2019). Superabsorbent polymers: A review on the characteristics and applications of synthetic, polysaccharide-based, semi-synthetic and “smart” derivatives. *European Polymer Journal*, 117, 165–178. <https://doi.org/10.1016/j.eurpolymj.2019.04.054>
- Nnadi, F., & Brave, C. (2011). Environmentally friendly superabsorbent polymers for water conservation in agricultural lands. *Journal of Soil Science and Environmental Management*, 2(7), 206–211.
- Oladosu, Y., Rafii, M. Y., Samuel, C., Fatai, A., Magaji, U., Kareem, I., Kamarudin, Z. S., Muhammad, I., & Kolapo, K. (2019). Drought resistance in rice from conventional to molecular breeding: A review. *International Journal of Molecular Sciences*, 20(14), 3519. <https://doi.org/10.3390/ijms20143519>
- Origin Lab Corporation (2016). *Origin Pro 2016*. Origin Lab Corporation.
- Ortec (2015). *ScintiVision-32*. Ortec.
- Prasad, C., Park, S. Y., Lee, J. S., Park, J. J., Jang, Y., Lee, S. W., Lee, B. M., Nam, Y. R., Rao, A. K., & Choi, H. Y. (2023). Modeling and investigation of swelling kinetics of sodium carboxymethyl cellulose/starch/citric acid superabsorbent polymer. *International Journal of Biological Macromolecules*, 253(4), 127013. <https://doi.org/10.1016/j.ijbiomac.2023.127013>
- Wang, Y., Fu, E., Saghir, S., & Xiao, Z. (2024). Novel superabsorbent polymer composite embedded with sodium alginate and diatomite for excellent water absorbency, water retention capacity, and high thermal stability. *Journal of Molecular Structure*, 1300, 137542. <https://doi.org/10.1016/j.molstruc.2023.137244>
- Wang, K., Dong, K., Guo, J., & Du, H. (2024). Absorption and Release mechanism of superabsorbent polymers and its impact on shrinkage and durability of internally cured concrete – A review. *Case Studies in Construction Materials*, 21, e03909. <https://doi.org/10.1016/j.cscm.2024.e03909>

Summary

Effect of soil nutrients on the stability of superabsorbent polymers as a tool for climate change mitigation. The aim of this study was to assess the effect of soil nutrients on the stability of superabsorbent polymers (SAPs). In agriculture, SAPs are known to increase productivity in arid regions by improving plant water availability, optimizing root nutrient uptake, and increasing plant drought tolerance. In this study, we tested SAPs derived from starch and mixtures of acrylic acid and acrylamide. First, a physicochemical characterization of the SAPs was performed, which included optimizing the water absorption volume, determining the maximum absorption capacity, and analyzing the water binding kinetics. We then also investigated the effects of elements, such as Na, K, Zn and Cu, on the stability of SAPs. The results showed that the SAPs exhibited a high-water absorption capacity. However, reduced swelling capacity was observed in the presence of Hoagland's medium and solutions of metal ions (Na, K, Zn, Cu) with equimolar concentrations to potassium in the SAP.

Yureana WIJAYANTI  

Oki SETYANDITO 

Bina Nusantara University, Faculty of Engineering, Civil Engineering Department, Indonesia

Enhancing urban water utilities: a case study of Utility of the Future framework implementation in Indonesia

Keywords: Utility of the Future, UoF, water utility, water management, action plan, sustainable improvement

Introduction

The provision of reliable and sustainable water services is a big challenge faced by rapidly urbanizing cities worldwide. The water provider should be able to conduct a self-assessment of its current condition, set targets, and make plans for future target implementation programs. There are tools for assessing current water management practices, such as the current situation analysis and management system (CSAS) (Kiliç et al., 2023), and the asset life-cycle management (ALCM) mode (Haffejee & Brent, 2008). Regarding tackling the sustainability issues, some approaches are being used, such as One Water (OW), which is an integrated planning and implementation approach to managing finite water resources for long-term resilience and reliability (Pokhrel et al., 2022; Dezfooli et al., 2023). In response to the complex and evolving water management outlook, the Utility of

the Future (UoF) concept has emerged as a transformative approach, integrating innovative technologies, sustainable practices, and advanced management strategies to enhance water utilities' performance (Cordoba et al., 2021). It employs participatory approaches in which utility teams are actively involved and empowered to drive the transformation of their utility (Gallandat et al., 2023).

The history of the UoF dates back to 2018 when the World Bank introduced the Framework for Performance Improvements, also known as the Turnaround Framework (Soppe et al., 2018) initiative aimed to support the enhancement of underperforming utilities. Building upon this foundation, the World Bank, in collaboration with Isle Utilities and Castalia, further strengthened the framework in 2019, leading to the development of the Utilities Framework Front, now known as the UoF. Building on the valuable insights gained from previous trials, the World Bank introduced the UoF Toolkit 2.0 in 2022 (Cordoba, 2022; World Bank, 2022). This updated toolkit incorporated lessons learned and best practices, offering more robust guidance for utilities seeking to adopt UoF principles. In 2020, UoF trials were conducted in ten utilities across eight countries, including Albania, Belarus, Brazil, Ethiopia, Ghana, the Philippines, Timor-Leste, and Turkey. These trials sought to evaluate the effectiveness of the UoF in diverse settings and utility contexts (Gallandat et al., 2023). Subsequently, in 2021, the Philippines embarked on a national pilot deployment of the UoF, marking a significant step toward a broader implementation.

The primary goal of the UoF is to deliver a service that is safe, reliable, transparent, inclusive, and responsive to customers. "Safe" implies adhering to quality standards, "reliable" denotes continuous 24/7 supply, and "transparency" means disclosing financial, operational, and performance information that is clear, and accurate (Schnackenberg & Tomlinson, 2016), "inclusive" means not excluding any party or group from the provision of service and/or within the utility, and finally, "responsive" signifies having sufficient capacity to provide customers with quality and timely responses, ensuring customer satisfaction. This objective relies on technical and commercial operations, organization and strategy, financial management, and human resource management. The operational environment of the utility is molded by the legal and governance framework. Other factors influencing the success of the UoF are resilience, innovation, market and customer-orientation, and inclusion. "Inclusion" means the process of increasing the opportunity for people with disadvantages based on their identity to take part in the utility's operations for better living conditions in the neighborhoods (Puente et al., 2021).

Among the beneficiaries of the UoF program was the country of Indonesia, where the UoF Toolkit 2.0 was successfully implemented. One of the water utilities that had the opportunity to participate in the UoF program was the local government-owned enterprise [Perusahaan Umum Daerah (Perumda)] Tirta Musi in Palembang City, South Sumatra. After undergoing rigorous assessments by the UoF Team from the World Bank, Perumda Tirta Musi Palembang emerged as a promising candidate for UoF adoption, opening up new avenues for empowering citywide water service provision in the region. This study hypothesizes that performing a thorough gap analysis within the UoF framework improves the focus and prioritization of methods for enhancing short-term and long-term utility performance.

This research aims to demonstrate the performance of the UoF framework as a systematic approach for performance evaluations, formulating action plans, and attaining world-class benchmarks in water utilities.

Material and methods

This study focused on the case of the water utility Perumda Tirta Musi Palembang. In the year 2022, when the UoF was starting to be implemented, Palembang City had 1,362,256 people in its service area, with the average number of people in a single family being 4.36 people (Badan Pusat Statistik, 2023). The water utility had a total water production volume of 138,707,289 m³ per year and a total water sell volume of 108,943,367 m³ per year (Ministry of Public Works and Housing, 2022). It is projected that service coverage will be 100% in 2030 (Kurniawan et al., 2021). Data collection methodologies include both quantitative and qualitative approaches. Quantitative methods were employed to gather performance indicator data from utility records, such as service level, operational efficiency, and financial metrics. Qualitative methods involve focus group discussions with employees to collect insights on gaps and goals, as well as document reviews (e.g., policy reports, historical evaluations).

The UoF methodology operates concurrently along two dimensions to enhance performance and stimulate the transformation of water and sanitation utilities: management and operations (a “hard” dimension that primarily focuses on processes and practices) and change management (a “soft” dimension that emphasizes staff engagement, empowerment, and team building). The management and operational aspect of the process involves five phases such as: (1) decision and preparation,

(2) rapid in-depth analysis, (3) ignition and short-term action plan, (4) strategic vision and long-term action plan, and (5) sustainable transformation.

The initial phase of the UoF program involves assessing the present condition of the utility and outlining the target advancement of five distinct domains: performance, service, UoF level, maturity, and enabling environment. These aspects are connected to various segments.

The service assessment evaluates the service quality based on the five elements of the diagnostic area (Table 1) using a scale ranging from 1 (elementary) to UoF. An example of the scoring is that, when assessing the performance of the utility service, with a drinking water coverage rate below 50%, it receives a score of 1, while a utility with a 100% coverage rate of drinking water is rated at the UoF service level. The assessment consists of five components, which are reliable, safe, inclusive, transparent, and responsive. Every element is evaluated using one or more indicators. For instance, reliability is appraised through metrics like continuity (hours of supply per day) and availability (averaged domestic water per person per day).

TABLE 1. Service assessment criteria

Diagnostic area	Analysis process
Service	Qualitative and quantitative data analysis
Performance	Qualitative and quantitative data analysis
Maturity	Selecting practices that match the utility's current state using maturity matrices
UoF level	Selecting emerging practices that match the utility's current state using UoF elements
Enabling environment	Selecting practices that match the utility's current enabling environment using enabling environment assessment criteria

Source: own work.

Cobweb plots visually compare the utility's performance in commercial, technical, financial management, human resource management, and organization and strategy, rated from 1 (elementary) to 5 (world-class), as seen in Table 2. Every element is assessed within one or two indicators, for instance, commercial operations are evaluated by the metering rate and collection rate, while the technical performance is evaluated through non-revenue water (NRW). Predicting the NRW provides advantages for budget balances and sound water utility decision-making, planning, and investment (Şişman & Kızılöz, 2020).

TABLE 2. Performance level assessment

Domain	Level				
	elementary (1)	basic (2)	good (3)	well performing (4)	world class (5)
Commercial					
Collection rate [%]	< 60	≥ 60–70	> 70–90	> 90–95	> 95
Metering rate (customers metered) [%]	< 25	≥ 25–60	> 60–85	> 85–95	> 95
Technical					
Non-revenue water (NRW) per connection when the system is pressurized [L·h ⁻¹]	> 50	> 25–50	> 12–25	> 6–12	≤ 3–6
Financial management					
Earnings before interest, taxes (EBITDA) margin [%]	negative	< 5%	≥ 5–19	> 19–30	> 30
Human resource management					
Staff per 1 000 connections	> 10	> 6–10	> 5–6	> 3–5	≤ 3
Organization and strategy					
Fulfillment of the strategic plan [%]	no performance targets	< 40	≥ 40–80	> 80–90	> 90

Source: Cordoba (2022).

Results and discussion

The result of service performance analysis using the criteria in Tables 1 and 2 shows that the Palembang water utility’s current status is at the world-class level in the categories “safe” and “responsive” (Fig. 1). Safe and responsive imply high quality standards, and sufficient capacity to deliver customers with quality and prompt responses, respectively. The water utility has put a lot of effort into ensuring that no party or group is excluded from the provision of service and/or within the utility, as shown in the inclusive category with a score of 80%, or the well-performing level. It underscores its dedication to guarantee that all communities and demographic groups have access to water services. This inclusion signifies a commitment to social equality and suggests that the utility actively endeavors to assist underrepresented and underserved communities. This may encompass customized outreach programs, community involvement activities, and cost-effective pricing strategies, enhancing the overall social sustainability of the utility’s services.

Also, at this level, the reliable category represents the continuous 24/7 supply, which is another significant advantage for the utility. Reliability is crucial for addressing the needs of an expanding urban populace and guaranteeing regular service provision. The utility’s capacity to ensure continuous supply enhances its performance in the perception of customers, businesses, and other stakeholders reliant on dependable water access for everyday operations.

Nonetheless, the utility’s performance in the transparency category, achieving a basic level (40%), suggests significant potential for improvement. Transparency is an essential factor in establishing confidence among stakeholders, such as customers, regulatory agencies, and financial investors. The low score indicates that, although the utility may be functioning effectively in its operations, it likely falls short in transparent and precise financial reporting, disseminating operational data, and performance measures. The lack of transparency may stem from difficulties in data administration, an absence of established reporting standards, or inadequate communication regarding the utility’s financial status and operational performance to the public. Furthermore, openness in utility administration is vital for promoting accountability and guaranteeing the effective allocation of resources, particularly in publicly owned utilities.

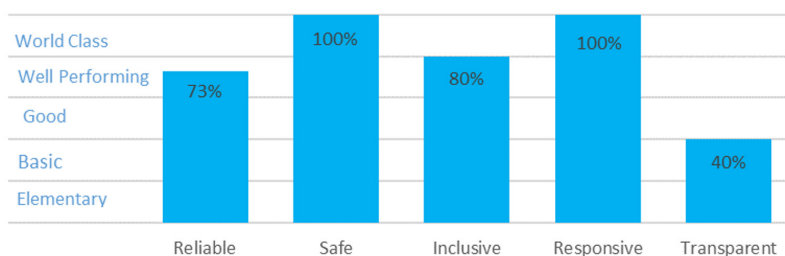


FIGURE 1. Service at the water utility in Palembang in 2022

Source: Perumda Tirta Musi Palembang (2023a).

Figure 2 shows that performance has a higher score than maturity for the commercial operations, financial management, and human resource management elements. This indicates that to maintain its current level of performance, the utility should increase its maturity. On the other hand, the technical operations element has a higher score for maturity than for performance, thus the utility should continue consolidating and optimizing its processes. The circle surrounding the maturity cobweb illustrates the advancement in adopting all UoF implementations over the various components, and the extent of the orange shading reflects

the overall percentage of UoF implementations integrated by the utility. It also shows that the utility has implemented about 36% of all innovation practices, which is the lowest implementation among other practices. The highest implementation is resilience, which is as much as 63%. The utility has implemented about 57% and 54% of the inclusion, and market and customer orientation practices, respectively. Comprehensive indicators are needed to carry out the planning and programming in an integrated manner (Mendoza Gómez et al., 2022). Tools of UoF provide graphics showing the gap between the current condition and future goal, hence the CEO understands which elements need to be addressed. The use of the “gap” feature in water service companies has been found effective at improving water utilities’ performance (Han et al., 2017).

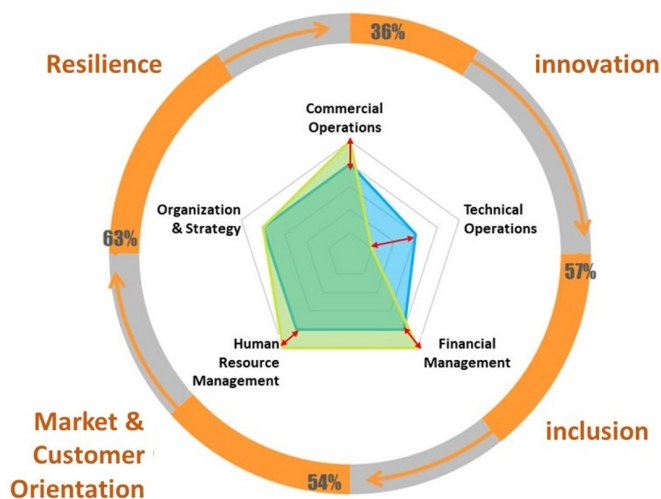


FIGURE 2. Cobwebs and Utility of the Future dimensions of performance and maturity of Perumda Tirta Musi Palembang

Source: Perumda Tirta Musi Palembang (2023a).

Figure 3a shows the results of identifying where gaps appear between the existing and future levels in the business strategy, monitoring and reporting, and strategy ability elements. Under the existing conditions, the business strategy element revealed that the mission, vision, and strategic objectives exist, but have not been updated and are not known to employees, the annual plans and budgets are not aligned with the strategic goals, mission, and vision, and the strategic objectives are documented at the executive management level, which includes an implementation plan and several performance indicators, but that this has not

been fully implemented. A strategic framework, including vision, mission, values, and strategic objectives, is available in the future but has not been updated, while some annual plans are already aligned with the strategic framework. Furthermore, strategic objectives for key performance aspects (e.g. customer service, operations, maintenance, asset management, policies, procedures, and financial reporting) have been defined for at least five years. Future scenarios for asset management should be developed strategically (de-Almeida-e-Pais et al., 2023), for example, the repairs planning of the pipe network (Scholten et al., 2014).

Figure 3b shows the results of the identifying where gaps appear between the existing and future levels in the commercial management areas, where a gap appears in the customer service area. Under the topic of “method for customers to submit complaints and questions,” the current state includes at least two media for delivery, including one that is electronic (e.g. call center and service provider website) during business hours (Monday to Friday). The desired level will be achieved when various methods, including kiosks and social media, and convenience levels are implemented. This also includes a 24/7 call center and web service, and public service standards and customer rights to escalate complaints being accessible to the public. The existing conditions align with another study that shows that the water utility sector uses social media less effectively to engage with customers compared to the electric utility sector (Mix et al., 2020).

Figure 3c shows the results of identifying where gaps appear between the existing and future levels in the technical operation elements, where gap appear in three areas. The first of these is asset management, as in its current state, it has a documented baseline plan but not a financial or asset life cycle plan, so the desired level consists of these documented plans, including implementation plans and performance monitoring measures, but excludes long-term financial planning. The second area is the technical operation process, which in its current state has an inventory of all processes/handbooks/guidance manuals and their respective update statuses, but not all processes are up to date. Efficient information management is essential for infrastructure asset management; however, numerous utilities struggle with missing or expired data (Carriço et al., 2020). These inventory documents are not always used for operations. The desired level consists of conducting an annual review of the process status and delivering plans to update key processes subject to staff consultation. The third area of the technical operation element consists of distribution and non-revenue water (NRW), which in its current state is undergoing comprehensive strategies to address actual water losses, apparent water losses,

and unbilled consumption in priority areas, including time-bound targets for multi-year periods, and establishing policies to assess, monitor and control NRW elements. The desired condition is a practical implementation (including the required capital investments and operating activities) of the NRW strategy. Strategies for lowering the amount of NRW must be consistent with the overall corporate goals, including achieving financial sustainability, minimizing environmental consequences, and enhancing service reliability (Farouk et al., 2023). Also, cross-functional collaboration is crucial, combining technical, financial, and customer service departments to formulate a comprehensive NRW management strategy (Lai et al., 2020).

Figure 3d shows the financial management element, where gaps appear in three areas. The first area is financial model and forecasting, which in its current state reveals a full-cost recovery tariff analysis (OPEX, depreciation, and return) with disaggregation by customer category, irregularly done per year. Tariff design is profoundly affected by social and environmental issues, requiring a theoretical framework that can incorporate these complexities (Granda-Aguilar et al., 2024). The desired level is a multi-year cost recovery tariff analysis, which is updated annually. The second area is accounting and financial reporting, with the current state of the detailed fixed asset register (including cost, location), and defined assets. The desired level is an asset management system that incorporates the condition, maintenance planning, and management of the assets. The third area is control and transparency, where the accounts are not published in their current state. The desired level is in the world-class category, where the accounts are published regularly. The domains of accounting and financial reporting, along with control and transparency, are essential to the utility's evolution into an excellent company. The former emphasizes operational efficiency and asset optimization, whereas the latter fosters trust and accountability. Overall, they constitute interconnected pillars of financial resilience and governance, ensuring that the utility is both efficient in service delivery and transparent and responsible in its operations. These adjustments, though challenging, are essential for the utility's aim of sustainability and excellence.

Figure 4a shows the results of the identification of the current state and desired level in the human resource element, where a gap appears in the performance management area. The current state of this area is an annual performance evaluation with semi-annual follow-up based on progress toward employee goals. Evaluation includes supervisory feedback, improvement plans, mentoring, and supervisory

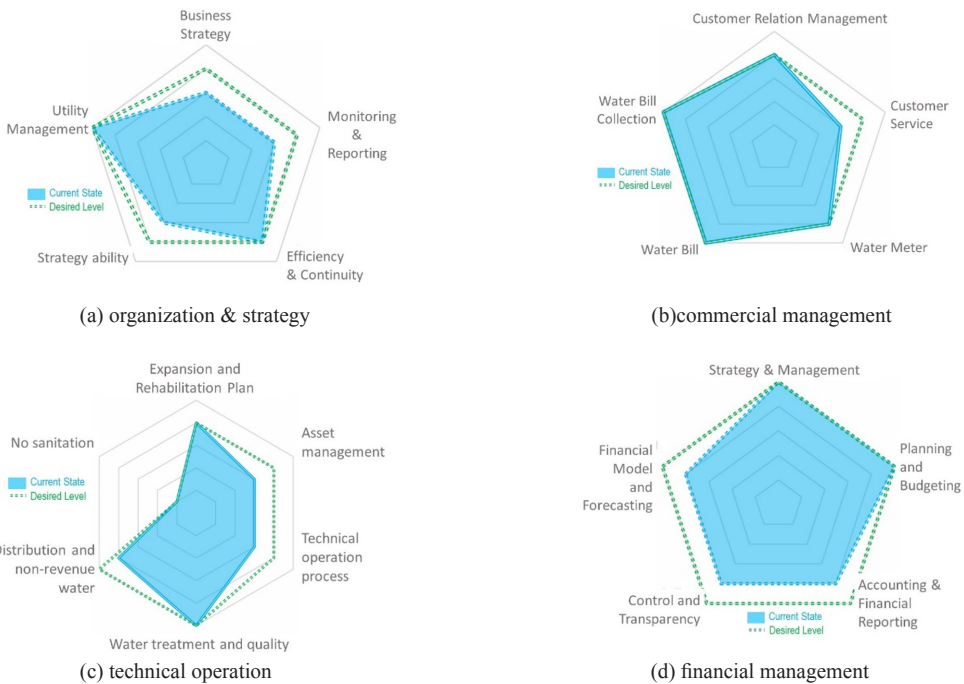


FIGURE 3. Cobweb of current states and desired levels of the elements: organization and strategy (a), commercial management (b), technical operation (c), and financial management (d)

Source: Perumda Tirta Musi Palembang (2023a).

commitment to implementing improvement plans. The desired level is an annual performance evaluation with quarterly or semi-annual follow-up.

The green management element has a gap in the greenhouse gas (GHG) emissions area (Fig. 4b). In the current state, GHG emissions have not been considered, so at the desired level, GHG measurements have been included in the water utility’s objectives but have not been completed.

There are four areas with gaps in the energy efficiency element, as shown in Figure 4c. The first area is strategy and management. Another area is energy monitoring and reporting, where its current state is energy tariffs, and contracts are known and managed by the administrative team. The desired level is that key consumption points that have driven contract/tariff optimization and optimization opportunities are considered by operations. The third area is vendor and procurement, where energy efficiency is the main criterion for vendor selection at the current level of “good”. The “well-performing” level is where every appliance

purchase has an energy efficiency component, updated regularly to follow the latest technology and tools. The fourth area is power system and assets, where in its current state, dedicated teams use modern tools to optimize maintenance plans and schedule proactive steps. To meet the world-class level, maintenance plans are digital and based on data-driven interactions to trigger proactive steps.

Figure 4d highlights a significant deficiency in the culture and value domain, particularly on the gender equality component. The utility currently operates at a “basic” level, indicating limited advancement in the integration of gender-sensitive practices. Although fundamental guidelines for minimizing sexual harassment are available, they are predominantly compliance-oriented rather than focused on fostering proactive cultural transformations. This suggests that the utility’s strategy for gender equality is reactive instead of proactive, lacking the necessary depth to cultivate an inclusive organizational atmosphere. The desired state, referred to as the “good” level, emphasizes advancements in formalizing gender equality initiatives, including the documenting of policies. The lack of implementation methods and training programs signifies a substantial deficiency in the operationalization of these policies. In the absence of explicit procedures, both personnel and management may lack the requisite guidance to implement the policy effectively, thereby diminishing its efficacy (Imonikhe & Moodley, 2018). The lack of training on sexual harassment prevention results in a knowledge deficit, hindering the organization’s capacity to enhance awareness, modify behavior, and cultivate a workplace culture that actively supports equality and safety.

Based on the gap analysis from the cobwebs, an action plan to close these gaps is then developed. The action plan is tailor-made, incorporating careful near-future actions and an expansive perspective on enduring strategies. Table 3 shows the final 100-day action list that has been validated by the water utility’s team. Such a tailored plan is a crucial component of strategic management planning for water utilities, to enable effective management (Almeida et al., 2021). The 100-day action plan was successfully implemented from October 2022 until 27 January 2023.

The 100-day action plan implementation evaluation demonstrated that the UoF framework effectively supports the water utility in assessing its current state, identifying gaps toward future goals, and formulating a five-year plan to achieve those objectives. Another finding indicates that leaders who are dedicated and devoted are crucial for the successful execution of the UoF. Leadership and purposeful knowledge management are critical to the implementation of the plan’s success in any water utility (Omar et al., 2017; Ruiz-Palomino et al.,

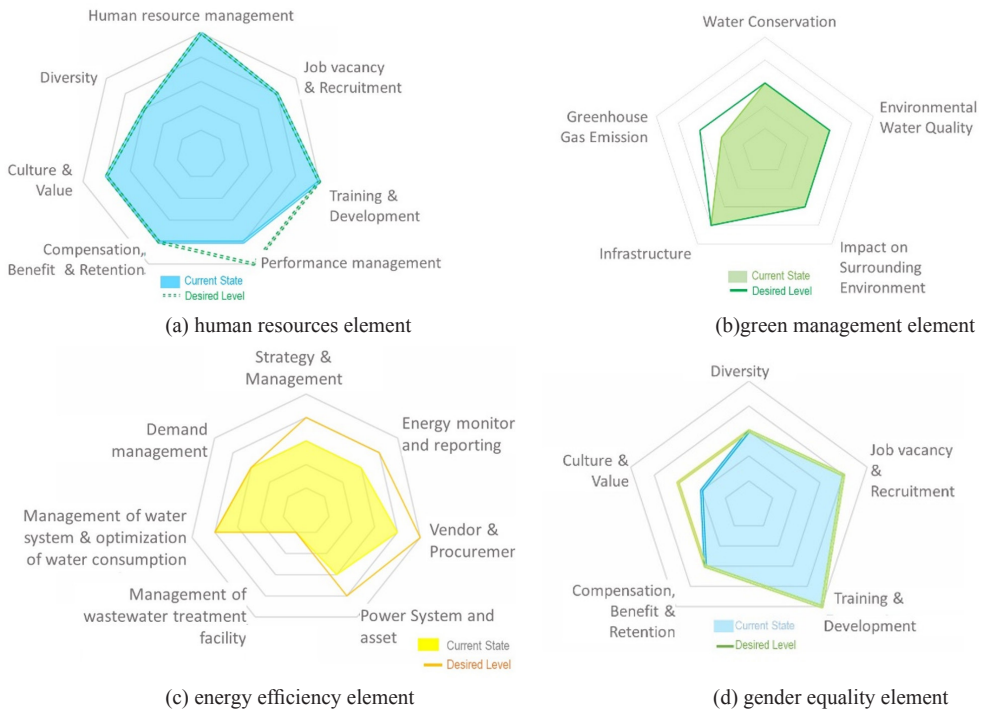


FIGURE 4. Cobweb of current state and desired level of elements
 Source: Perumda Tirta Musi Palembang (2023a).

TABLE 3. Matrices of 100-day action plan

Area	Topic	Action	Time [week]
Element: Organization & strategy			
Business strategy	strategic architecture	Strategic framework available but not yet updated, including vision, mission, values, and strategic goals. Some of the annual plans are aligned with the strategic framework.	8
Efficiency & continuity	process optimization	Accommodate ideas to improve company performance, create a team that will accommodate, evaluate, and select the best ideas (rewarded), and then report to management.	10
Strategic capability	procurement management	Analyze historical data of the procurement process (1–2 years) by categorizing purchases and contracts (services) based on value, supplier, etc.	6

TABLE 3 (cont.)

Area	Topic	Action	Time [week]
Element: Commercial management			
Customer relation management	communication strategy	Website updates and social media (Instagram, Facebook etc.) direct information about zones to be repaired, flow disturbances, tariff structures, publication of water quality test results, bills from large customers, etc.	15
Element: technical operation			
Asset management	asset recording	Adding criteria to asset applications regarding good, normal, and bad conditions, must be replaced, maintenance.	10
	maintenance notes	Develop an asset management application for water meters regarding the condition of the water meters, the amount, replacement, and removal of water meters that were previously only connected to PKA and service units to the budget and asset sections.	12
Water treatment & quality	water quality test method	Obtain laboratory certification according to ISO 17025:2017 (International Organization for Standardization [ISO], 2017).	15
Distribution & non-revenue water	average true range (ATR) of management strategy	Reports to management on the state of non-revenue water in the district metered area (level of non-revenue water, critical areas, key issues, etc.), as well as possible solutions in the short- and long-term (estimated cost of possible solutions).	12
Element: Financial management			
Planning & budgeting	budget system	Install financial software for work units to monitor budget realization online by budget users (programs can also be monitored by management), and carry out application usage training.	5
Accounting & financial reporting	asset register	Uploading audited financial reports (annual reports) to the website, for example, profit and loss balance.	4
Element: Human resource			
Compensation, benefits & retention	reward & acknowledgement	Create a set of rules including indicators for employees who innovate and their rewards.	12
Culture & value	organizational culture	Change the habits of employees to carry out energy efficiency (there is already an official memorandum followed by a socialization program for each work unit).	10
Element: Energy efficiency			
Energy monitoring & reporting	study & audit regarding energy	Analyze the main sources of energy consumption and the average annual cost of each building/pump. Energy efficiency: pumping, offices.	10

Source: Perumda Tirta Musi Palembang (2023b).

2021). Tianingrum (2021) performed a case study in a city in Indonesia, revealing that leadership has a positive and significant influence on organizational culture, and following this, organizational culture then has a positive and significant influence on employee performance. This study found that the framework can be adapted to the unique challenges and conditions of local contexts. Also, through the performance gap analysis, a comprehensive performance and maturity assessment can be drafted to pinpoint specific focus areas, such as technical operations, and integrate these insights into the planning process.

Conclusions

The UoF approach to the planning and sequencing methodology begins with an assessment of the present condition of the utility in terms of services, maturity, performance, and assessment of ecological responsibility. After that, the framework pinpoints its focused elements by recognizing the gaps during its assessments. In the case study, technical operation was identified as an area of focus that scored lower in the performance assessment compared to the other areas. The UoF framework's objective is to steer utility companies and professionals in formulating action plans while considering their specific areas of emphasis and enduring aspirations. The outcome is a tailor-made 100-day action plan encompassing meticulous short-term steps, provisional medium-term measures, and a broad overview of long-term actions. The UoF methodology is suitable to be used to support the water utility in understanding its current condition effectively and thoroughly, and its gaps between the present benchmark to future goals. Later, this gap can be incorporated into the formulation of an inclusive action plan to finally achieve a world-class water utility. Future studies will explore implementations of the UoF in more water utilities across Indonesia, offering insights into sustainable performance improvement.

Acknowledgments

The authors would like to extend their appreciation to Popy Indrawati from the Water Section, the World Bank Group, for her insights into the development of this paper, and to Andi Wijaya Andini as the director of Perumda Tirta Musi Palembang, South Sumatra.

References

- Almeida, M. C., Brito, R. S., Jorge, C., & Cardoso, M. A. (2021). Performance assessment system to wastewater utilities strategic planning. *Water*, 13(18), 2489. <https://doi.org/10.3390/w13182489>
- de-Almeida-e-Pais, J. E., Raposo, H. D., Farinha, J. T., Cardoso, A. J. M., Lyubchyk, S., & Lyubchyk, S. (2023). Measuring the performance of a strategic asset management plan through a balanced scorecard. *Sustainability*, 15(22), 15697. <https://doi.org/10.3390/su152215697>
- Badan Pusat Statistik (2023). *Palembang Municipality in figures 2023*. Badan Pusat Statistik. <https://palembangkota.bps.go.id/publication/2023/02/28/d11792eb5fee5963efd9f0bb/kota-palembang-dalam-angka-2023.html>
- Carriço, N., Ferreira, B., Barreira, R., Antunes, A., Grueau, C., Mendes, A., Covas, D., Monteiro, L., Santos, J., & Brito, I. S. (2020). Data integration for infrastructure asset management in small to medium-sized water utilities. *Water Science and Technology*, 82(12), 2737–2744. <https://doi.org/10.2166/wst.2020.377>
- Cordoba, C. L., Gustavo, S. P., & Penalosa, F. P. (2022). *Utility of the future: taking water and sanitation utilities beyond the next level 2.0 – a methodology to ignite transformation in water and sanitation utilities* (English). World Bank Group. <http://documents.worldbank.org/curated/en/099325005112246075/P1655860d146090dc097dc0165740604044>
- Dezfooli, D., Bolson, J., Arabi, M., Sukop, M. C., Wiersema, I., & Millonig, S. (2023). A Qualitative Approach to Understand Transitions toward One Water in Urban Areas across North America. *Water*, 15(14), 2499. <https://doi.org/10.3390/w15142499>
- Farouk, A. M., Rahman, R. A., & Romali, N. S. (2023). Non-revenue water reduction strategies: a systematic review. *Smart and Sustainable Built Environment*, 12(1), 181–199. <https://doi.org/10.1108/SASBE-04-2021-0071>
- Gallandat, K., Schlumpberger, S., Penalosa, F. P., & Cordoba, C. L. (2023). *Empowering utilities to accelerate universal access: Introducing the Utility of the Future Center of Excellence in the Western Balkans*. <https://blogs.worldbank.org/en/water/empowering-utilities-accelerate-universal-access-introducing-utility-future-center-excellence>
- Granda-Aguilar, F., Benavides-Muñoz, H. M., Arteaga-Marín, J., Massa-Sánchez, P., & Ochoa-Cueva, P. (2024). Sustainable water service tariff model for integrated watershed management: a case study in the Ecuadorian Andes. *Water*, 16(13), 1816. <https://doi.org/10.3390/w16131816>
- Haffejee, M., & Brent, A. C. (2008). Evaluation of an integrated asset life-cycle management (ALCM) model and assessment of practices in the water utility sector. *Water SA*, 34(2), 285–290. <https://doi.org/10.4314/wsa.v34i2.183651>
- Han, S., Koo, D. D., Kim, Y., Kim, S., & Park, J. (2017). Gap analysis based decision support methodology to improve level of service of water services. *Sustainability (Switzerland)*, 9(9), 1578. <https://doi.org/10.3390/su9091578>
- Imonikhe, O. M., & Moodley, K. (2018). The challenge of effective policy implementation in Nigerian urban water utilities. *Water Supply*, 18(5), 1696–1705. <https://doi.org/10.2166/ws.2017.231>
- International Organization for Standardization [ISO]. (2017). *General requirements for the competence of testing and calibration laboratories* (ISO/IEC 17025:2017).

- Kiliç, S., Firat, M., Yılmaz, S., & Ateş, A. (2023). A novel assessment framework for evaluation of the current implementation level of water and wastewater management practices. *Water Supply*, 23(5), 1787–1809. <https://doi.org/10.2166/ws.2023.117>
- Kurniawan, M. A., Fitriani, H., & Hadinata, F. (2021). Analisis Kebutuhan Penyediaan Air Bersih di Kota Palembang [Analysis of water demand supply in Palembang City]. *Saintis*, 21(02), 105–112. [https://doi.org/10.25299/saintis.2021.vol21\(02\).7611](https://doi.org/10.25299/saintis.2021.vol21(02).7611)
- Lai, C. H., Tan, D. T., Roy, R., Chan, N. W., & Zakaria, N. A. (2020). Systems thinking approach for analysing non-revenue water management reform in Malaysia. *Water Policy*, 22(2), 237–251. <https://doi.org/10.2166/wp.2020.165>
- Mendoza Gómez, M., Tagle-Zamora, D., Morales Martínez, J. L., Caldera Ortega, A. R., Mora Rodríguez, J. D. J., & Delgado-Galván, X. (2022). Water Supply Management Index: Leon, Guanajuato, Mexico. *Water*, 14(6), 919. <https://doi.org/10.3390/w14060919>
- Ministry of Public Work and Housing. (2022). *Water Utility Performance 2022*. Ministry of Public Work and Housing.
- Mix, N., George, A., & Haas, A. (2020). Social media monitoring for water quality Surveillance and response systems. *AWWA Water Science*, 112(8), 44–55. <https://doi.org/10.1002/awwa.1555>
- Omar, Y. Y., Parker, A., Smith, J. A., & Pollard, S. J. T. (2017). Risk management for drinking water safety in low and middle income countries – cultural influences on water safety plan (WSP) implementation in urban water utilities. *Science of the Total Environment*, 576, 895–906. <https://doi.org/10.1016/j.scitotenv.2016.10.131>
- Perumda Tirta Musi Palembang. (2023a). *Final report. Utility of the future*. Perumda Tirta Musi Palembang.
- Perumda Tirta Musi Palembang. (2023b). *Report of UoF implementation at water utility Perumda Tirta Musi Palembang*.
- Pokhrel, S. R., Chhipi-Shrestha, G., Hewage, K., & Sadiq, R. (2022). Sustainable, resilient, and reliable urban water systems: making the case for a “one water” approach. *Environmental Reviews*, 30(1), 10–29. <https://doi.org/10.1139/er-2020-0090>
- Puente, F. A., Penalosa, F. P., Cordoba, L., & Sadik, N. (2021). *Utility of the future challenge: delivering water and sanitation services in 2050*. <https://blogs.worldbank.org/en/water/utility-future-challenge-delivering-water-and-sanitation-services-2050>
- Ruiz-Palomino, P., Linuesa-Langreo, J., & Elche, D. (2023). Team-level servant leadership and team performance: The mediating roles of organizational citizenship behavior and internal social capital. *Business Ethics, the Environment & Responsibility*, 32, 127–144. <https://doi.org/10.1111/beer.12390>
- Schnackenberg, A. K., & Tomlinson, E. C. (2016). Organizational Transparency. *Journal of Management*, 42(7), 1784–1810. <https://doi.org/10.1177/0149206314525202>
- Scholten, L., Scheidegger, A., Reichert, P., Mauer, M., & Lienert, J. (2014). Strategic rehabilitation planning of piped water networks using multi-criteria decision analysis. *Water Research*, 49, 124–143. <https://doi.org/10.1016/j.watres.2013.11.017>
- Şişman, E., & Kızıloöz, B. (2020). Trend-risk model for predicting non-revenue water: an application in Turkey. *Utilities Policy*, 67, 101137. <https://doi.org/10.1016/j.jup.2020.101137>

- Soppe, G., Janson, N., & Piantini, S. (2018). *Water utility turnaround framework. A guide for improving performance*. World Bank Group. <https://documents1.worldbank.org/curated/en/515931542315166330/pdf/Water-Utility-Turnaround-Framework-A-Guide-for-Improving-Performance.pdf>
- Tianingrum, A. S. (2021). Effect of leadership and organizational culture on employee performance. *APTISI Transactions on Management (ATM)*, 6(2), 158–166. <https://doi.org/10.33050/atm.v6i2.1746>
- World Bank. (2022). *Taking water and sanitation utilities beyond the next level 2.0. A methodology to ignite transformation in water and sanitation utilities*. <https://documents.worldbank.org/en/publication/documents-reports/documentdetail/099325005112246075/p1655860d146090dc097dc0165740604044>

Summary

Enhancing urban water utilities: a case study of the Utility of the Future framework implementation in Indonesia. Utility companies worldwide face unique challenges in innovation, inclusivity, market focus, and resilience. A uniform approach to action plans is impractical. The Utility of the Future (UoF) framework aims to guide companies in developing tailored action plans that reflect their specific areas of focus and long-term objectives. Therefore, the objective of this paper is to elaborate on the implementation of the UoF approach in reviewing the utility's performance and in developing the 100-day action plans. The case study is a local government-owned enterprise of the water utility, Perumda Tirta Musi, in Palembang City, South Sumatra, Indonesia. The outcome is a 100-day action plan with short-term steps and a five-year plan with long-term actions. It shows that the UoF methodology can help water utilities understand their current condition and gaps from the current benchmark to their future goals, enabling inclusive action plans for world-class water utilities. Future studies will explore further UoF implementations in Indonesia to provide insights into sustainable performance improvement strategies.

Instruction for Authors

The journal publishes in English languages, peer-reviewed original research, critical reviews and short communications, which have not been and will not be published elsewhere in substantially the same form. Author of an article is required to transfer the copyright to the journal publisher, however authors retain significant rights to use and share their own published papers. The published papers are available under the terms of the principles of Open Access Creative Commons CC BY-NC license. The submitting author must agree to pay the publication charge (see Charges).

The author of submitted materials (e.g. text, figures, tables etc.) is obligated to restricts the publishing rights. All contributors who do not meet the criteria for authorship should be listed in an Acknowledgements section of the manuscript. Authors should, therefore, add a statement on the type of assistance, if any, received from the sponsor or the sponsor's representative and include the names of any person who provided technical help, writing assistance, editorial support or any type of participation in writing the manuscript.

Uniform requirements for manuscripts

The manuscript should be submitted by the Open Journal System (OJS) at <https://srees.sggw.edu.pl/about/submissions>. All figures and tables should be placed near their reference in the main text and additionally sent in a form of data files (e.g. Excel, Visio, Adobe Illustrator, Adobe Photoshop, CorelDRAW). Figures are printed in black and white on paper version of the journal (color printing is combined with an additional fee calculated on a case-by-case basis), while on the website are published in color.

The size of the manuscript should be limited up to 10 pages including overview, summary, references and figures (the manuscript more than 13 pages is unacceptable); Please set the text format in single column with paragraphs (A4 paper format), all margins to 25 mm, use the font Times New Roman, typeface 12 points and line spacing one and half.

The submitted manuscript should include the following parts:

- name and SURNAME of the author(s) – up to 5 authors
- affiliation of the author(s), ORCID Id (optional)
- title of the work
- key words
- abstract (about 500 characters)
- text of the paper divided into: Introduction, Material and Methods, Results and Discussion, Conclusions, References and Summary
- references in APA style are listed fully in alphabetical order according to the last name of the first author and not numbered; please find the details below
- post and mailing address of the corresponding author:

Author's address:

Name, SURNAME

Affiliation

Street, number, postal code, City

Country

e-mail: `adres@domain`

- Plagiarism statement (<https://srees.sggw.edu.pl/copyright>)

Reference formatting

In the Scientific Review Engineering and Environmental Sciences the APA 7th edition style is used.

Detailed information

More information can be found: <https://srees.sggw.edu.pl>

